ANALYSIS OF SOUTHWESTERN UTAH

PRECIPITATION EVENTS ASSOCIATED WITH FLASH FLOODING

by

James T. Powell

A thesis submitted to the faculty of
The University of Utah
in partial fulfillment of the requirements for the degree of

Master of Science

Department of Atmospheric Sciences

The University of Utah

May 2022

Copyright © James Terry Powell 2023

All Rights Reserved

The University of Utah Graduate School

STATEMENT OF THESIS APPROVAL

The thesis of **James T. Powell**

has been approved by the following supervisory committee members:

John D. Horel	, Chair	Date Approved
W. James Steenburgh	, Member	Date Approved
Lawrence Dunn	, Member	Date Approved

and by **John D. Horel** , Chair/Dean of

the Department/College/School of **Atmospheric Sciences**

and by David B. Kieda, Dean of The Graduate School.

ABSTRACT

Extreme precipitation and flash floods during the summer North American Monsoon (NAM) season have led to extensive property damage and fatalities in the southwestern United States. While many studies have examined extreme precipitation events during the NAM in Arizona and New Mexico, less attention has focused on the NAM's extension into southwestern Utah. This study relates flash flood reports and precipitation to atmospheric moisture content and instability during the 2021 and 2022 active monsoon seasons across southwestern Utah. The utility of operational analyses from the Multi-Radar Multi-Sensor (MRMS) and High-Resolution Rapid Refresh (HRRR) systems of the National Centers for Environmental Prediction is examined for this purpose.

MRMS quantitative precipitation estimates over southwestern Utah during summer depend largely on the areal coverage of the high elevation National Weather Service WSR88-D radar (KICX). Those estimates are generally consistent with the frequency of lightning strikes arising from convective storms and precipitation gauge reports in the region except at extended distances from the radar. A strong relationship is evident between days with heavy precipitation and flash flood reports and days with above average precipitable water (PWAT, PWAT> 1.5 cm) and afternoon convective available potential energy (CAPE, CAPE > 500 J kg^{-1}) estimated from HRRR analyses. These results are established on the basis of statistical summaries over the two seasons as well as specifically for three flash flood cases with differing environmental conditions.

An additional objective of this study is to assess whether 3-h time-lagged ensembles of HRRR forecasts issued either 13-18 or 10-15 h prior to the afternoon period when convection is initiating across the region (18-21 UTC; 12-15 MDT) are useful for

situational awareness of heavy precipitation events. There is no expectation that such forecasts would pinpoint the specific timing or location of heavy precipitation or flash flooding within the region. HRRR ensemble precipitation forecasts at these lead times underestimate substantively the amount of precipitation analyzed by the MRMS. The time-lagged ensembles of HRRR forecasts are skillful for identifying days with heavy precipitation when the HRRR PWAT and CAPE ensemble forecasts are above their two-summer seasonal averages. While the available flash flood reports in the region likely substantively underreport their occurrence, 40 of 56 days with one or more flash flood reports were correctly identified by the "midnight" HRRR ensemble (initialization times from 03-06 UTC) when PWAT and CAPE were above average. The "early morning" HRRR ensemble (initialization times from 6-8 UTC) identified two fewer flash flood days (38). The skill of this relatively simple metric from the HRRR forecasts is comparable to that of the flash flood potential rating developed by the Salt Lake City National Weather Service Forecast Office.

TABLE OF CONTENTS

LIST OF FIGURES

LIST OF TABLES

ACKNOWLEDGEMENTS

Accomplishing this Master's thesis has been one of the most challenging but rewarding things I have ever done. While many people have made this work possible, I will only be able to name a few. First, I would like to thank my chairman/mentor Dr. John Horel for all the guidance given from the undergraduate through the Masters and the many hours spent revising. I hope to be able to represent his teachings well in the field as he is truly a pillar in the science community. I would also like to express my appreciation to my other committee members Dr. Jim Steenburgh and Dr. Larry Dunn or the time spent editing and giving helpful feedback. I thank Jim for the times when he boosted my moral when I came into his office and, I thank Larry for his guidance in teaching me about forecasting in the undergraduate as well as his expert knowledge regarding the North American Monsoon.

I would also like to express my appreciation to Jeff Massey for the many hours mentoring, furthering my connections, and educating me on how to excel in the professional environment. I will owe much of my early career to your guidance and connections you helped me build. I know it will help me for years to come. I also want to express my appreciation for the Salt Lake City National Weather Service Office, especially Darren Van Cleave and Glen Merrill, for the background and data given during the duration of this thesis.

This work was possible thanks to The University of Utah Center for High Performance Computing (CHPC), for the computational hardware and the NOAA/National Weather Service Collaborative Science, Technology, and Applied Research (CSTAR) Program, Award NA20NWS4680046, through which this research is supported.

Lastly but most importantly, I could not have done any of this without the help of my loving wife and advocate Gracie Powell. Through this thesis she has helped me handle my many church duties, overcome the loss of a brother, and given me encouragement to press on while being pregnant with our first child. I will never be able to express in full my gratitude for how much you mean to me, I dedicate this thesis to you.

CHAPTER 1

INTRODUCTION

The summer North American Monsoon (NAM) is responsible for frequent heavy precipitation events that tend to originate along the Mexican cordillera and over the mountain ranges of the Southwestern United States (Douglas et al. 1993; Dunn and Horel 1994a,b; Maddox et al. 1995. Adams and Comrie 1997; Yang et al. 2019; Boos and Pascale 2021). Many studies have looked at the conditions leading to extreme precipitation events associated with the NAM in this region and ways to predict their occurrence (Gutzler et al. 2009; Serra et al. 2016; Risanto et al. 2021). Not surprisingly, the fundamental building blocks for intense convection are necessary for such events to occur: lift, instability, and moisture (Doswell et al. 1996). Afternoon surface heating of elevated terrain (Figure 1.1) can provide the orographic lift that aids thunderstorm development. Mazon et al. (2016) classified extreme NAM weather events primarily in Arizona based on atmospheric instability, precipitable water vapor, and upper level conditions. Figure 1.2 illustrates the precipitation during such events is largest over the higher terrain of the Colorado Plateau, including over southern Utah.

Smith et al. (2019) provide a detailed climatological evaluation of the seasonality and locations of thunderstorms in northern Arizona and southern Utah motivated by the flash flood event in Hilldale UT on 14 September 2015 that resulted in 20 fatalities. They

note on the basis of lightning, radar, and streamflow records that while the details regarding the occurrence and track of NAM thunderstorms vary widely across the Colorado Plateau, summer convective storms tend to move from southwest to northeast modulated by the underlying terrain and synoptic/mesoscale setting. They also found frequent lightning begins in June and peaks during July – September. Some flash floods, such as that in Hilldale UT, result from short duration, highly intense, and very localized convection near canyon/basin outlets that are embedded within an ambient environment of enhanced water vapor transport by the prevailing flow.

Flash floods are defined by the National Weather Service (NWS) as "Flooding that begins within 6 hours, and often within 3 hours, of the heavy rainfall (or other cause)" (NWS website). Two key factors determine whether an event's precipitation will lead to flash flooding in southern Utah: precipitation intensity and the location where the precipitation lands. As noted by Smith et al. (2019), flash flood water volumes in Colorado Plateau watersheds are not well related to basin scale, as is often the case in other regions of the United States where flash flooding may result from heavy precipitation falling synchronously across large basins. Rather, the flash flood response is tied to the spatial scale of thunderstorms (10-50 km^2) and their proximity to slot canyons, channel narrows, and basin outlets.

Quantifying the total number of flash flood events in Utah is difficult since they often happen in remote locations. To identify as many flash flood periods as possible, this study uses the storm report data base available from the National Center for Environmental Information (NCEI 2022) and summaries of NWS Flash Flood Warnings (Figures 1.3 and 1.4, respectively). Over one hundred flash floods were reported during summer 2013 while

the next most active flash flood seasons were the 2021 and 2022 seasons during which over 14 million dollars in property damage occurred in southwestern Utah. Forecasting flash floods at short lead times (<6 h) often leads to the issuance of NWS flash flood warnings and relies on careful evaluation by forecasters of model guidance focusing on interpretation of satellite and radar imagery of convective environments. The NWS offices in Salt Lake City and Grand Junction issued the first and third highest numbers of flash flood warnings (i.e., flash flood conditions occurring or imminent) during 2021 and 2022 within the 1996-2022 period.

Providing forecasts for the potential for organized convection and heavy precipitation that might lead to flash floods within areas of complex terrain at lead times longer than 6 h requires greater reliance on numerical model output from operational convection allowing models, such as the High Resolution Rapid Refresh (HRRR, Smith et al. 2008; Sun et al. 2014; Blaylock and Horel 2020; Dowell et al. 2022). For longer lead times, the NWS issues flash flood watches. In order to avoid too many watches during the monsoon season, the Salt Lake City NWS office issues them only on days when multiple basins are likely to be impacted, so fewer are made as seen in Figure 1.5. In addition, they issue flash flood potential forecasts for 11 government entities responsible for public safety across Utah. Flash flood potential forecasts are provided in southwestern Utah for Zion National Park, Bryce National Park, Capitol Reef National Park, and Grand Staircase-Escalante National Monument.

This study focuses on the meteorological conditions during the 2021 and 2022 summer monsoon seasons when convection was more extensive in southwestern Utah than during other recent summers. This study defines the monsoon season as falling between 15

June and 30 September. The area of interest is limited to southwestern Utah, which encompasses multiple plateaus and distinct mountain ranges as well as the Virgin River and other smaller basins (Figure 1.1). A significant consideration for focusing on this region is the higher risk for injuries and fatalities due to flash floods in slot canyons within national parks and monuments (Zion, Bryce, Capitol Reef, Grand Staircase-Escalante) in this region as well as public safety and property damage in the populated centers located near stream outlets. In addition, the availability of the Cedar City NWS radar (see Figure 1.1) within this region provides better estimation of convective activity and precipitation than is available for other parts of the state influenced frequently by the NAM.

The objective of this study is to first estimate the occurrence of widespread and heavy precipitation events during the two summer seasons in southwestern Utah. Many of these heavy precipitation episodes were accompanied by reports of flash floods. Then, the interplay is studied between location and terrain and the large-scale conditions (moisture availability and instability) analyzed by the HRRR leading to heavy precipitation across southwestern Utah. Day-to-day variability during the two summers of precipitation, flash floods, moisture availability, and instability are contrasted. Case studies of three significant flash flood days are presented to show in more detail the conditions often present during these heavy precipitation events. Finally, the skill of specific HRRR forecasts are examined at lead times from 6-18 h as a possible aid for situational awareness of the large-scale summer-afternoon conditions commonly observed during heavy precipitation events. One approach evaluated relies on 3-h time-lagged ensembles of HRRR forecasts issued either 13-18 or 10-15 h prior to the afternoon period when convection is initiating across the region (18-21 UTC; 12-15 MDT). There is no expectation that HRRR forecasts at these

lead times will provide an indication of the specific regions where heavy precipitation may fall or flash floods may occur in specific canyon or basins.

Questions addressed in this study are:

1. What are the spatial and temporal variations in precipitation and lightning during the 2021 and 2022 summer seasons?
2. What are the prevailing large-scale conditions commonly observed during heavy precipitation episodes across southwestern Utah?
3. To what extent do HRRR forecasts of large-scale conditions at lead times of 6-18 h have the potential to provide situational awareness of increased likelihood of heavy precipitation during summer afternoons?

The data and model used in this research are discussed in Chapter 2. Chapter 3 relies on observations and HRRR analyses to estimate the spatial and temporal variations in precipitation across southwestern Utah during the two summers. Three case studies of days when flash floods occurred in different regions of southwestern Utah are also presented. Chapter 4 examines the skill of F06-F18 HRRR model forecasts for moisture availability, stability, and precipitation during both seasons as well as for the three case studies. Chapter 5 provides a concluding discussion including suggestions on how this approach might be applicable for examining future trends in the intensity of the NAM across southwestern Utah.

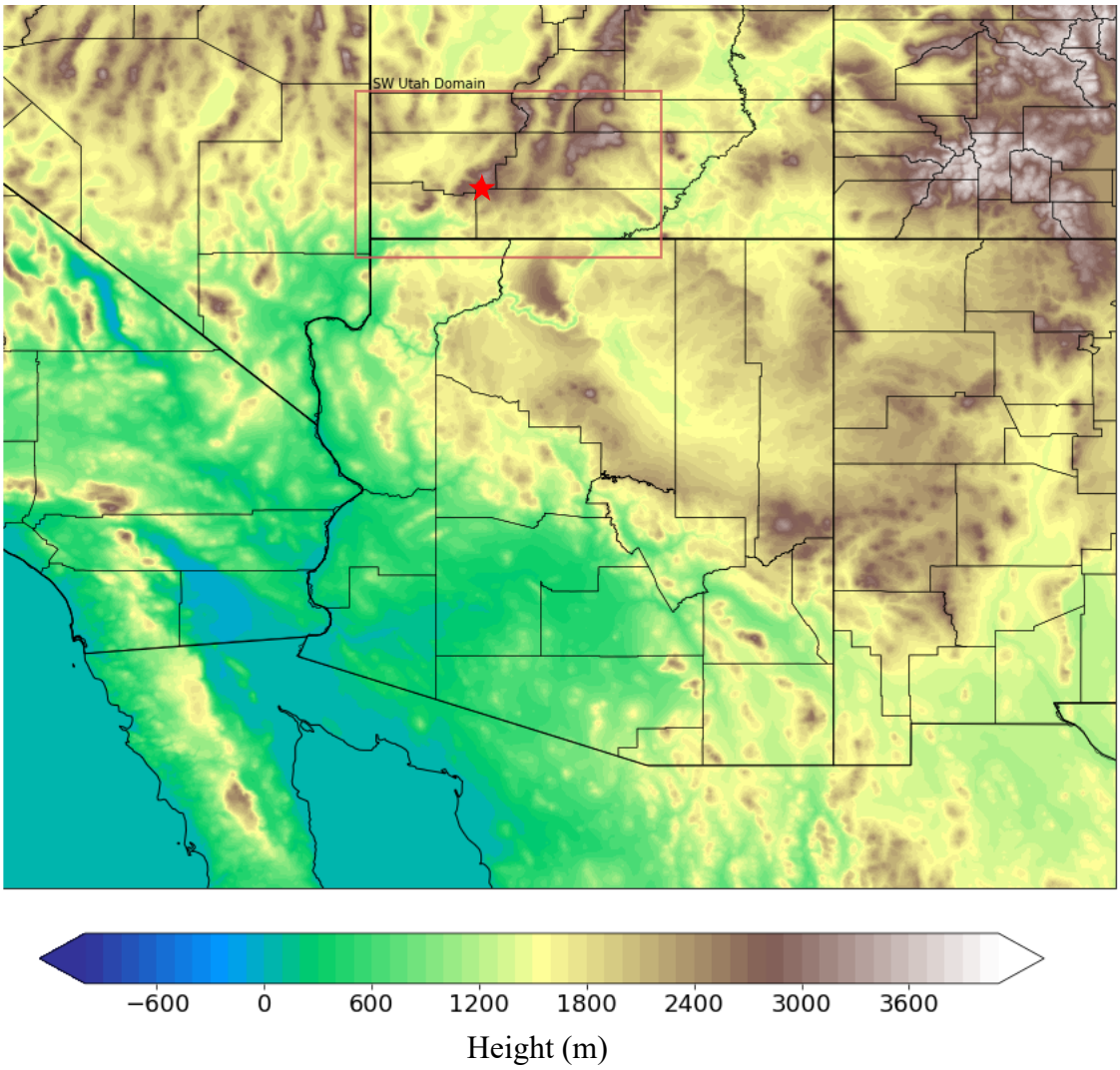

Figure 1.1: Topography (m) of the southwestern United States at 3 km horizontal resolution. Thin black lines denote county outlines while the red rectangle highlights the area of interest for this study. The Red star denotes the location of the Cedar City Radar (KICX) on the Markagunt plateau.

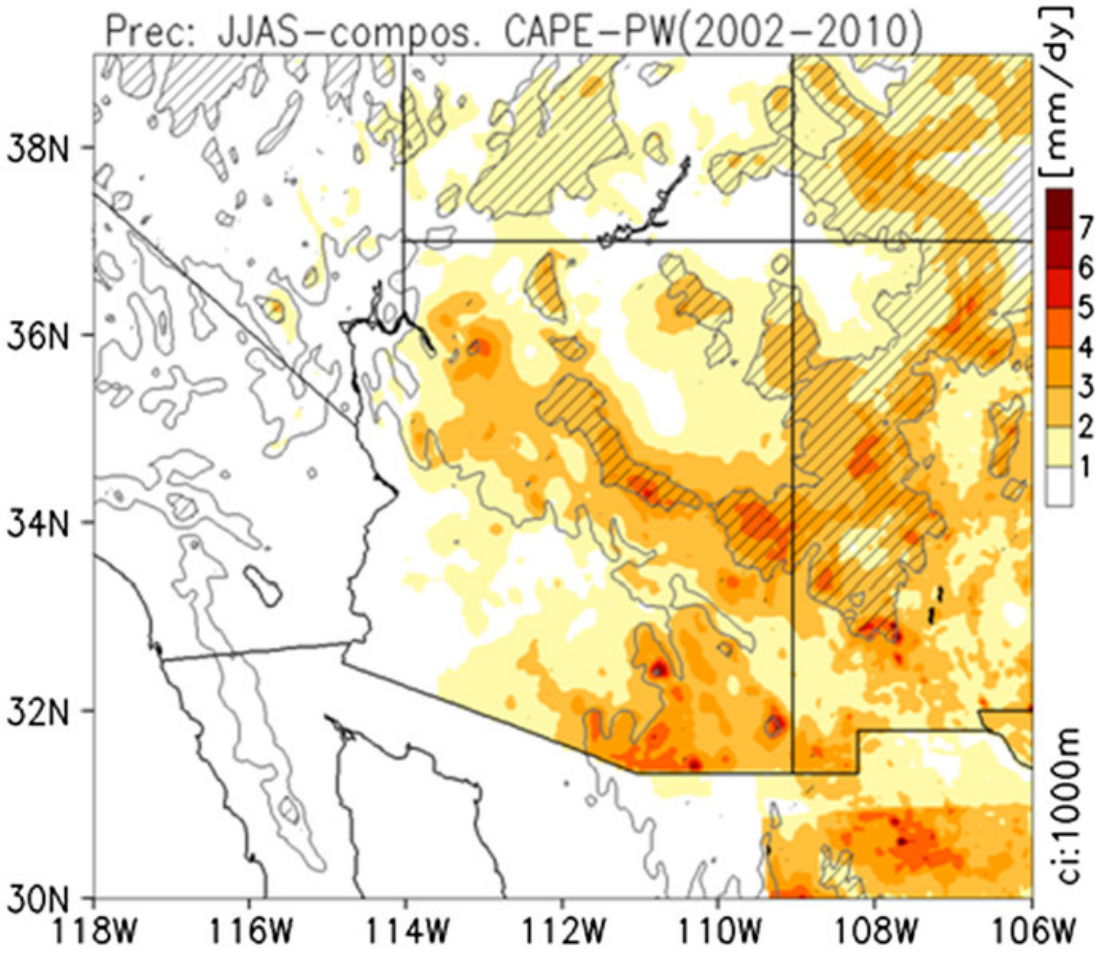

Figure 1.2: Average precipitation (mm/day) from the stage IV product for thermodynamically favorable severe weather events during 2002–2010. Terrain elevation is indicated as contours at intervals of 1000 m. Regions over 2000 m in elevation are shown in hatching. The figure is adapted from Mazon et al. (2016).

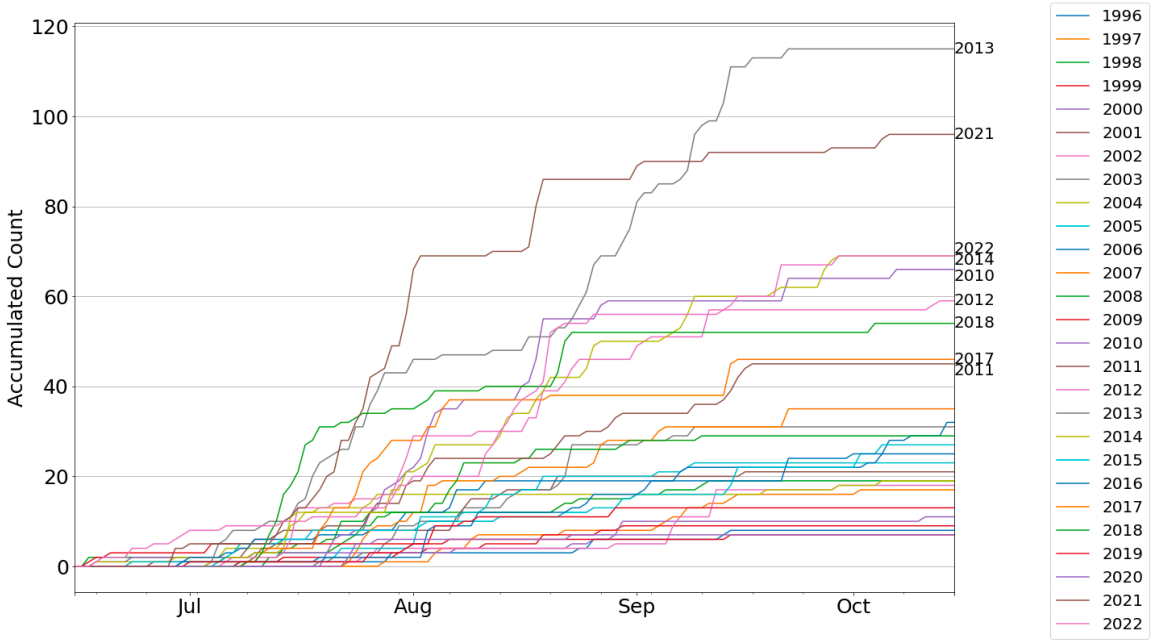

Figure 1.3: Accumulated counts of summer Utah flash flood storm reports from 1996 to 2022. Source: National Center for Environmental Information (NCEI 2022).

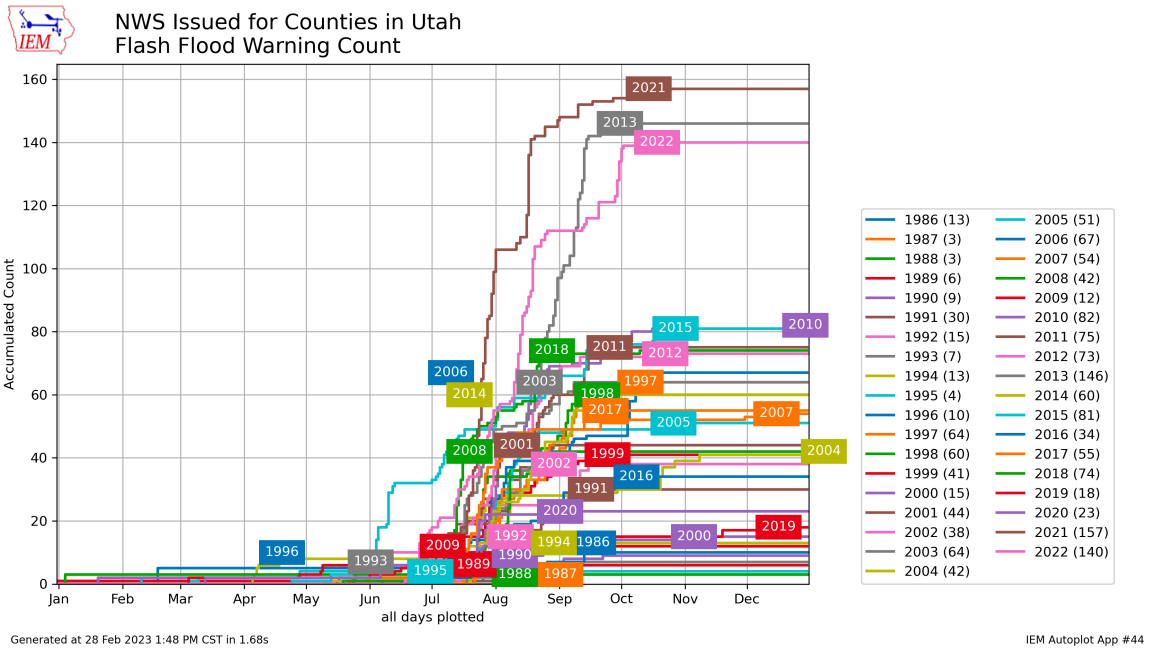

Figure 1.4: Accumulated counts during the year of NWS flash flood warnings issued within Utah from 1986 to 2022. Source: Iowa State University Automated Data Plotter (Iowa State University 2023)

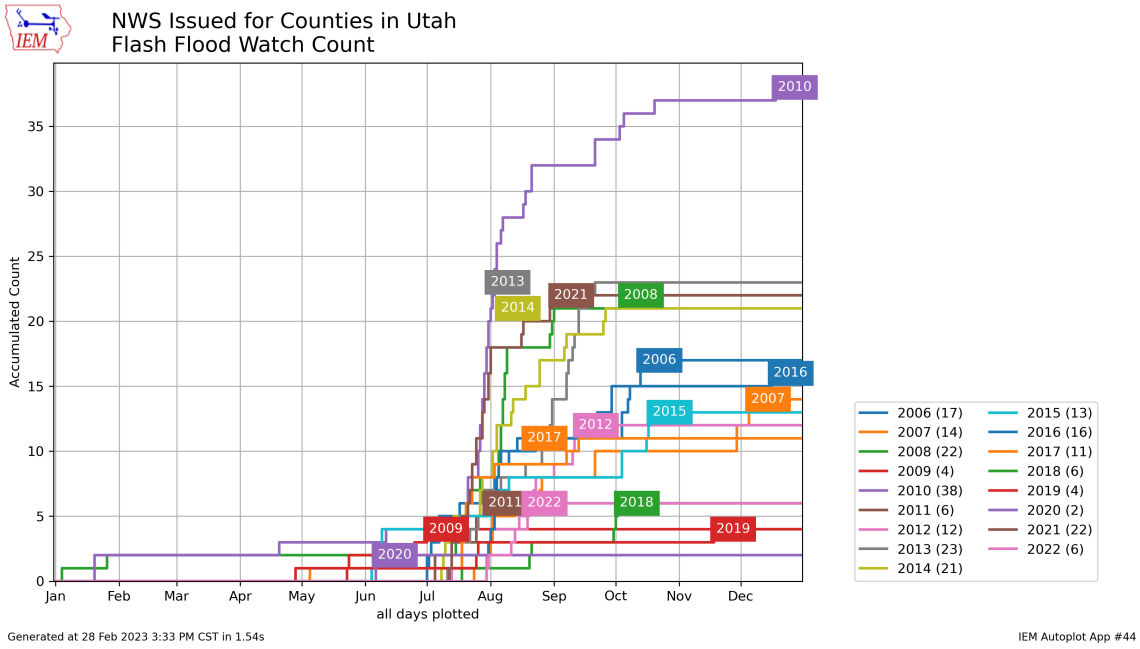

Figure 1.5: Accumulated counts during the year of NWS flash flood watches issued within Utah from 1986 to 2022. Source: Iowa State University Automated Data Plotter (Iowa State University 2023)

CHAPTER 2

DATA AND MODELS

2.1 Precipitation, Radar, Lightning

Although providing limited coverage across southwestern Utah, precipitation observations from stations in the NWS and Remote Automated Weather Stations (RAWS) networks are used in this study for seasonal totals and flash flood case studies. Precipitation observations from other networks (e.g., Hydrological Meteorological Data System) were examined for the case studies to help fill in observing gaps. The precipitation observations were accessed using the API services of Synoptic Data PBC.

Deep convection over the southwestern Utah domain of interest in this study is largely detected by the Cedar City WSR-88D Doppler RADAR (KICX). This radar is located 3230 meters above sea level near the southwestern edge of the Markagunt plateau (Figure 1.1). Due to its high elevation, 0.2^{o} degree elevation scans are made to capture conditions as much as possible over the surrounding desert regions at elevations typically between 1000-2000 m.

Widespread coverage of vigorous convection containing lightning is made possible from the ground-based National Lightning Detection Network (NLDN, Murphy et al. 2021). The Flash Energy Density (FED) product provided by the Multi-Radar Multi-

Sensor (MRMS) system, based upon the NLDN is used in this study. FED is an estimate of the number of cloud to ground flashes per km^2 during each 30 minute period.

2.2 Multi-Radar Multi-Sensor Quantitative Precipitation Estimates

The MRMS is an operational system of the National Centers for Environmental Prediction (NCEP) for estimating precipitation from radar, rain gauge, satellite, lightning, and numerical weather model data (Zhang et al. 2016; El Saadani et al. 2018; Sharif et al. 2020, Martinaitis et al. 2021). The MRMS Quantitative Precipitation Estimate (QPE) Pass II product for each hour and for each km^2 along with FED and other diagnostic fields are accessed from Iowa State University's Iowa Environmental Mesonet archive (Iowa State University 2023) .

Radar precipitation estimates are the primary input for MRMS QPE. As shown in Figure 2.1, MRMS processing involves quality control applied to radar data (e.g., accounting for beam blockage and non-precipitation echoes) and then computing a radar quality index for each location (Martinaitis et al. 2021). If an area has adequate radar quality, radar estimates may be adjusted using weighted corrections based on precipitation gauge data from trusted networks to then yield the final QPE. If the radar quality is poor during convective situations, then precipitation estimates may be adjusted based on gridded estimates of precipitation from the HRRR model.

2.3 High-Resolution Rapid Refresh Model

The HRRR is a convection allowing, short-range forecast model with 3km horizontal grid spacing run operationally every hour by the NCEP for the CONUS region

(Dowell et al. 2022). Forecasts at lead times out to 18 h are available every hour with lead times extended out to 48 h at 00, 06, 12, and 18 UTC. The HRRR benefits from advanced data assimilation techniques incorporating standard data observations (rawinsonde, aircraft, GPS precipitable water, etc.) and also includes 3-D radar reflectivity data from the MRMS and lightning data from the NLDN (Hu et al. 2017; James and Benjamin 2017; Dowell et al. 2022). Access to the high-resolution forecast model output in grib2 format is currently available through Amazon Web Services and Google's Cloud Platform (Dowell et al. 2022). This study relies on HRRR version 4 that was deployed 2 Dec 2020. Select model analysis (F00) and forecast (F01-F18) fields are retrieved in Zarr format from Amazon Web Services (Gowan et al. 2022). Supported by Amazon's Sustainability Data Initiative, the Zarr files are created in order to split the CONUS into 96 compressed chunks, allowing the downloading of data more efficiently for smaller domains (Gowan et al. 2022).

HRRR model F00 analyses and F06-F18 forecasts of deep moisture (precipitable water, PWAT) and instability (surface-based Convective Available Potential Energy, CAPE) are relied upon extensively in this study as a means to assess conditions favorable for widespread convection across southwestern Utah. Mazon et al. (2016) and Yang et al. (2019) used similar metrics to study the NAM in Arizona but relied primarily upon rawinsonde observations from Tucson. Surface based CAPE is assumed to be an adequate metric for estimating the potential for convective instability over elevated terrain due to the limited convective inhibition likely in these locations during summer afternoons. Several other CAPE parameters available from the HRRR were examined and it was found that

surface-based CAPE adequately represented the potential for afternoon convection in this region.

HRRR QPE at 06-18 h lead times is compared to MRMS QPE and NLDN FED as a means to assess the extent to which those forecasts might be useful for situational awareness for the likelihood of widespread precipitation across southwestern Utah. The forecast skill of short range (F01-F05) QPE HRRR forecasts is not examined since the HRRR initialization procedures rely in part on MRMS and NLDN products that are used for validation.

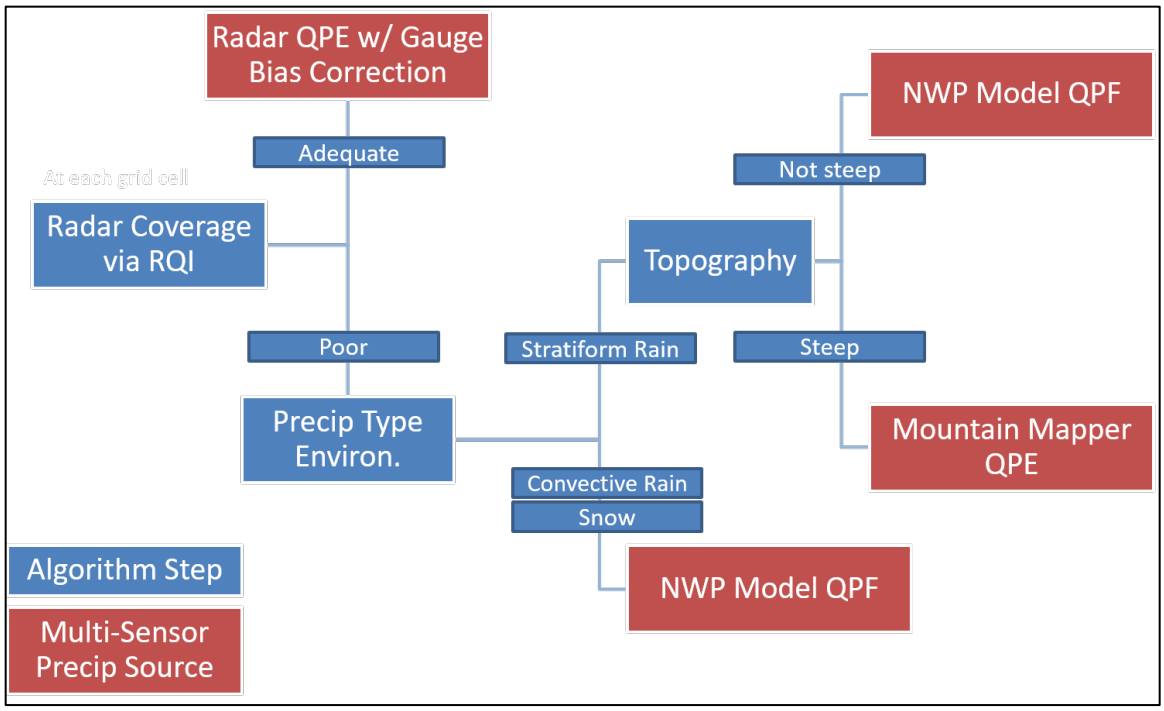

Figure 2.1: MRMS Decision tree for QPE estimation (MRMS Decision Tree 2022).

CHAPTER 3

2021 & 2022 MONSOON SEASONS

Characteristics of the typical conditions across southwestern Utah during both monsoon seasons are presented in the first subsection. A more detailed evaluation of the conditions during three days with heavy precipitation and multiple flash floods follow.

3.1 Seasonal Analyses

The large-scale conditions favorable for heavy precipitation events during the NAM are well established: deep moisture and instability are necessary for convection to break out during the afternoon and early evening over elevated terrain (Douglas et al. 1993; Dunn and Horel 1994ab; Adams and Comrie 1997; Adams and Souza 2009; Mazon et al. 2016; Smith et al. 2019; Yang et al. 2019; Blaylock and Horel 2020). Figure 3.1 illustrates the day-to-day evolution of moisture availability (PWAT) and instability (CAPE) averaged over southwestern Utah during the 2021 and 2022 summers. PWAT in Figure 3.1 represents the HRRR F00 precipitable water values averaged over ~10,000 grid points and over every hour of the day minus a reference value of 1.5 cm. CAPE in Figure 3.1 is the average of the daily maxima at each grid point of HRRR F00 surface-based CAPE values averaged over all grid points minus a reference value of 500 J kg^{-1}. The choices for these reference values were based roughly on the average of those quantities over the two summers (1.65 cm and 498 J kg^{-1}, respectively) and, as will be discussed later, approximate

thresholds based on the days when flash flood reports were common. Each summer had a sustained period of monsoonal moisture and instability (13 July – 2 August 2021 and 12 July– 26 August 2022) with occasional short episodes at later times.

The averages over southwestern Utah of daily MRMS QPE totals and NLDN FED are shown in Figure 3.2. Comparing Figures 3.1 and 3.2, periods of high moisture and instability over southwestern Utah tend to be associated with widespread thunderstorms and precipitation. Higher intensity outbreaks of lightning are evident during summer 2021 than 2022, for example. (FED values of .05 flashes km^{-2} correspond to over 3,000 flashes across the ~64,000 grid points in the domain).

For both NAM seasons the spatial distribution of average PWAT and average daily maximum surface CAPE are shown in Figures 3.3-3.4 for Utah and the surrounding areas from the HRRR analyses (F00) for the local day (MDT). PWAT decreases as the depth of the atmospheric column over elevated terrain decreases. The average maximum daily CAPE across both seasons shows lower CAPE values in northern Utah compared to southern Utah except for the artificially high values over surface water bodies, such as the Great Salt Lake. It should be noted that the CAPE values in Figure 3.4 over southwestern Utah may underestimate actual conditions. Prior work with earlier versions of the HRRR found the analyses had a slight stable bias compared to estimates from rawinsondes (Evans et al. 2018).

For reference, Figures 3.5-3.7 illustrate the spatial variability of rainfall and lightning flashes averaged over all days and both NAM seasons across Utah and adjacent areas. Comparing Figures 3.5 and 3.6 with Figure 1.2, Mazon et al. (2016) highlighted that rainfall totals in southern Utah tended to be substantively lower than those in northern

Arizona. As expected, all of the mountain ranges and plateaus of southwestern Utah exhibit higher MRMS QPE and FED than their surrounding deserts (e.g., Pine Valley Mountains and Markagunt, Paunsaugunt, Kairparowits, and Aquarius Plateaus) yet some of the isolated ranges in central and eastern Utah have very high FED and higher gauge totals but low QPE (Henry and Abajo Mountains, for example). The lack of radar coverage for these mountain ranges likely impacts the MRMS QPE estimates. The average daily FED over the past two years (Figure 3.7) is similar to the 1991-2016 lightning climatology done by Smith et al. (2019).

Focusing on southwestern Utah, the diurnal cycles of MRMS QPE and NLDN FED in southwestern Utah are examined in Figures 3.8-3.11. Figure 3.8 illustrates that rainfall begins to increase from around solar noon (13 MDT) and peaks during the 6 h period from 14 - 20 MDT. Evident from Figure 3.9 is that the precipitation initiates typically over the high terrain around solar noon and then develops substantively during late afternoon before weakening as solar forcing weakens.

As expected when looking at 3 hour bins, the diurnal cycle in NLDN FED (Figure 3.10) is consistent with that in MRMS QPE (Figure 3.8) with the most frequent occurrence of lightning during late afternoon (14-17 MDT). FED begins near higher elevations in the afternoon hours (Figure 3.10). Evening lightning is more common at lower elevations, e.g., along the Arizona and Utah border that are likely formed in Arizona and moving from southwest to northeast in the typical monsoonal flow (Smith et al. 2019).

Although the spatial and temporal variability of PWAT during the day is weak (not shown), Figure 3.12 illustrates the rapid increase of surface-based CAPE during the morning hours that peaks from 12-15 MDT. The shaded area in Figure 3.12 highlights the

period when CAPE reaches its maximum prior to the peak in precipitation typically from 15-17 MDT.

Figure 3.13 follows the work of Mazon et al. (2016) and Yang et al. (2019) for relating PWAT and CAPE values to the occurrence of extreme precipitation. While those studies relied on twice-daily Tucson rawinsonde data to estimate stability and moisture for the entire state of Arizona, hourly HRRR analyses at 3 km resolution across the southwestern Utah domain are available for that purpose here. The figure relates the environmental conditions of PWAT and CAPE to MRMS daily QPE in southwestern Utah during the two summers. Days with very limited rainfall (domain averaged rainfall < 0.01 cm (none of which had flash flood reports) are omitted. The CAPE values in Figure 3.13 represent domain averages of the maximum CAPE at every grid point during the 12-15 MDT period while the PWAT values are the domain averages of all the PWAT values during that time period. The size and color of each dot denotes the accumulated precipitation for that entire day, which predominantly falls between 11-23 MDT (see Figure 3.6).

MRMS QPE amounts tend to be low either if PWAT averaged over southwestern Utah is less than 1.5 cm or maximum CAPE is less than 300 J kg^{-1}. As PWAT and CAPE increase, then QPE increases commensurately. A total of 81 and 48 NCEI flash flood reports were available in southwestern Utah during the 2021 and 2022 seasons, respectively. Plus signs in Figure 3.13 denote those days when at least one NCEI flash flood storm report was recorded. Figure 3.13 suggests that widespread precipitation and flash flood reports were most common when PWAT > 1.5 cm and CAPE > ~500 J kg^{-1}, which contributed to the decision to subtract those approximate two-season average values

from the time series in Figure 3.1. Smith et al (2019) also found that lightning activity increased in the region when PWAT was greater than 1.5 cm and grew substantively after 2.0 cm. As summarized in Table 3.1, areal precipitation was limited and only 2 days with flash flood reports occurred when PWAT was less than 1.5 cm. The propensity is evident in Table 3.1 for heavy precipitation and flash floods to occur when the daily values exceed both the 1.5 cm PWAT and 500 J kg^{-1} CAPE thresholds. For example, 70% of days reported at least one flash flood when both of these thresholds were exceeded while the other 30% did not result in flash floods yet the average precipitation was high.

A quasi-linear increase in areal precipitation and flash flood reports with PWAT and CAPE is evident in Figure 3.13. A notable exception to this general relationship is evident by the relatively low CAPE on 19 Aug 2021. A trough digging across the region on the 17 and 18 of Aug 2021 led to heavy precipitation that continued overnight until the trough passage after which afternoon PWAT and CAPE dropped to the values highlighted by Point A in Figure 3.13. The 4 days surrounding Point B in Figure 3.13 exhibit much higher CAPE than might have been expected based on the available moisture. These days were two day events (17-18 Aug 2021 and 20-21 Aug 2022) associated with slow moving upper level troughs.

Also highlighted in Figure 3.13 are three days (29 June 2021, 26 July 2021, and 23 June 2022) when flash floods caused considerable damage in Springdale, Cedar City, and Capitol Reef National Park, respectively. The following case studies are provided to gain more insight into the meteorological conditions leading to those three events.

3.2 Springdale Flash Flood (29 June 2021)

During 29 June 2021, monsoonal moisture coupled with afternoon heating led to thunderstorm development that resulted in four flash flood reports with their locations marked in Figure 3.14 by red dots. The NCEI storm reports for those four events are listed in Table 3.2. The Hilldale flash flood (point B) occurred in the same Water Canyon drainage as the 2015 event examined by Smith et al. (2019). The extensive damage done to the western entrance to Zion National Park and nearby roads and commercial buildings in Springdale, UT received national media attention (Point C, e.g. CBS News, 2021). When averaged over the southwestern Utah domain, the PWAT and CAPE in southwestern Utah were approximately 1.75 cm and 650 J kg^{-1}, respectively (Figure 3.13). Ridging aloft to the north of Utah led to a sharp meridional gradient in PWAT across western Utah helping to define the northern boundary of the region affected by the monsoon during this afternoon (Figure 3.15). A similar sharp CAPE meridional gradient is evident across western Utah with values in excess of 800 J kg^{-1} during the afternoon over southwestern Utah (Figure 3.16). Considerable veering vertical wind shear over southwestern Utah was analyzed by the HRRR during this afternoon with southeasterly flow at 700 hPa (not shown), northerly flows at 500 hPa (Figure 3.17) and northeasterly winds at 250 hPa (not shown).

The GOES-West satellite image in Figure 3.18 near 20 UTC (2 PM MDT) highlights many thunderstorms across southwestern Utah that, based on the series of such images during the afternoon, were propagating roughly from north to south driven by the prevailing midtropospheric flow. The 1-hour maximum composite reflectivity from the Cedar City radar (KICX) shown in Figure 3.19 for the hour prior to the satellite image in Figure 3.18 suggests that individual cells developing within the north-south oriented

convective line tended to move from northeast to southwest into the prevailing inflow in the lower troposphere.

Hourly precipitation rates during the afternoon at RAWS and NWS stations and from the MRMS analyses are shown in Figures 3.20 and 3.21, respectively. Two weather stations near the extensive damage observed from the flash flooding near the mouth of Zion Canyon and Springdale recorded total rainfall between 1.8 - 3.0 cm (0.7 in – 1.2 in) of precipitation in four hours (only one appears in Figure 3.18 since the other is part of the Hydrometeorological Automated Data System network). The resulting flash flood resulted from multiple thunderstorm cells that transited across and down the very narrow drainage of the North Fork of the Virgin River within ZNP during the four hours of the event (18-22 UTC).

Heavy precipitation is evident as well during this afternoon over the Pine Valley mountains and across the Markagunt Plateau (Figure 3.21). Figure 3.22 shows the average hourly FED during this afternoon. The flashes associated with the cells transiting from north to south down the drainage of the North Fork of the Virgin River are evident as well as those resulting from many other thunderstorm cells across southwestern Utah in other drainages. Substantial lightning upstream of the city of Boulder in the Boulder Creek drainage (Point A) with less lightning evident in the narrow Buckskin Gulch slot canyon (Point D). This case shows that high precipitating storms with over 60 dBz values can form in southwestern Utah while having average PWAT and CAPE values (1.75 cm and 650 J kg^{-1}, respectively)

3.3 Cedar City Flash Flood (26 July 2021)

As shown in Figure 3.2, heavy precipitation and lightning were frequent across southwestern Utah with over 17 flash floods reported during the week preceding 26 July 2021. The most devasting property damage due to flash flooding during the two years of this study occurred on 26 July 2021 primarily near Cedar City, Utah. A total of 7 flash flood reports were made on this day or ~9% of all flash floods reported in 2021 (see their locations in Figure 3.23 and details in Table 3.3).

The PWAT analyzed during this afternoon from 18 UTC 26 July to 00 UTC 27 July (18-0z) is shown in Figure 3.24. The moisture transport from the south into western Arizona and Utah is more extensive in this case than the previous case with larger CAPE value across southwestern Utah as well (Figure 3.25). This corresponded with higher CAPE values for much of the same area with many values above 2000 J kg^{-1} in the HRRR analysis. When averaged over the southwestern Utah, domain the PWAT and CAPE in southwestern Utah were approximately 2.7 cm and 900 J kg^{-1}, respectively (Figure 3.13).

In contrast to the distinctive veering vertical wind profile in the first case, the prevailing flow in this case was deep southeasterly winds from 700 to 250 hPa as evident at 500 hPa (Figure 3.26). Animations of GOES-West satellite imagery and KICX composite radar reflectivity during this afternoon confirmed the prevailing southeast to northwest progression of thunderstorm cells during the afternoon as shown by the visible image near 20 UTC (Figure 3.27) and composite radar reflectivity during the preceding hour (Figure 3.28).

Average hourly precipitation rates are shown from RAWS and NWS weather stations in Figure 3.29 and the MRMS in Figure 3.30. While modest amounts of rainfall

were likely observed across many areas of southwestern Utah during this afternoon, heavy amounts were highly localized, most notably unofficial reports of over 5 cm (2 in) over portions of southwestern Cedar City as well as over the small drainages along the steep western rim of the Markagunt Plateau. The initial report of flooding across the Interstate southwest of Cedar City was associated with a strong cell (maximum composite reflectivity > ~65 dBz) from around 20-21 UTC (2-3 MDT) that contributed roughly 3.8 cm (1.5 in) of the precipitation reported by the aforementioned station. The channeling of much of this precipitation went directly into residential and commercial areas of Cedar City, a town with a population of 37,000.

Figure 3.31 shows the average hourly FED during 18-0z with many areas showing extensive lightning across southwestern Utah including frequent lightning over areas over and near Cedar City. This afternoon had more strong convective storms and flash flood storm reports than the Springdale flash flood case. Frequent lightning occurred near all of the locations reporting flash flooding that afternoon. This case highlights that with high areally-averaged PWAT and CAPE values (2.7 cm and 900 J kg^{-1}, respectively) many intense storms formed in southwestern Utah leading to many flash floods.

3.4 Capitol Reef Flash Flood (23 June 2022)

Much lower average PWAT and CAPE values (~1.6 cm and 550 J kg^{-1}, respectively) were observed across southwestern Utah on 23 June 2022 than during the previous two flash flood cases (Figure 3.13). These lower values corresponded with a relatively weak monsoonal moisture surge into southern Utah. Even with the weak signature, this led to a flash flood that would destroy over a half dozen vehicles with ~60

persons being stranded and many requiring helicopter evacuations (Table 3.4). Fortunately, no fatalities resulted and a video documented one family's experience escaping from the flood. The location of the Capitol Reef flood is shown in Figure 3.32. Details of the reports are provided in Table 3.4. The other flash flood report's location does not show on the figure as it is outside the boundary box further downstream along the Fremont River (locally referenced as Bull Creek in Table 3.4).

Figures 3.33 and 3.34 illustrate the plume of higher PWAT and CAPE extending northward across central Utah in this case compared to the north-south gradients in those fields evident in the previous two cases. Unidirectional southwesterly flow over southwestern Utah was analyzed upstream of the midtropospheric cyclonic circulation evident in Nevada during this afternoon from 700 hPa to 250 hPa as evident in the 500 hPa winds (Figure 3.35). Animations of satellite and radar imagery confirm the tendency for thunderstorm cells during this event to form earlier in the day than the other two cases and to track northeastward (Figures 3.36 and 3.37). Hourly precipitation rates evident from station and MRMS were weaker during this event (see Figures 3.38 and 3.39). One citizen science rain gauge near Capitol Gorge reported over 2.0 cm in three hours during this event (not shown). The large number of lightning strikes near Capitol Reef (Figure 3.40) is a better indicator of the intensity of the localized thunderstorm than that afforded by the MRMS precipitation estimates that rely heavily on the distant KICX radar.

A heavy precipitating storm formed and brought devastation to Capitol Gorge. This case resulted from average PWAT and CAPE values (~1.6 cm and 550 J kg^{-1}, respectively) that were near the two season averages, similar to the Springdale flash flood case. The Capitol Reef case, like all the other cases, had over 60 dBz values making them above the

90th percentile of flash flood producing storms done by Smith et al. (2019) even without the presence of significant wind shear.

3.5 Summary

The results presented in this chapter suggest that the MRMS precipitation adequately captures the day-to-day variation in precipitation across southwestern Utah except over high terrain at distances far from the radar. The daily precipitation and lightning indices presented in Figure 3.2 may be an adequate metric for studies over a larger sample of prior years and for use to monitor future NAM conditions across southwestern Utah. Daily mean PWAT and daily maximum surface CAPE (Figure 3.1) may also be useful proxies for monitoring the types of widespread conditions associated with heavy precipitation and flash floods in the area. When PWAT and CAPE both exceed their approximate two-summer averages, there is a greater likelihood for heavier precipitation and flash flooding to occur across the region (Figure 3.9). The three case studies in Sections 3.2-3.4 highlight differing vertical wind shear profiles that may influence the type and propagation of convection during those days within the generally moist and unstable environment, although differing PWAT and CAPE environments did have a dramatic effect on the number of flash floods reported on each day.

	CAPE < 500 J kg^{-1}				**CAPE > 500 J kg^{-1}**			
	NFF		*FF*		*NFF*		*FF*	
	days	*PPT*	*days*	*PPT*	*days*	*PPT*	*days*	*PPT*
PWAT < 1.5 cm	87	0.01	1	0.01	0	0	1	0.05
PWAT > 1.5 cm	53	0.05	8	0.3	20	0.22	46	0.34

Table 3.1: Counts of days with no flash floods (NFF) and days with flash floods (FF) across southwestern Utah binned relative to CAPE and PWAT thresholds. Average daily precipitation (PPT, cm) across southwestern Utah during these sets of days also shown.

Fig 3.14 Identifier	Location	Report Time (MDT)	Source	Event Narrative
A	BOULDER	1430	Park / Forest Service	Flash flooding was observed at the state Route 12 overpass of the Escalante River. Additional reports of flash flooding were observed upstream, including in Escalante River Canyon and at Death Hollow. The Escalante River gauge climbed from no flow to 400 CFS.
B	HILLDALE	1431	Fire Department / Rescue	Hildale Fire Department personnel reported multiple road closures in town, multiple flooded residences, and several stranded motorists due to flash flooding in the area.
C	SPRINGDALE	1447	Park / Forest Service	Significant flash flooding occurred from the entrance of Zion National Park, across the eastern portions of the park. State Route 9 within the park closed due to flooding and debris on the roadway.
D	BUCKSKIN GULCH	1700	Park / Forest Service	Widespread flash flooding occurred from Wire Pass to the mouth of Buckskin Gulch. Several hikers were stranded between Wire Pass and the entrance to Buckskin Gulch, with muddy water levels rising to waist deep. Another group was trapped within Buckskin Gulch overnight due to Flash Flooding. The group was able to climb onto narrow ledges above the flood waters, where they remained overnight, then evacuated the next day.

Table 3.2: NCEI flash flood storm reports on 29 June 2021.

Fig 3.23 Identifier	Location	Report Time (MDT)	Source	Event Narrative
A	SPRINGDALE	1250	Park / Forest Service	A significant flash flood wave in Pine Creek was reported by Zion National Park staff.
B	CEDAR CITY	1342	Department of Highways	Water flowed across many roadways in Cedar City, including across Interstate 15 near milepost 59.
C	ESCALANTE	1430	Newspaper	A video showed flash flooding at the confluence of Birch and North Creeks into the Escalante River.
D	ESCALANTE MUNI ARPT	1430	Official NWS Observations	The Escalante River gauge near Escalante indicated a rise from 3 CFS to 1060 CFS, a rise of 4 feet.
E	ADAIRVILLE	1900	Park / Forest Service	Grand Staircase-Escalante National Monument officials reported that significant damage was sustained on House Rock Road near Wire Pass due to flash flooding.
F	GLEN CANYON	2042	Storm Chaser	A received video showed a flood wave with significant debris moving through Big Water, UT.
G	ADAIRVILLE	2215	Official NWS Observations	The Paria - Kanab gauge on the Paria River indicated a rise from 23 CFS to 1450 CFS with the primary flood wave. The time above 1000 CFS was from 2315 MDT to 0130 MDT.

Table 3.3: NCEI flash flood storm reports on 26 July 2021.

Fig 3.14 Identifier	Begin Location	Begin Time	Source	Event Narrative
A	FRUITA	1130	Park / Forest Service	Capitol Reef National Park reported SR-24 was impassable near milepost 83 due to flood waters from grand wash. Scenic drive was also closed, and the parking lot at the Grand Wash trailhead flooded. The flooding stranded nearly 60 people, and trapped or washed away several vehicles. Numerous water rescues were conducted by Utah Department of Public Safety helicopter operations to bring people to safety.
B	HANKSVILLE	1509	Public	Bull Creek flowed across the road near Main Street, bringing with it large debris.

Table 3.4: NCEI flash flood storm report data for 6/23/22. Note that the second flash flood (B) occurred soon after (A) to the east of the eastern edge of Figure 3.29.

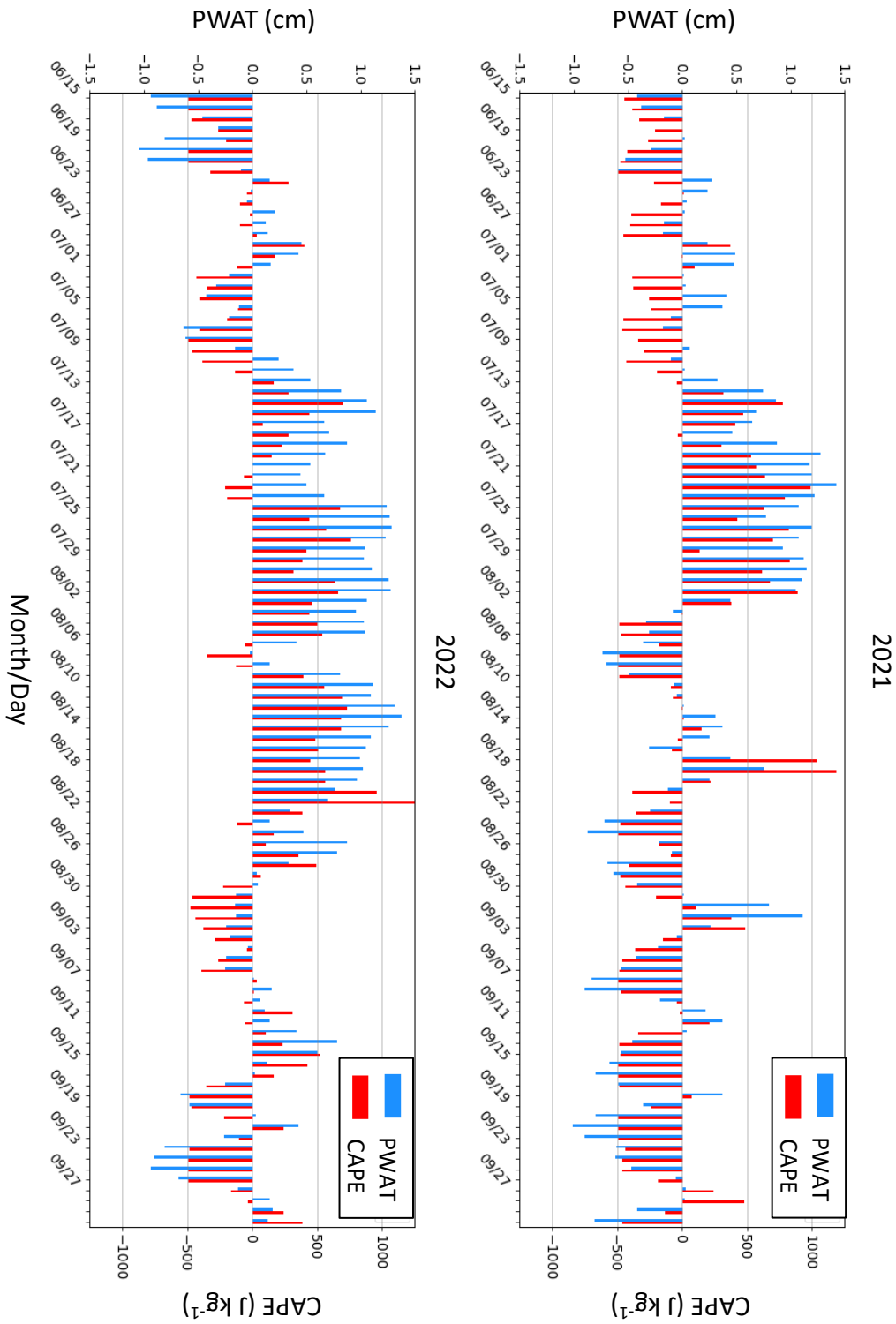

Figure 3.1: Averages computed over all grid points in southwestern Utah of local day (MDT) PWAT (cm) and daily maximum CAPE (J kg^{-1}) relative to approximate two monsoon season averages of 500 J kg^{-1} and 1.5 cm respectively.

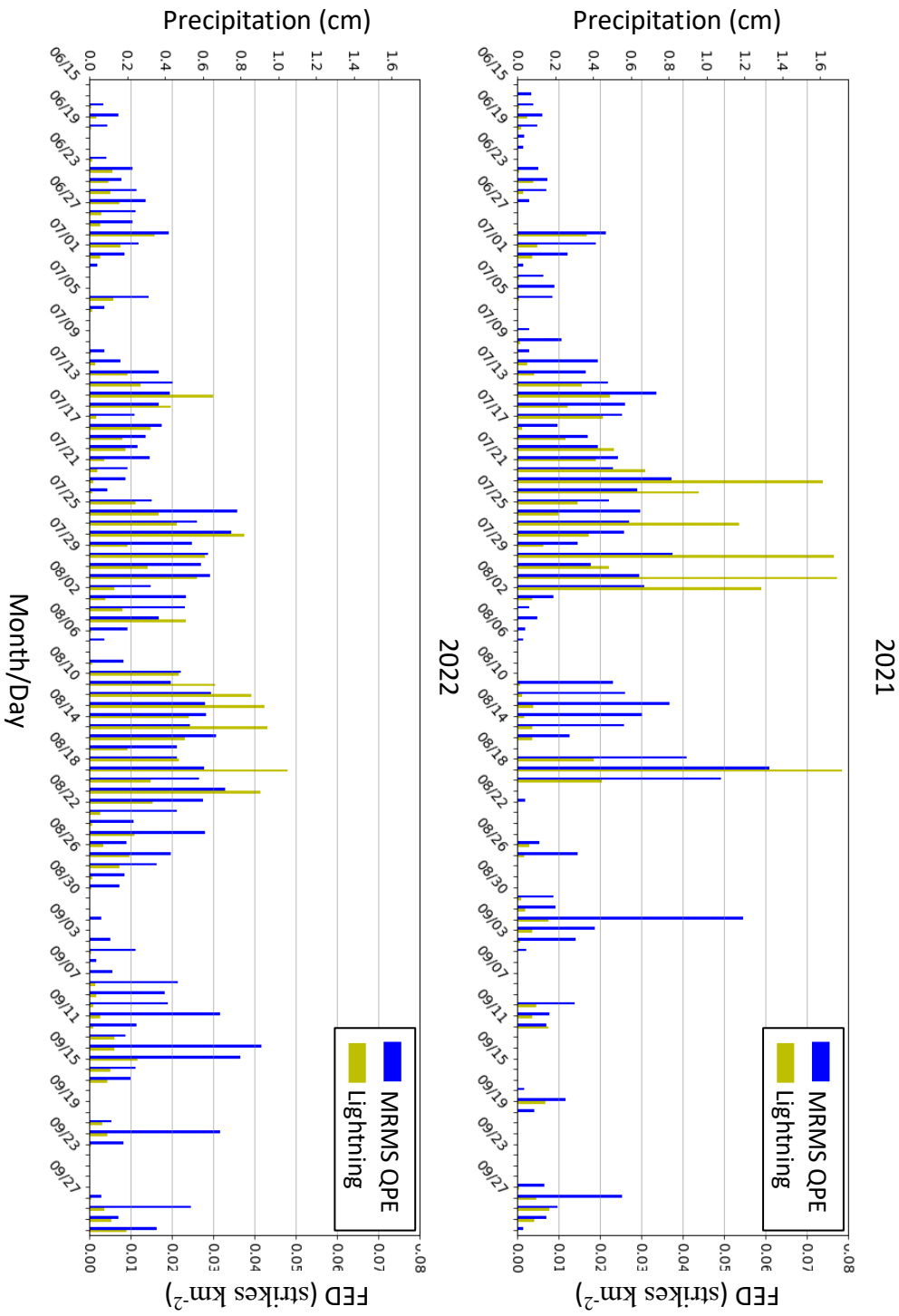

Figure 3.2: Averages computed over all grid points in southwestern Utah of local day (MDT) MRMS precipitation (cm) and NLDN FED (strikes km^{-2}).

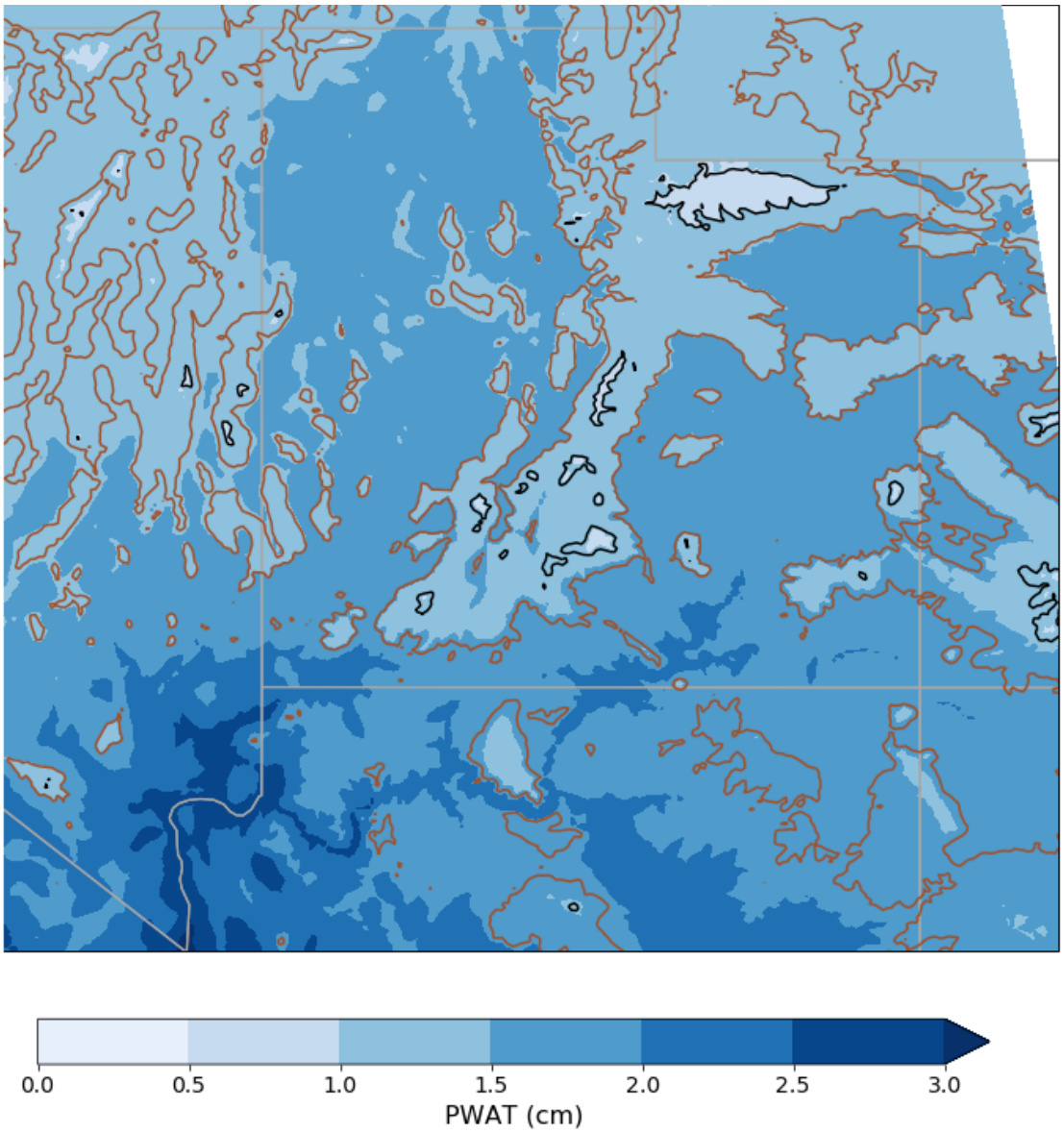

Figure 3.3: Mean HRRR PWAT (cm) during the 2021 – 2022 monsoon seasons. Heavy solid lines denote terrain elevation at 2000m (brown) and 3000m (black).

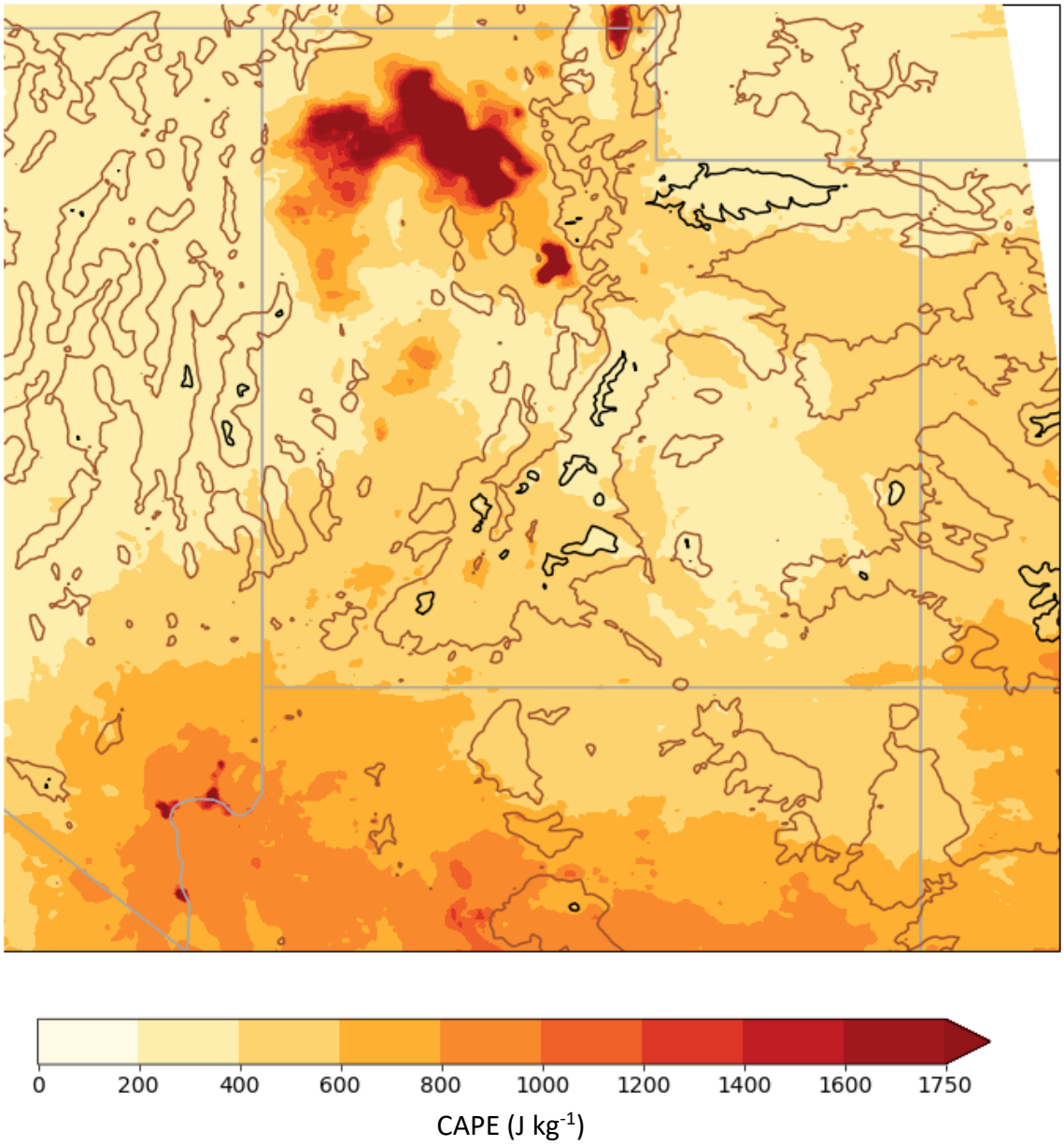

Figure 3.4: Mean computed over the 2021 – 2022 monsoon seasons of daily maximum HRRR CAPE (J kg^{-1}). Heavy solid lines denote terrain elevation at 2000m (brown) and 3000m (black).

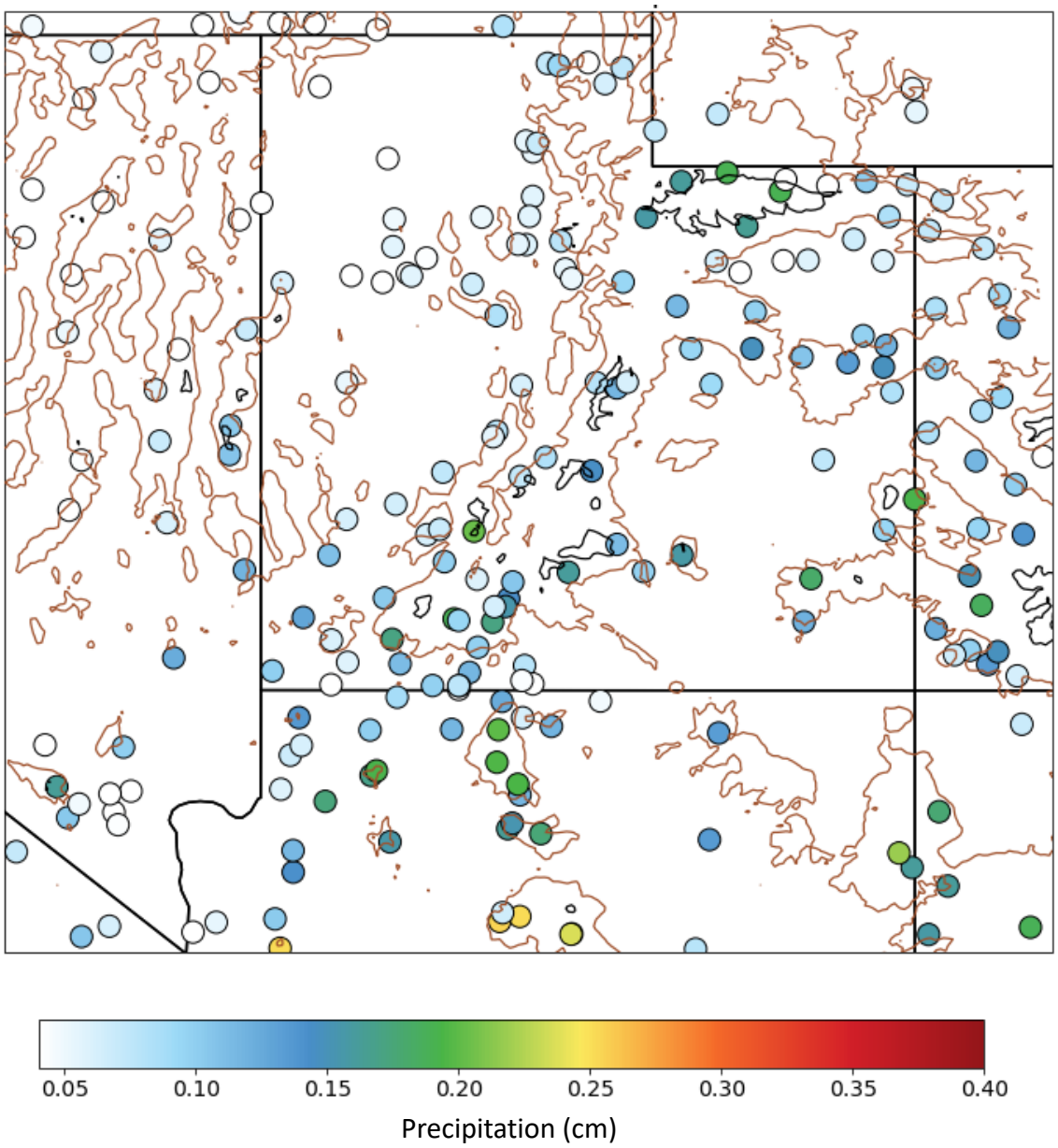

Figure 3.5: Mean daily precipitation (cm) during the 2021 – 2022 monsoon seasons at NWS/RAWS stations. Heavy solid lines denote terrain elevation at 2000m (brown) and 3000m (black).

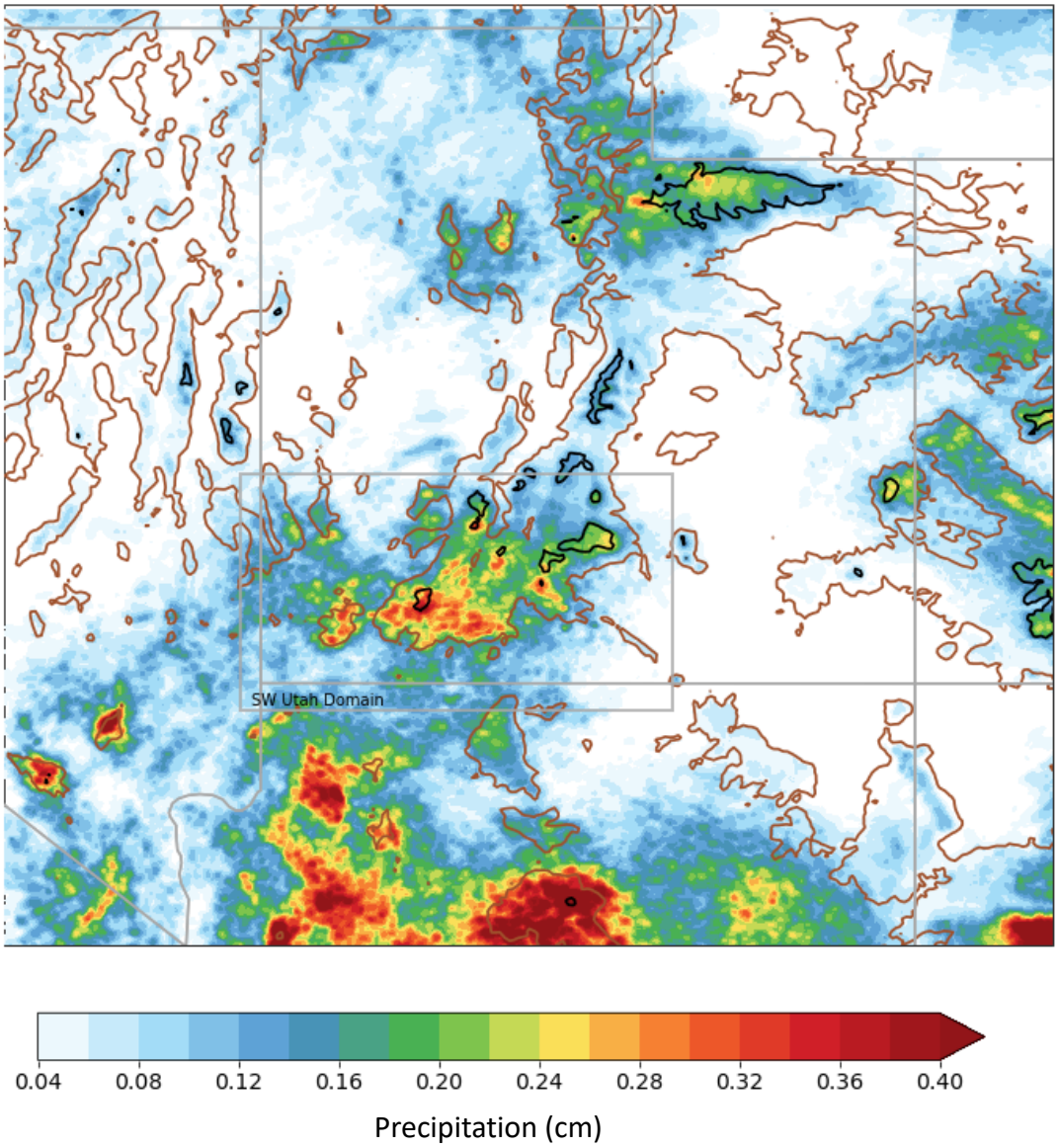

Figure 3.6: Mean daily MRMS precipitation (cm) during the 2021 – 2022 monsoon seasons. Heavy solid lines denote terrain elevation at 2000m (brown) and 3000m (black).

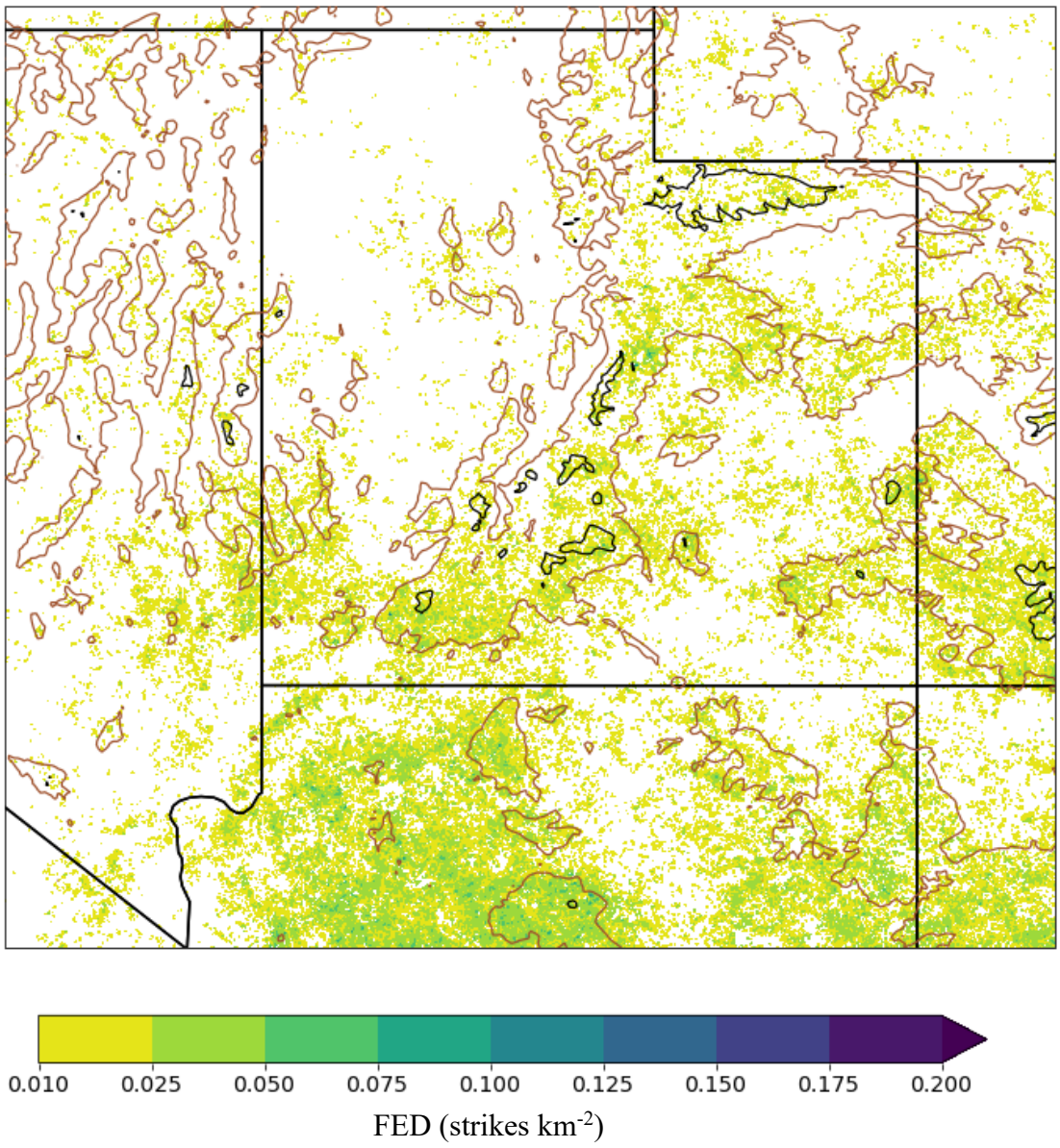

Figure 3.7: Mean daily NLDN FED (strikes km^{-2}) during the 2021 – 2022 monsoon seasons. Heavy solid lines denote terrain elevation at 2000m (brown) and 3000m (black).

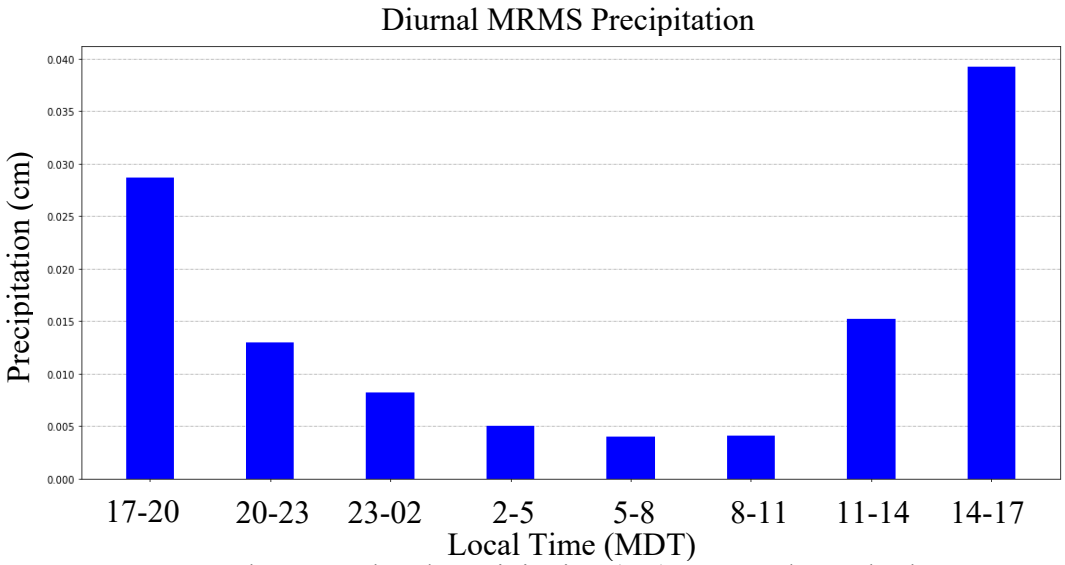

Figure 3.8: MRMS 3-h accumulated precipitation (cm) averaged over both seasons and over the southwestern Utah domain.

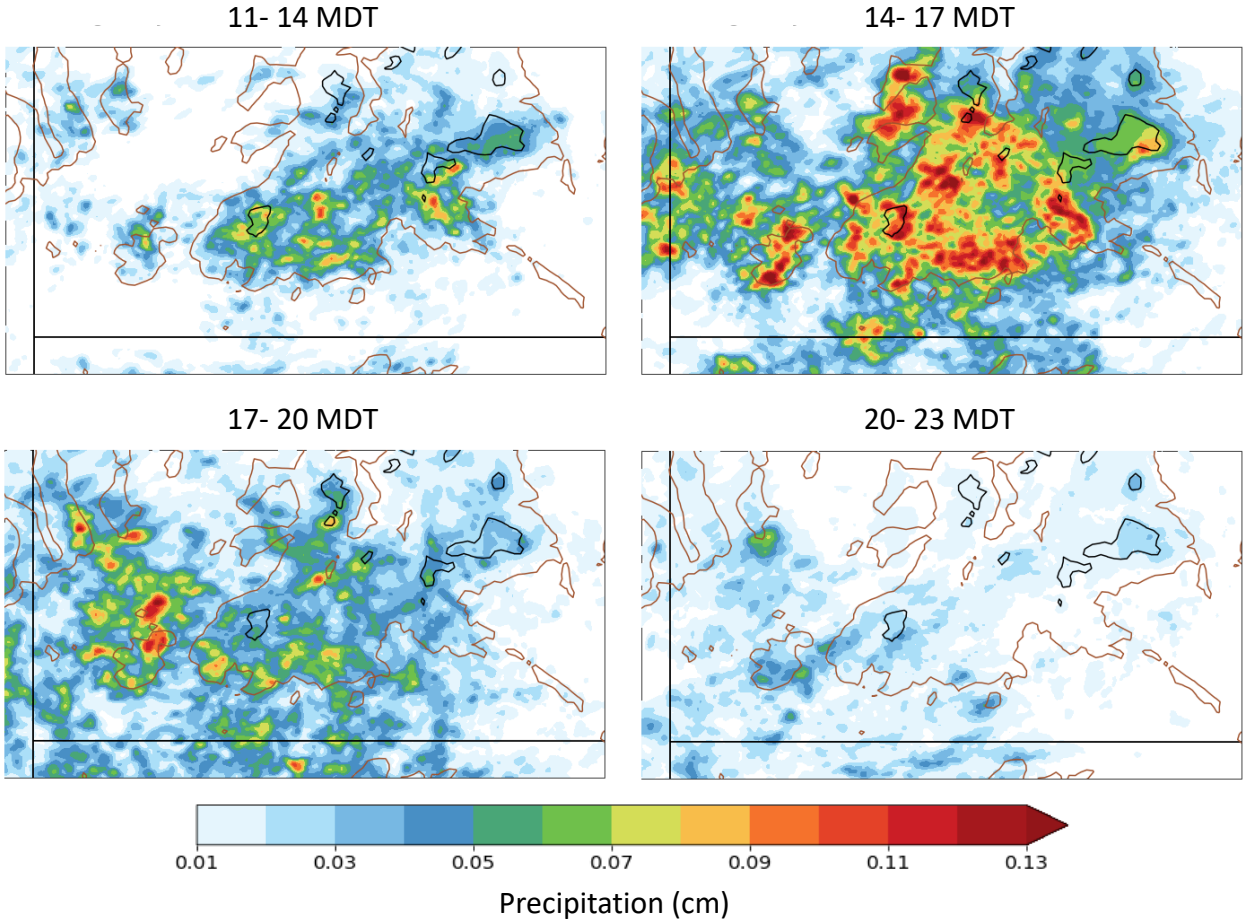

Figure 3.9: MRMS 3-h accumulated precipitation (cm) averaged over both seasons. Heavy solid lines denote terrain elevation at 2000m (brown) and 3000m (black).

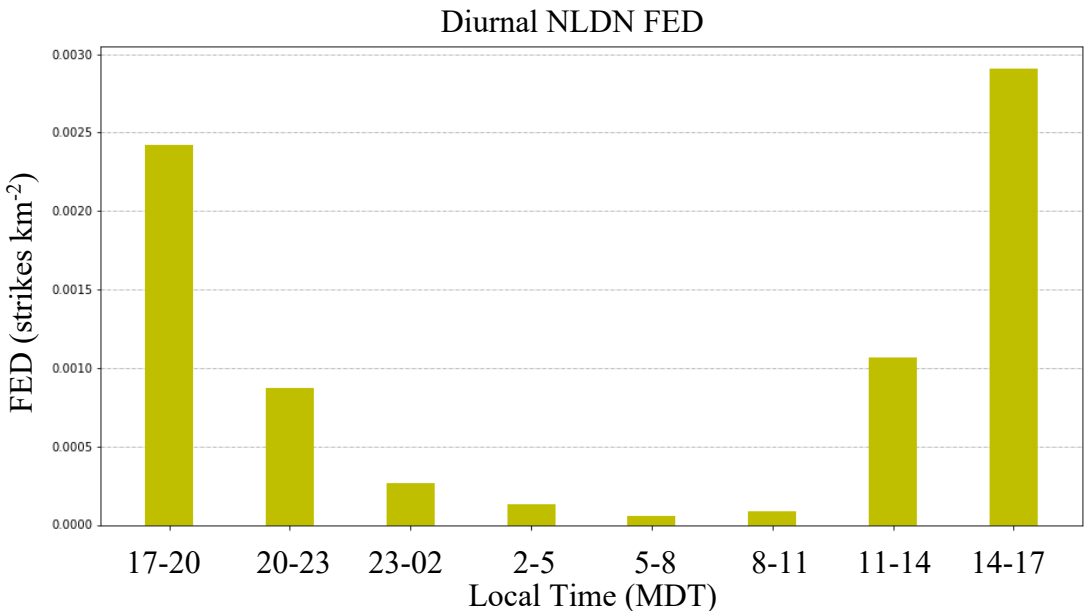

Figure 3.10: NLDN 3-h average FED (strikes km^{-2}) averaged over both seasons and over the southwestern Utah domain.

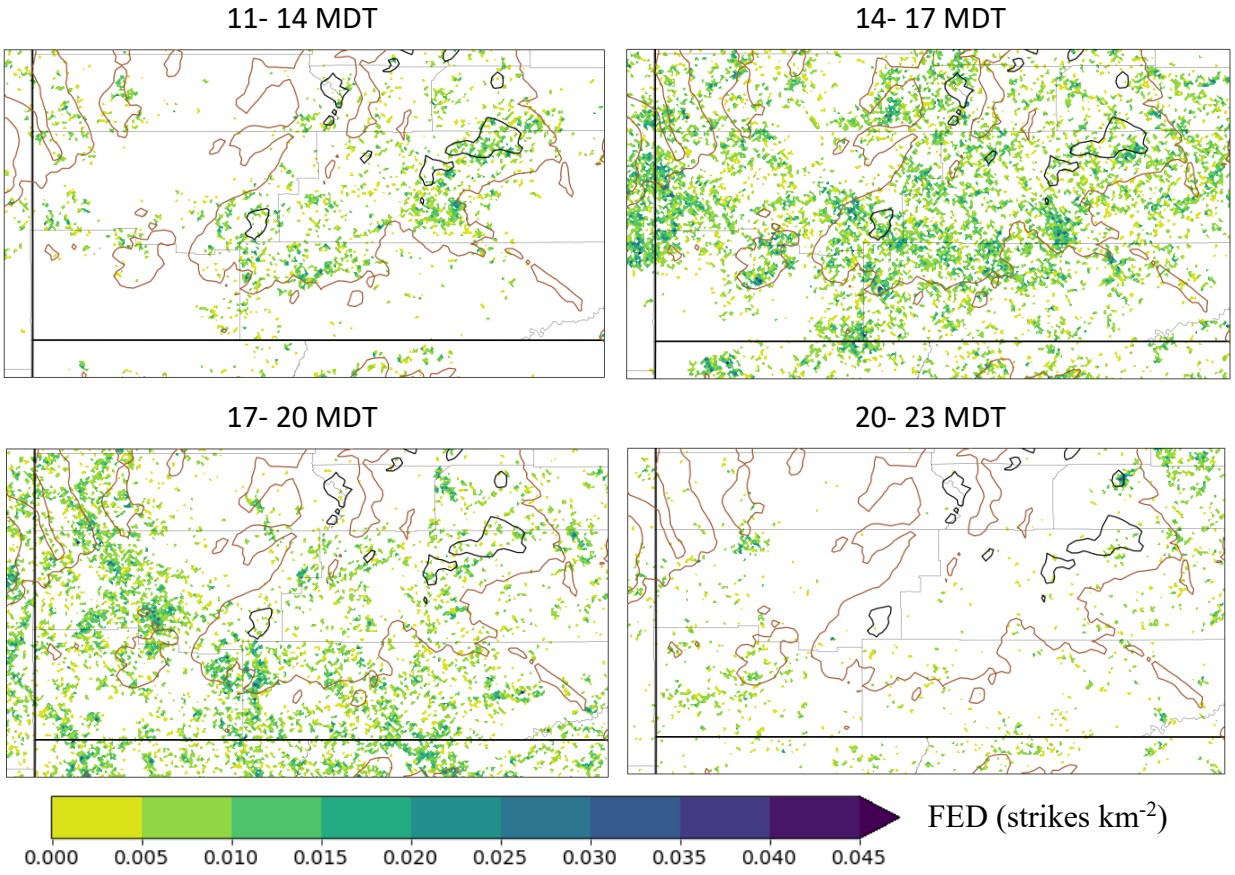

Figure 3.11: NLDN 3-h accumulated flash extent density (FED, strikes km^{-2}) averaged over both seasons. Heavy solid lines denote terrain elevation at 2000m (brown) and 3000m (black).

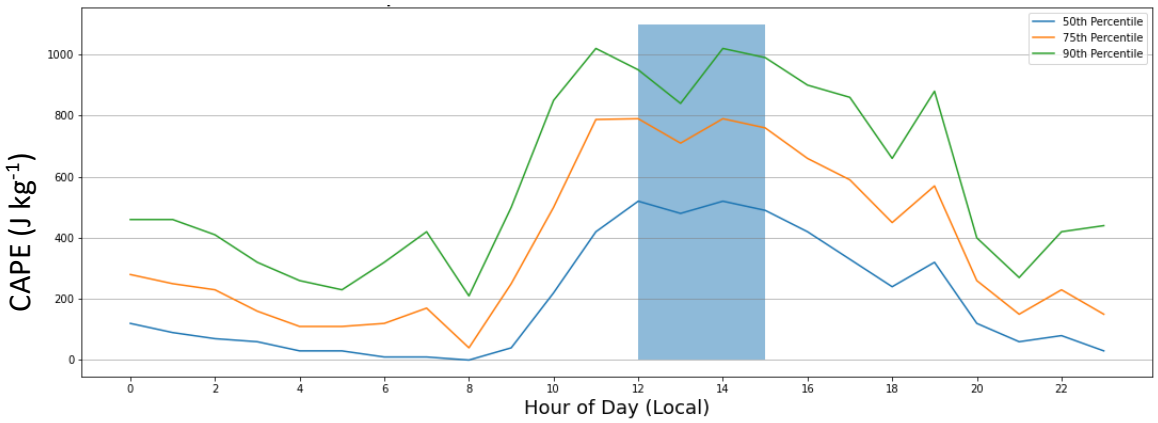

Figure 3.12: HRRR 50th, 75th, and 90th percentile of surface CAPE (J kg^{-1}) over the southwestern Utah domain. Shaded region highlights the afternoon hours (12-15 MDT) that are critical for convective initiation that are addressed later in this study.

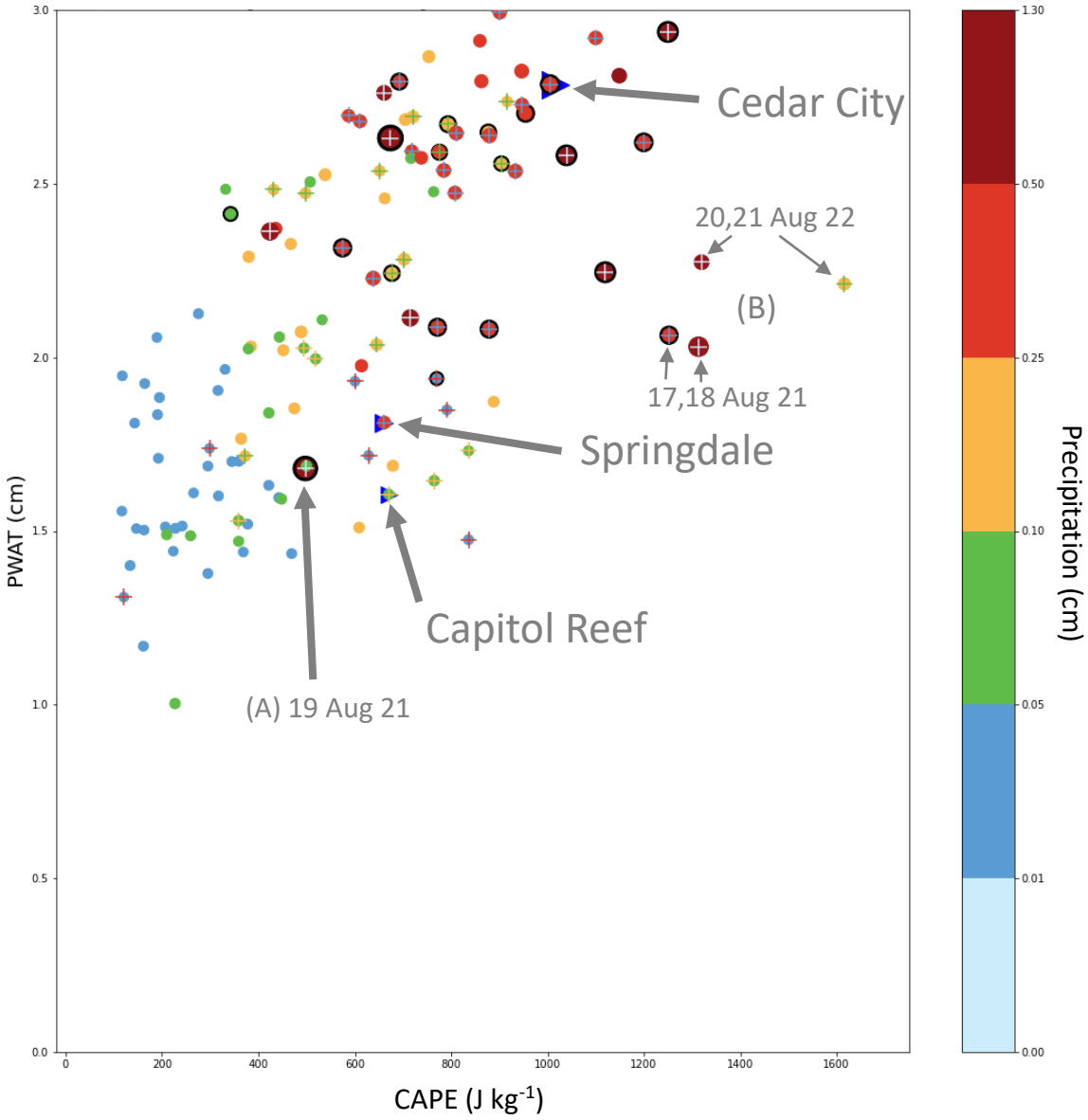

Figure 3.13: Daily maximum CAPE (J kg^{-1}) and PWAT (cm) from 18-21 UTC (12-15 MDT) for southwestern Utah domain from the HRRR analyses with the color and size of the circle denoting daily MRMS precipitation (cm). Plus symbols denote days with at least one flash flood report. A blue sideways triangle was placed under the three case study days and labeled. A and B label outliers that are discussed in the text.

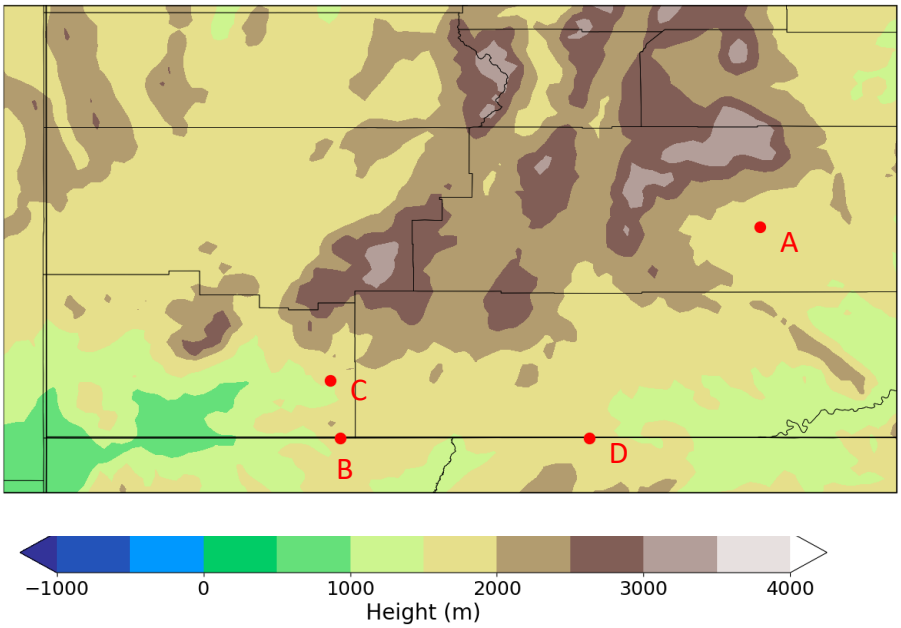

Figure 3.14: Terrain (m) within southwestern Utah domain shaded according to the color bar. Red dots are the locations of flash flood storm reports on 29 June 2021 listed in Table 3.2.

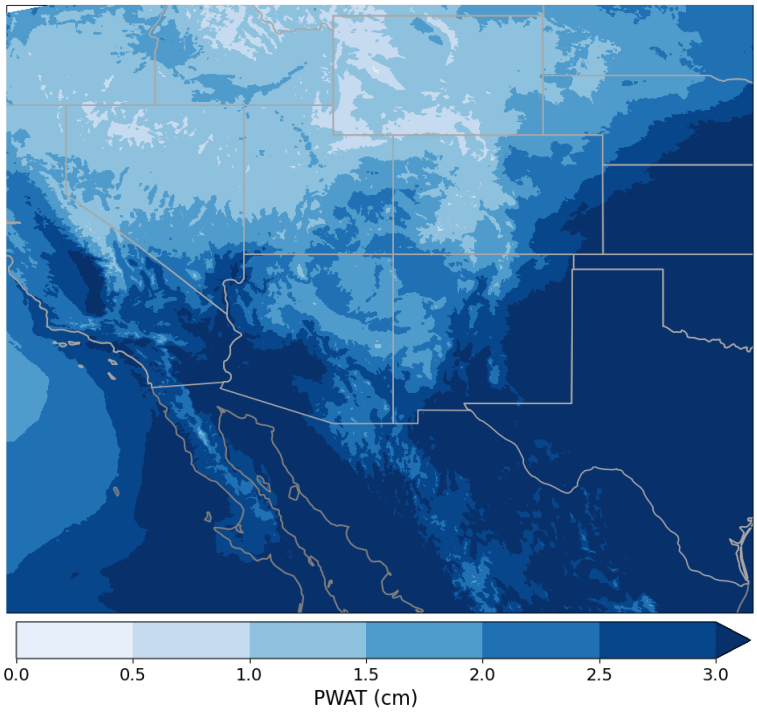

Figure 3.15: Mean HRRR PWAT (cm) during the period 12 – 16 MDT 29 June 2021.

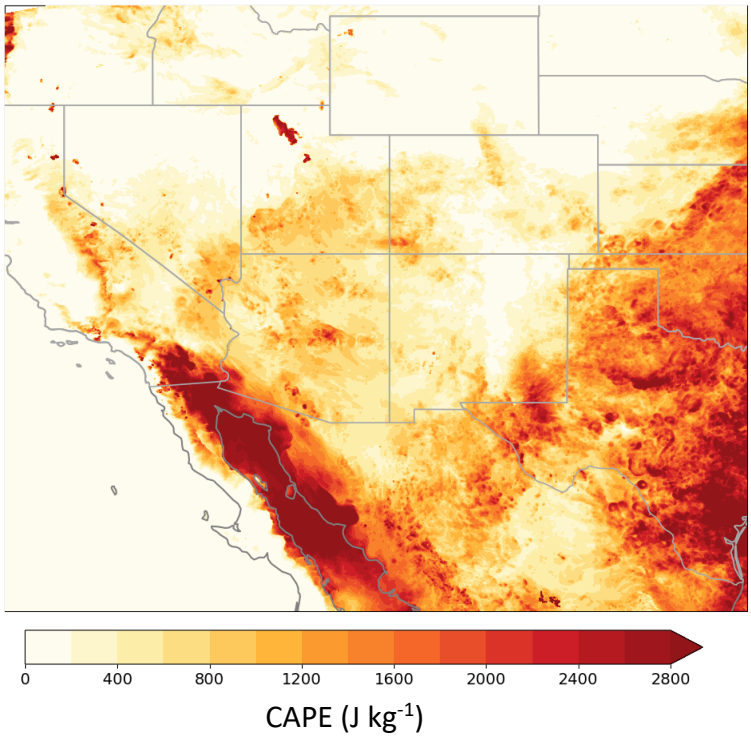

Figure 3.16: Maximum HRRR CAPE (J kg^{-1}) during the period 12 – 16 MDT 29 June 2021.

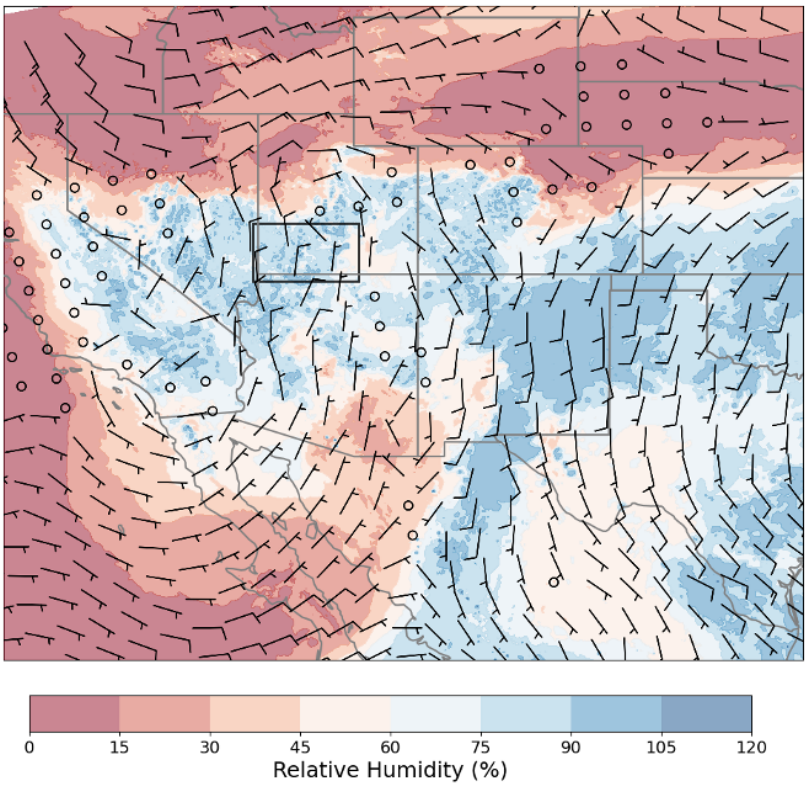

Figure 3.17: HRRR analysis of 500 hPa relative humidity (shading in %), geopotential height, and vector wind (10 m s^{-1} denoted by a full barb) valid at 14 MDT 29 June 2021.

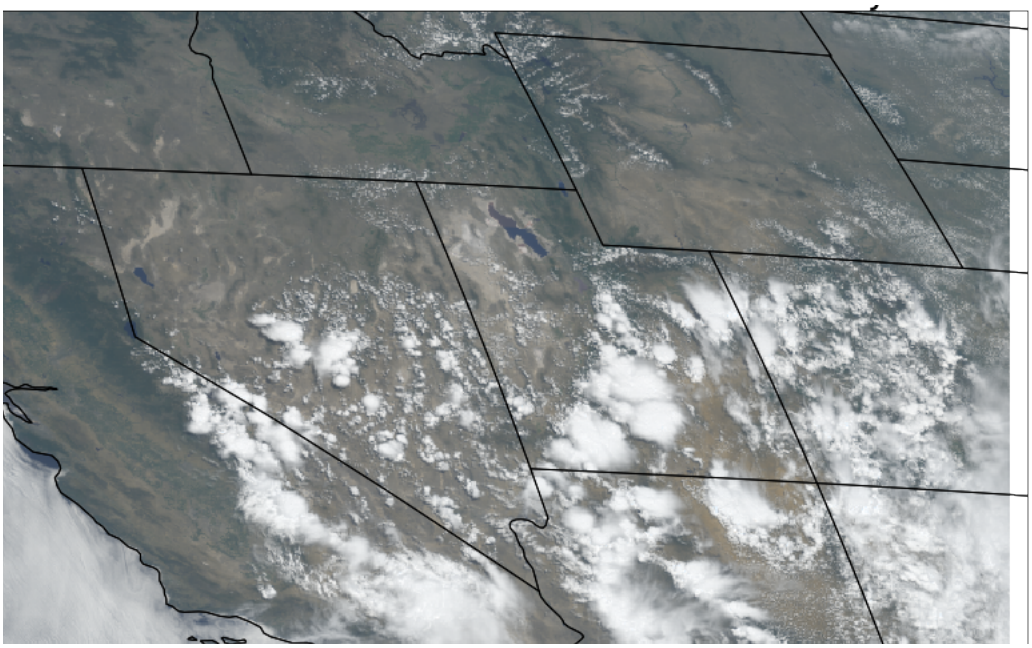

Figure 3.18: True color visible image at 13:42 MDT 29 June 2021.

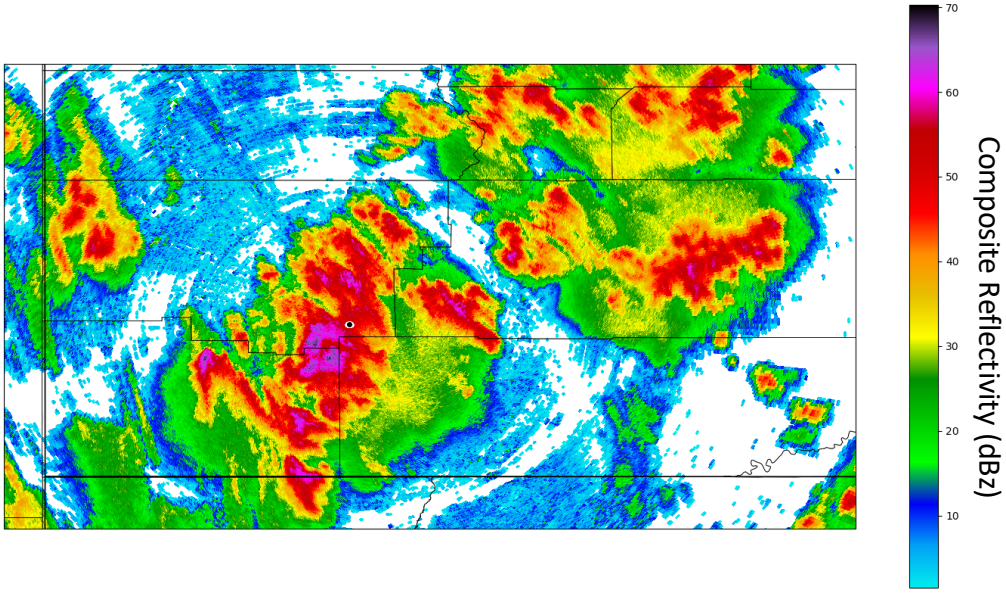

Figure 3.19: Maximum composite reflectivity (dBz) from the KICX radar above 1.5 dBz during 13 – 14 MDT 29 June 2021. The Black dot shows the radar's location.

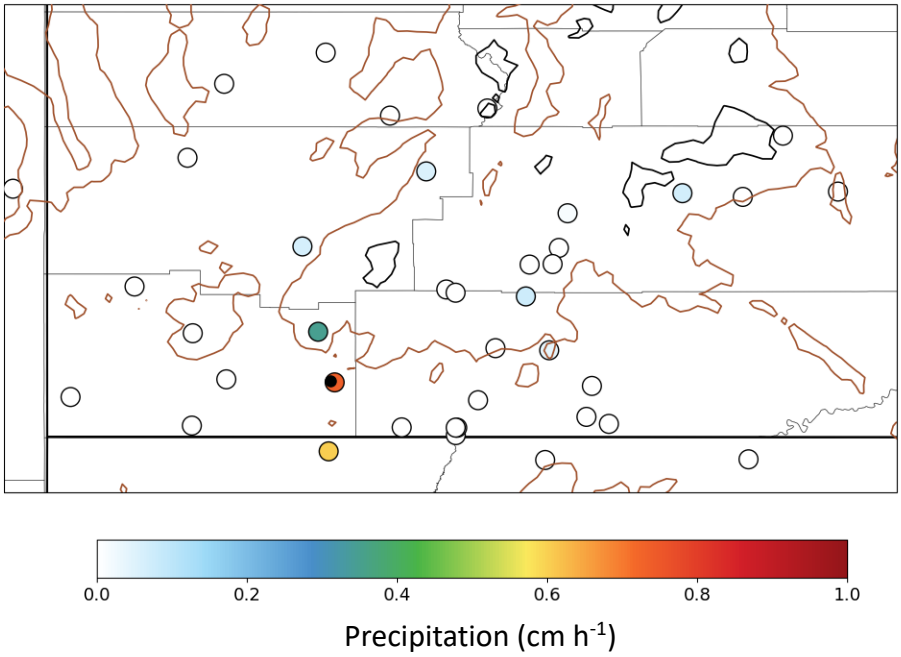

Figure 3.20: Average hourly precipitation (cm h^{-1}) from NWS and RAWS stations during the period 12 – 16 MDT 29 June 2021. Black dot shows the location of Springdale flash flood. Heavy solid lines denote terrain elevation at 2000m (brown) and 3000m (black).

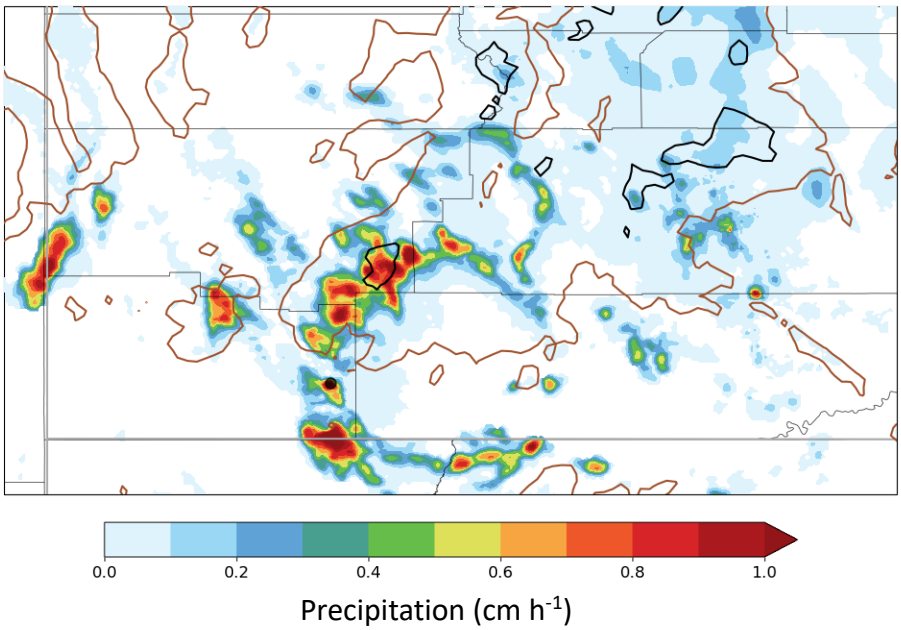

Figure 3.21: Average hourly precipitation (cm h^{-1}) from MRMS analyses during the period 12 – 16 MDT 29 June 2021. Black dot shows the location of Springdale flash flood. Heavy solid lines denote terrain elevation at 2000m (brown) and 3000m (black).

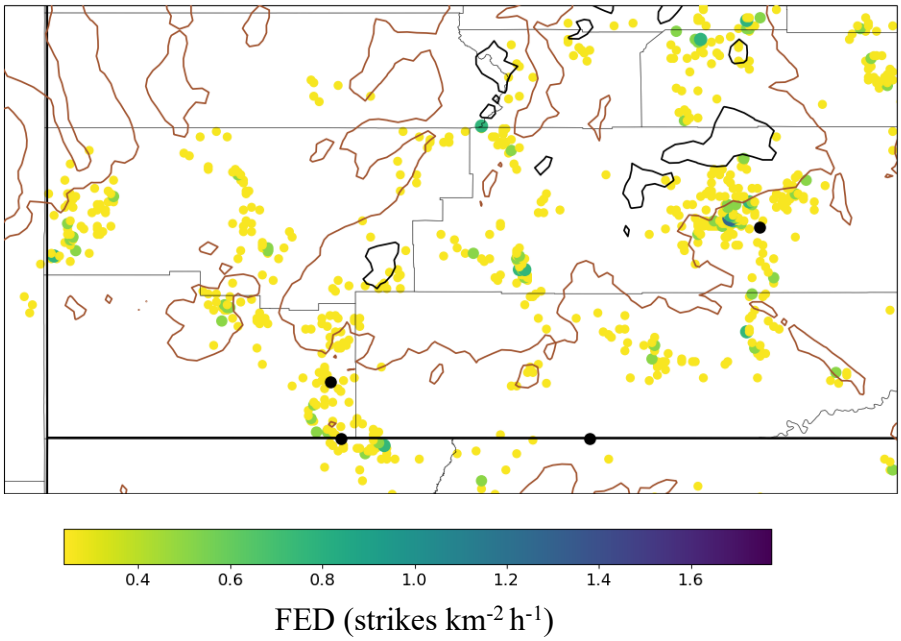

Figure 3.22: Average NLDN FED (strikes km^{-2} h^{-1}) during the period 12 – 16 MDT 29 June 2021. Black dots show the locations of each flash flood report on that day as described in Table 3.2. Heavy solid lines denote terrain elevation at 2000m (brown) and 3000m (black).

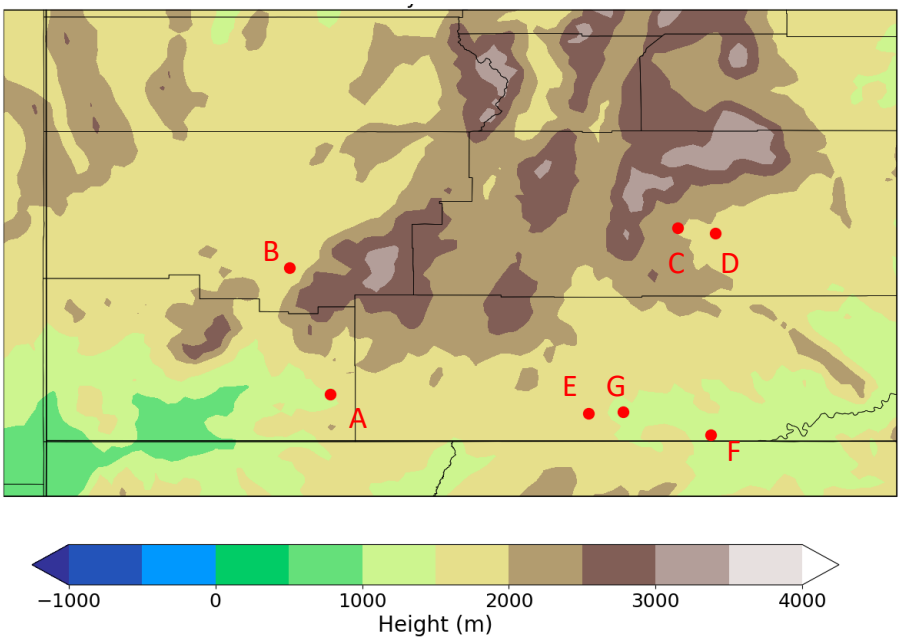

Figure 3.23: Terrain map of southwestern Utah domain at 500 meter contours levels. Red dots are the locations of flash flood storm reports on 26 July 2021 described in Table 3.3.

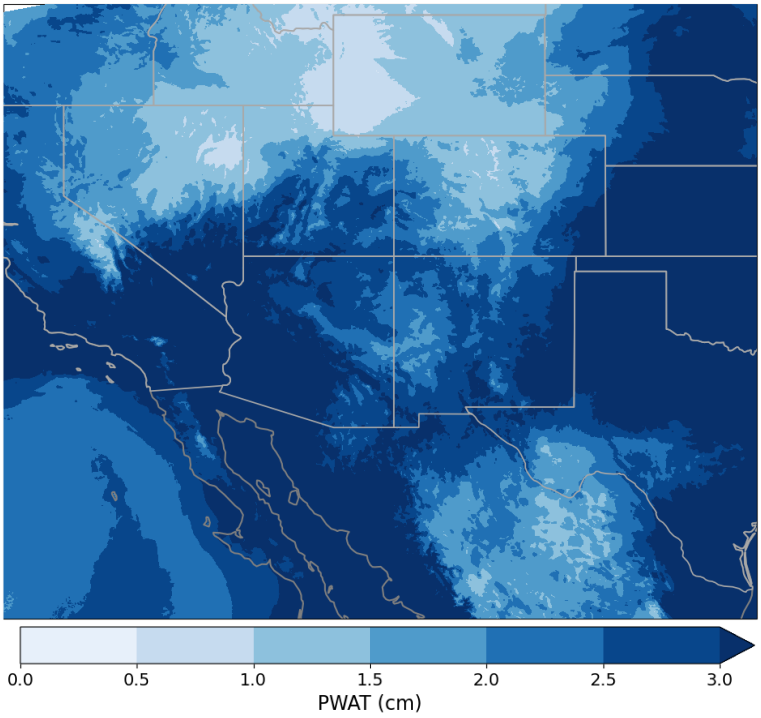

Figure 3.24: Mean HRRR PWAT (cm) during the period 12 – 18 MDT 26 July 2021.

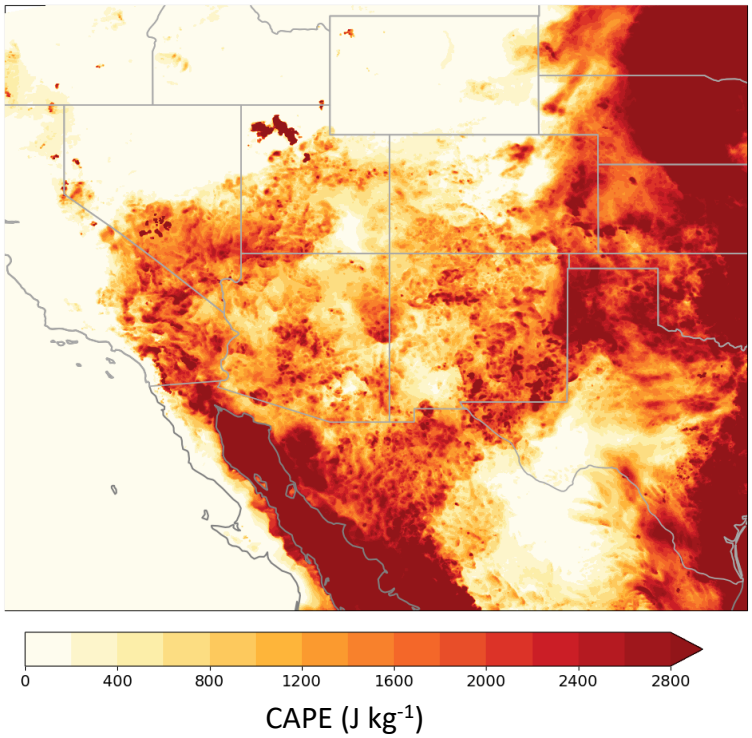

Figure 3.25: Maximum HRRR CAPE (J kg^{-1}) during the period 12 – 18 MDT 26 July 2021.

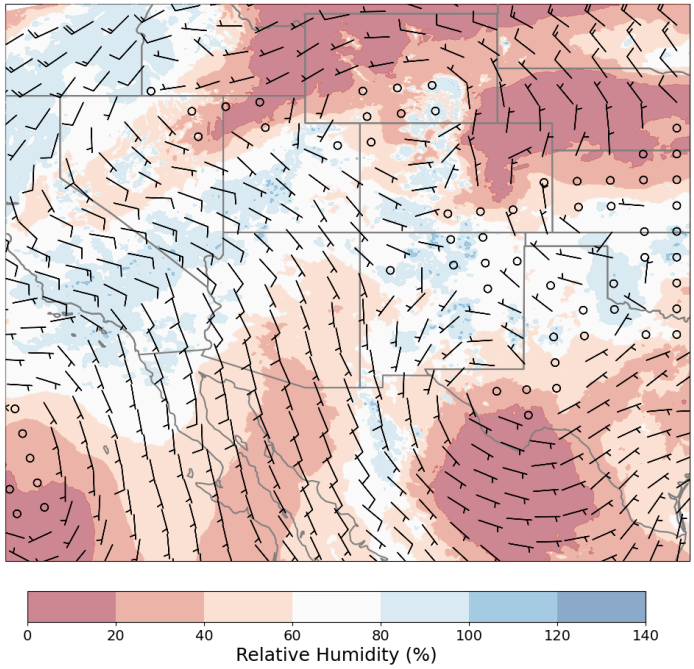

Figure 3.26: HRRR analysis of 500 hPa relative humidity (shading in %), geopotential height, and vector wind (10 m s^{-1} denoted by a full barb) valid at 14 MDT 26 July 2021.

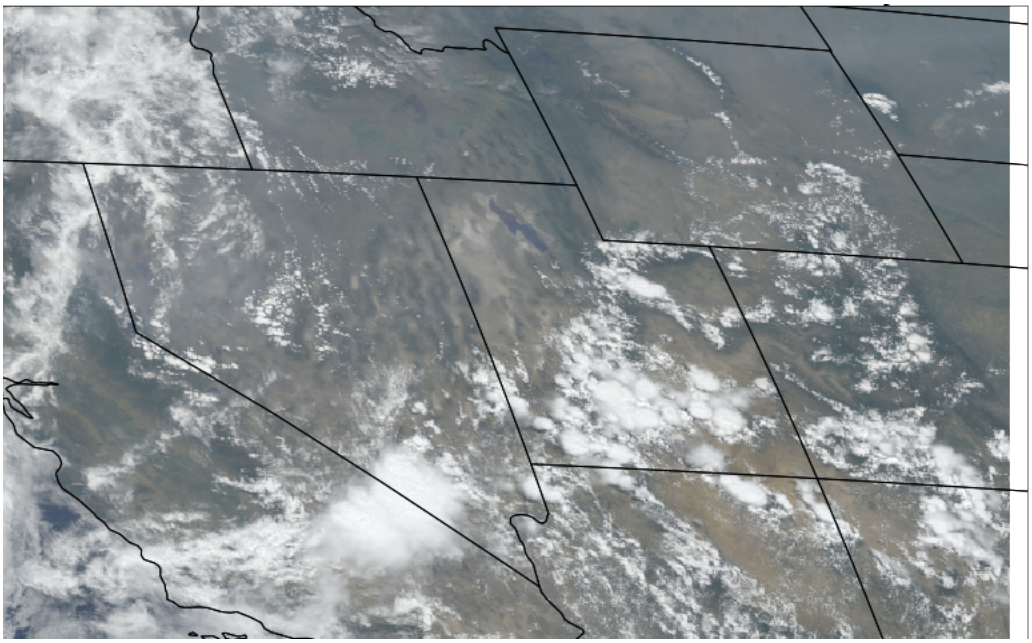

Figure 3.27: True color visible image at 14:02 MDT 26 July 2021.

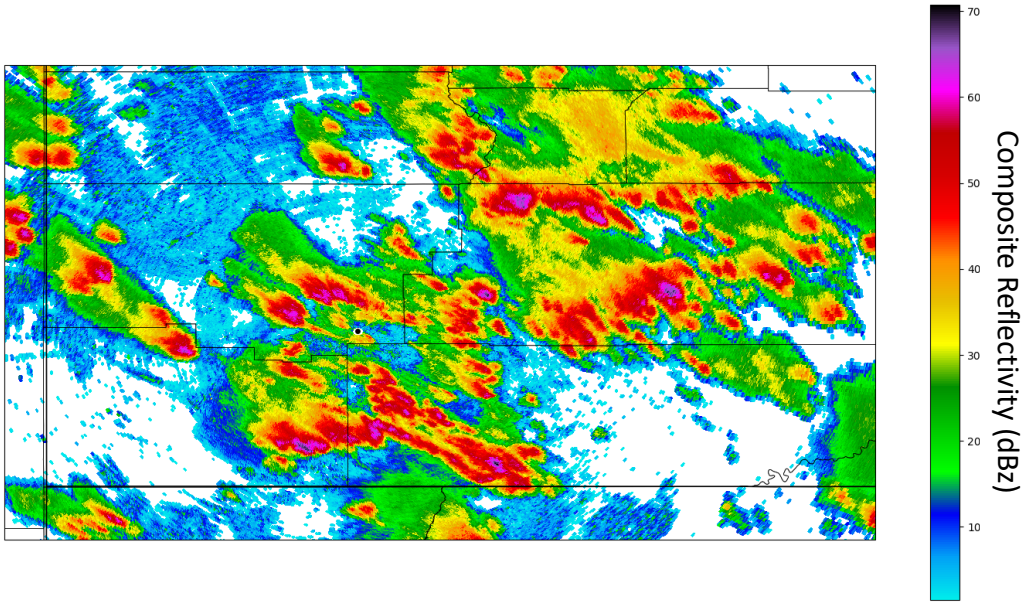

Figure 3.28: Maximum composite reflectivity (dBz) from the KICX radar above 1.5 dBz during 13 – 14 MDT 26 July 2021. The Black dot shows the radar's location.

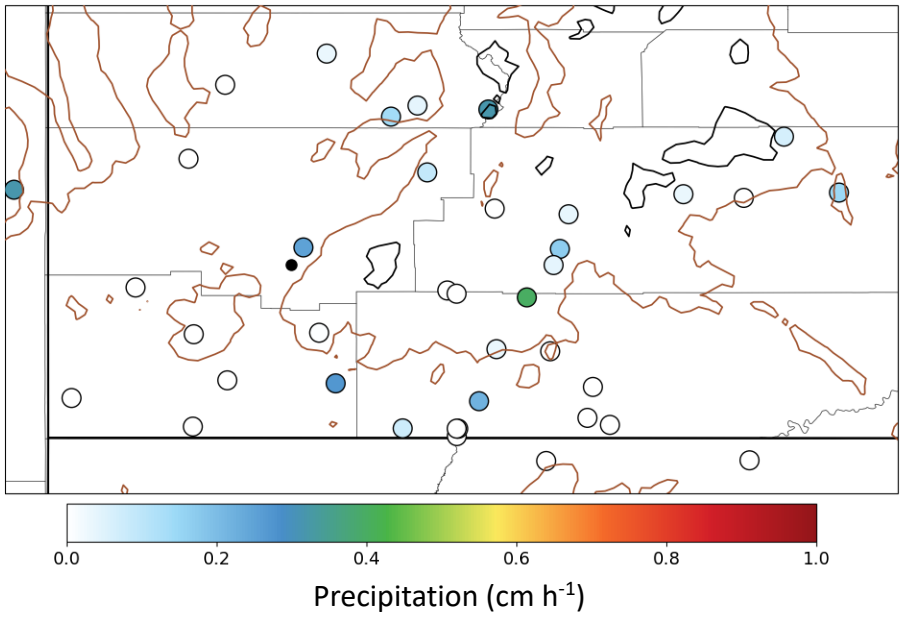

Figure 3.29: Average hourly precipitation (cm h^{-1}) from NWS and RAWS stations during the period 12 – 18 MDT 26 July 2021. Black dot shows the location of Cedar City flash flood. Heavy solid lines denote terrain elevation at 2000m (brown) and 3000m (black).

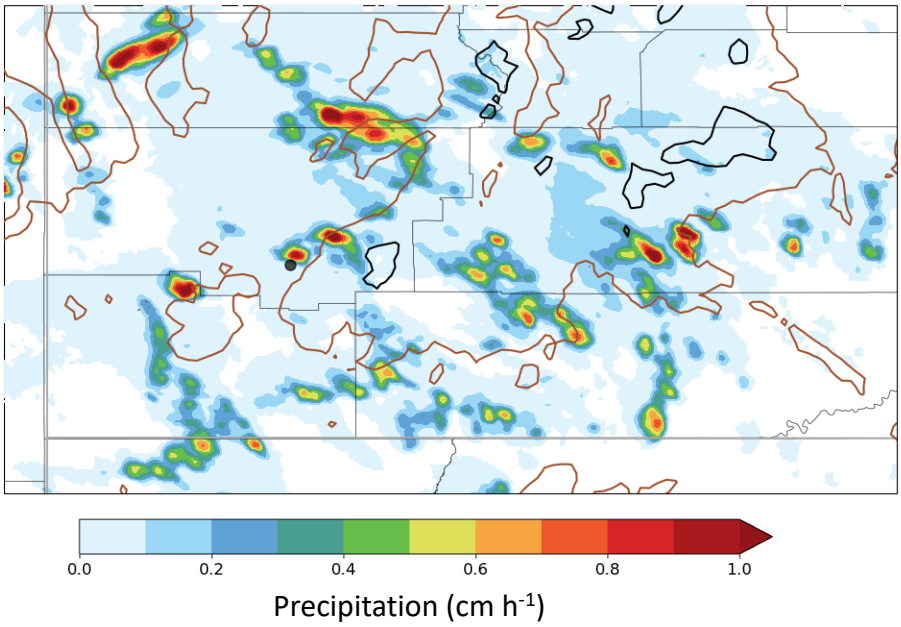

Figure 3.30: Average hourly precipitation (cm h^{-1}) from MRMS analyses during the period 12 – 18 MDT 26 July 2021. Black dot shows the location of Cedar City flash flood. Heavy solid lines denote terrain elevation at 2000m (brown) and 3000m (black).

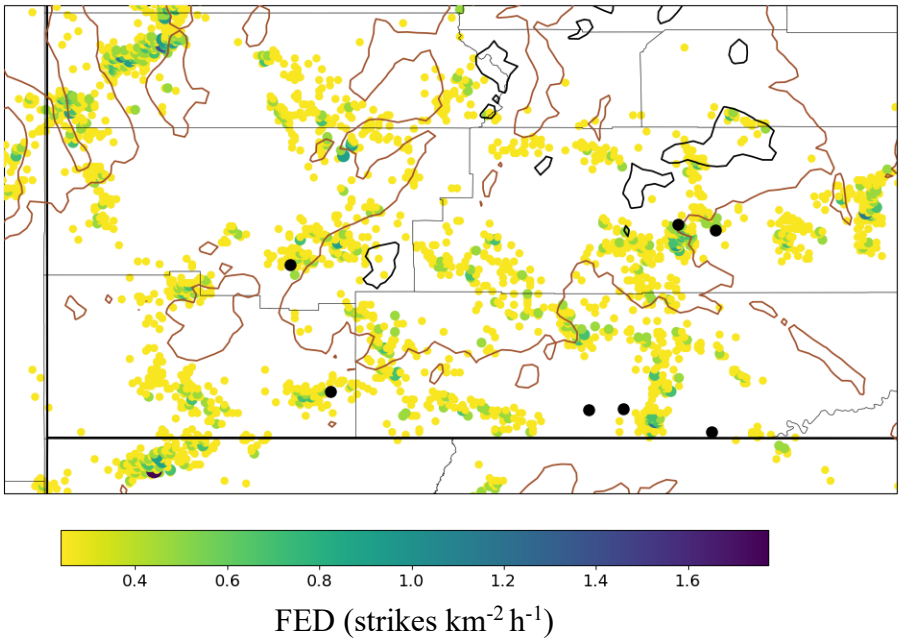

Figure 3.31: Average NLDN FED (strikes km^{-2} h^{-1}) from NLDN during the period 12 – 18 MDT 26 July 2021. Black dots show the locations of all flash flood reports that day as described in Table 3.3. Heavy solid lines denote terrain elevation at 2000m (brown) and 3000m (black).

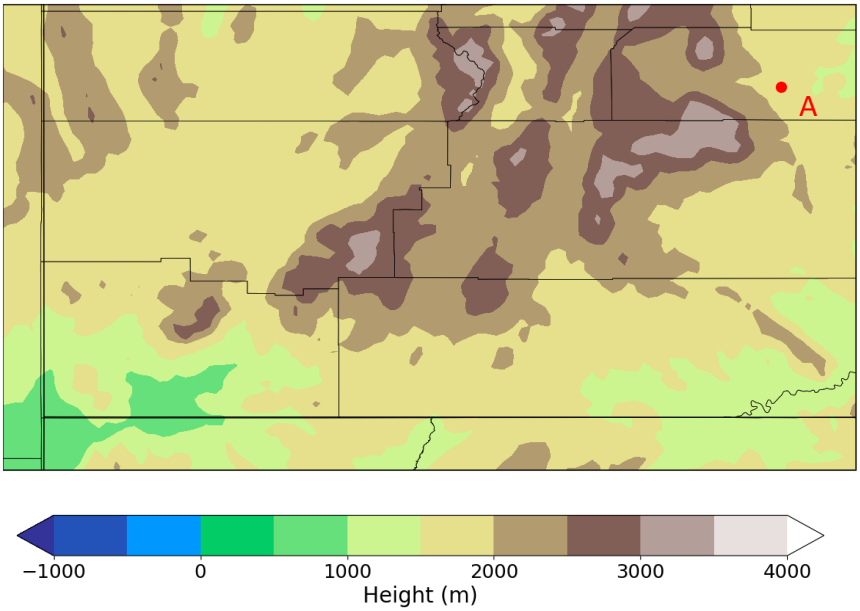

Figure 3.32: Terrain map of southwestern Utah domain at 500 meter contours levels. Red dot is the location of flash flood storm report on 23 June 2022, described in Table 3.4. A second storm report on this day is just outside the northeast edge of the domain.

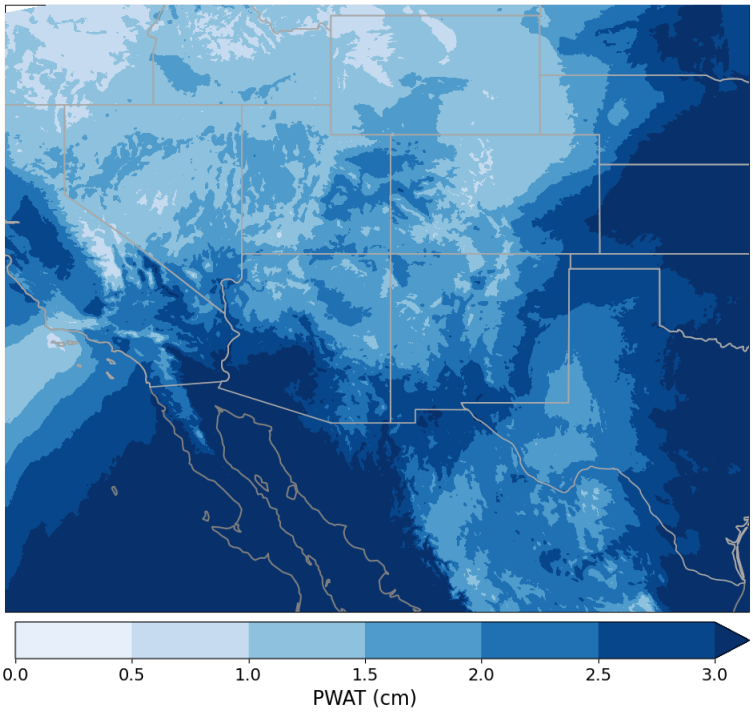

Figure 3.33: Mean HRRR PWAT (cm) during the period 11 – 18 MDT 23 June 2022.

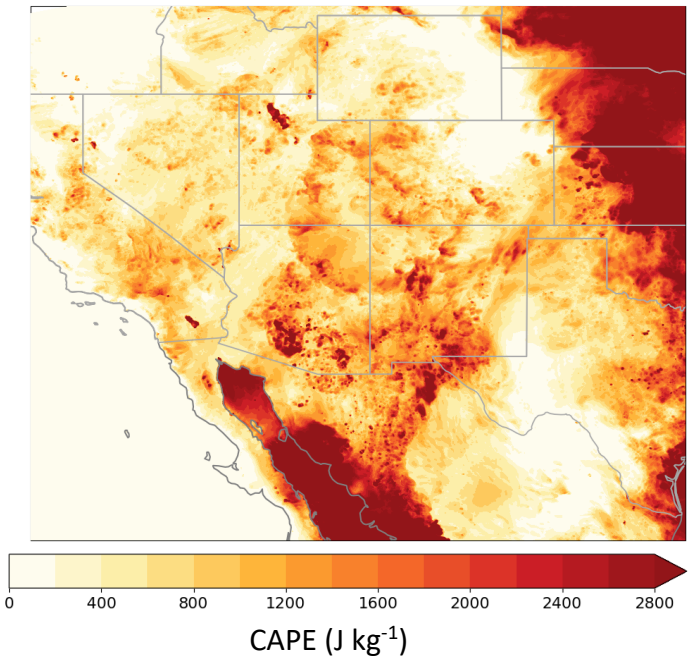

Figure 3.34: Maximum HRRR CAPE (J kg^{-1}) during the period 11 – 18 MDT 23 June 2022.

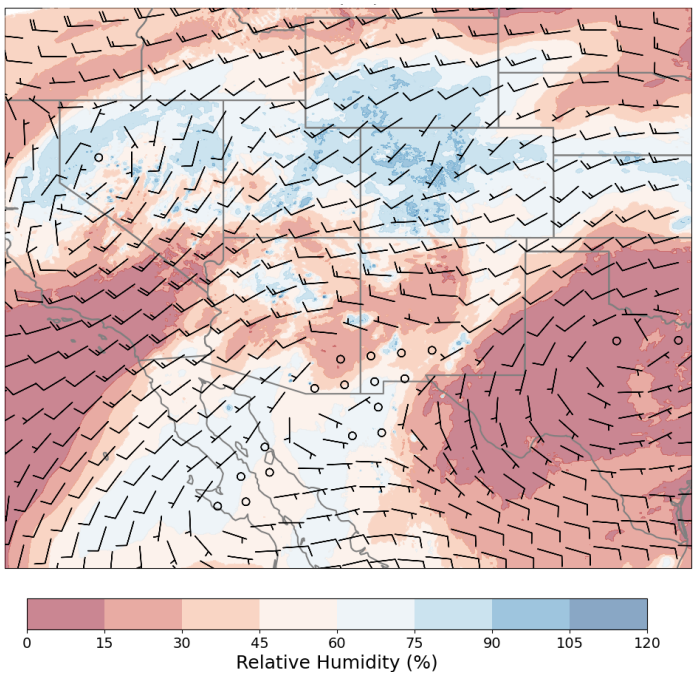

Figure 3.35: HRRR analysis of 500 hPa relative humidity (shading in %), geopotential height, and vector wind (10 m s^{-1} denoted by a full barb) valid at 13 MDT 23 Jun 2022.

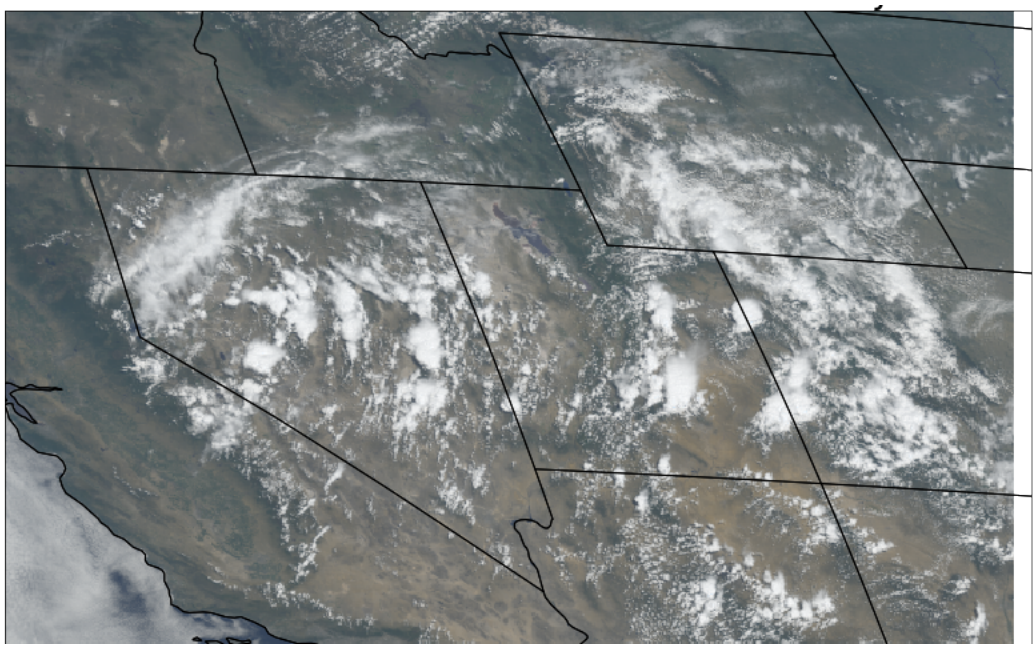

Figure 3.36: True color visible image at 13:02 MDT 23 June 2022.

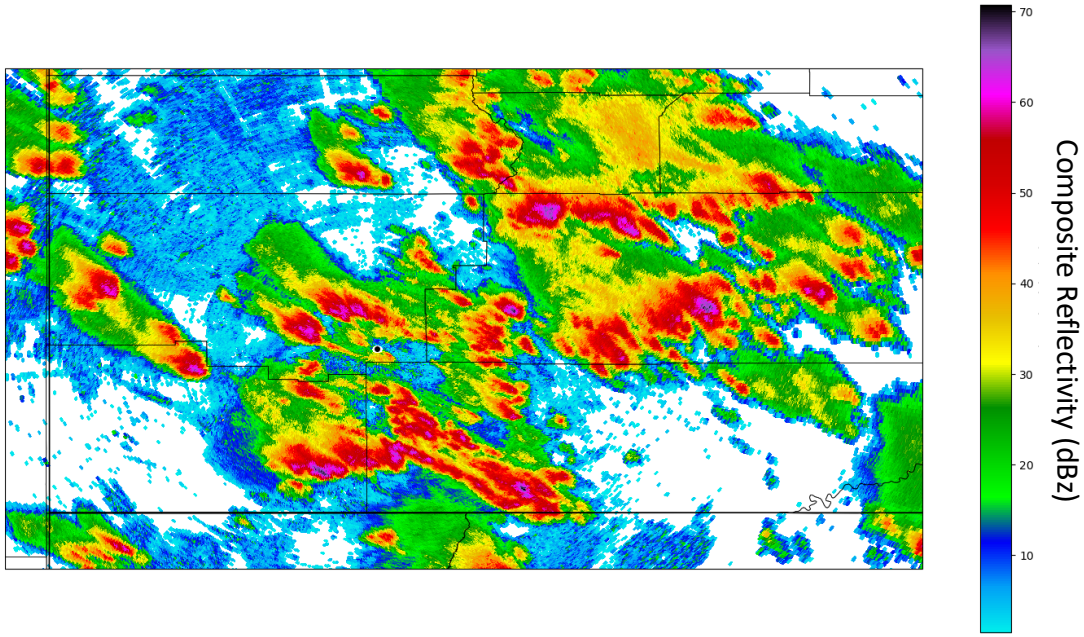

Figure 3.37: Maximum composite reflectivity (dBz) from the KICX radar above 1.5 dBz during 12 – 13 MDT 23 June 2022. The Black dot shows the radar's location.

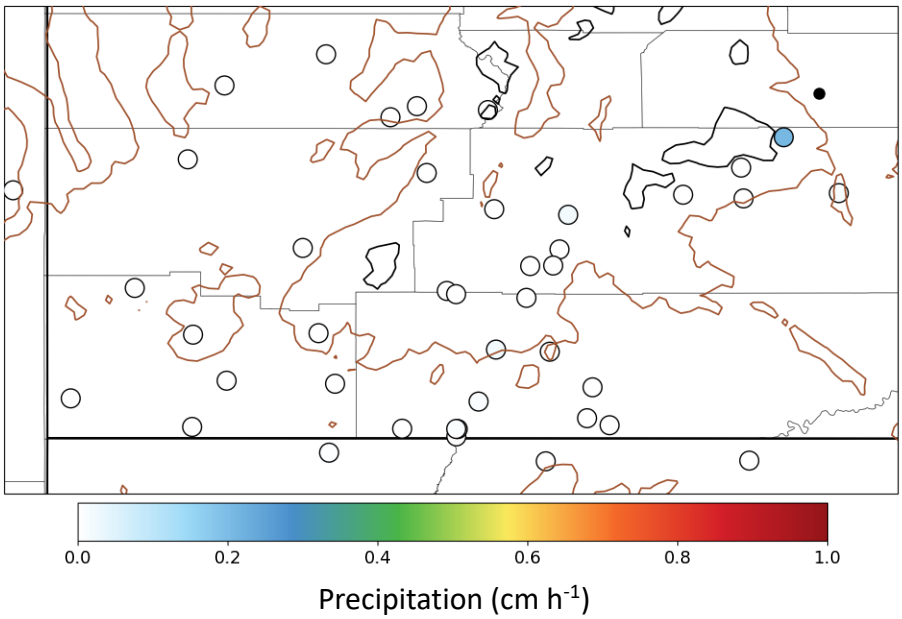

Figure 3.38: Average hourly precipitation (cm h^{-1}) from NWS and RAWS stations during the period 11 – 18 MDT 23 June 2022.Black dot shows the location of Capitol Reef flash flood. Heavy solid lines denote terrain elevation at 2000m (brown) and 3000m (black).

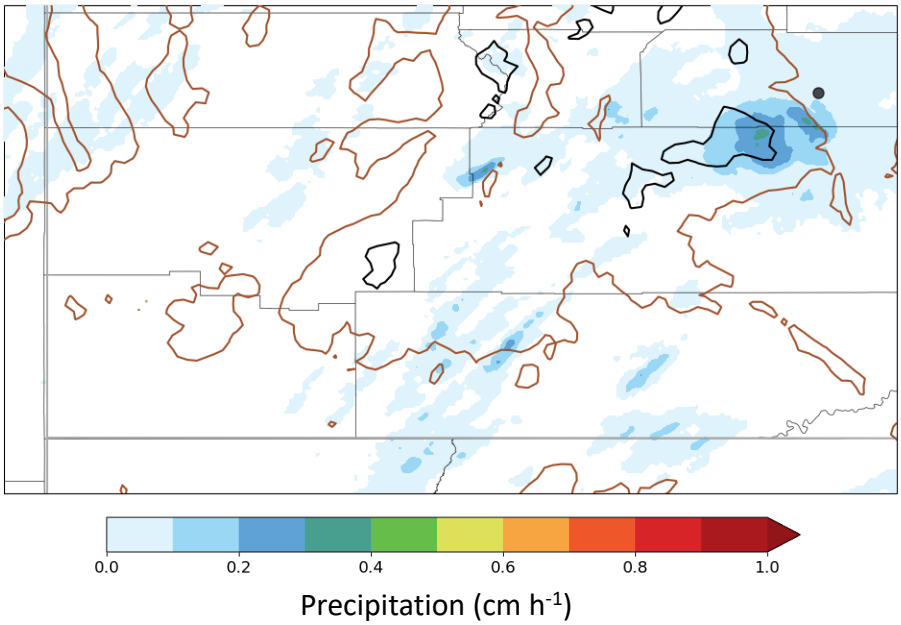

Figure 3.39: Average hourly precipitation (cm h^{-1}) from MRMS analyses during the period 11 – 18 MDT 23 June 2022. Black dot shows the location of Capitol Reef flash flood. Heavy solid lines denote terrain elevation at 2000m (brown) and 3000m (black).

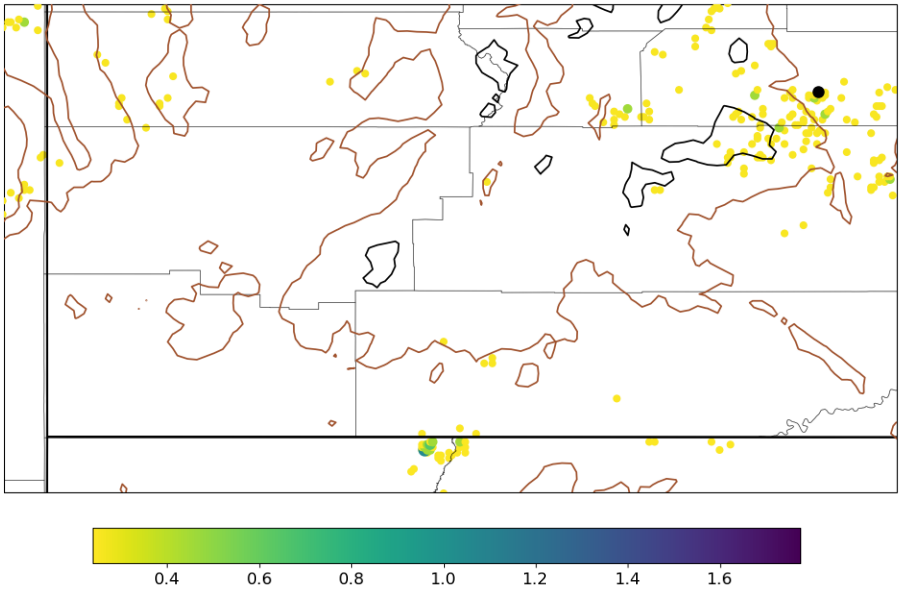

Figure 3.40: Average NLDN FED (strikes km^{-2} h^{-1}) from NLDN during the period 11 – 18 MDT 23 June 2022. Black dot shows the location of Capitol Reef flash flood. Heavy solid lines denote terrain elevation at 2000m (brown) and 3000m (black).

CHAPTER 4

HRRR MODEL FORECAST SKILL

Chapter 3 focused on analyzing characteristics of the 2021 and 2022 monsoon seasons on the basis of daily and seasonal statistics as well as three case studies of specific days representative of different types of monsoonal situations leading to flash floods. This Chapter uses HRRR and MRMS analysis fields as estimates of what transpired across southwestern Utah to help evaluate the extent to which HRRR forecasts at lead times from 6-18 h may be useful to recognize the general conditions that may lead to heavy precipitation across southwestern Utah. There is no attempt here to expect that model forecasts at these lead times could provide specific guidance on where heavy precipitation or flash floods might occur within southwestern Utah. Rather, the objective is to assess the extent to which HRRR forecasts of basic fields such as PWAT and CAPE at lead times from 6-18 h may help identify those afternoons when heavy precipitation is more likely than others.

4.1 Flash Flood Potential Rating

As a reference for the skill of the HRRR model forecasts, an alternative approach being used by the Salt Lake City NWSFO is first examined. The Salt Lake City forecasters have extensive experience issuing watches and warnings for flash flood

conditions across southwestern Utah on the basis of many data and numerical model resources. Based on their experience and the desire of the constituents, the flash flood potential ranking (FFPR) has been developed and issued by the WFO to benefit government agencies responsible for public safety in national parks, monuments, and recreational areas across the state. FFPR values are issued daily often in the early morning (8-10 UTC; 2-4 MDT) and then updated if necessary throughout the day for specific subregions in southwestern Utah: Zion National Park, Bryce Canyon National Park, Capitol Reef National Park, and Grand Staircase-Escalante National Monument. These four subregions are referred to simply as Parks hereafter. For this study, the first FFPR report of the day was used to align more closely with this study's objective to forecast conditions 6-18 h in advance. While the Parks prefer that the FFPR be defined by text descriptors, Salt Lake City forecasters have assigned loosely probabilities to them as follows (Darren Van Cleave, personal communication): Not Expected (12.5%), Possible (37.5%), Probable (62.5%), and Expected (87.5%).

Figure 4.1 shows the NWS first FFPR for each day in the southwestern Utah domain when there was a flash flood reported at any location in southwestern Utah. By this metric, forecasters are appropriately forecasting for flash floods to be Probable or Expected across the region during the major monsoon periods evident in Figure 3.2 during the latter half of July 2021 and mid-August 2022. Table 4.1 summarizes the FFPR values compared to the days with and without flash flood reports. While the number of flash floods within many of the remote regions of southwestern Utah may be underestimated, ones that occur in the Parks are more likely to be reported. Table 4.1 suggests that the FFPR roughly aligns with a broad interpretation of how the public may

perceive a Possible forecast for flash floods (e.g., less likely to happen than not) and Probable (equal chances of it happening or not). The small number of days with flash floods when Not Expected or the small number of no flash flood days when Expected also align with how those would be understood by the public.

4.2 Evaluation of PWAT, CAPE, and Precipitation Forecasts

For reference, Figure 4.2 compares the averages computed from every hour during the two summers of HRRR PWAT from F00 analyses and F06, F12, and F18 forecasts. There are no perceptible differences between the forecasts and analyses and all highlight the dependence of PWAT on surface elevation. In order to focus on days when the monsoon was observed and analyzed to be active, the variations in PWAT during the 82 days during 2021 and 49 days during 2022 when flash floods were reported within southwestern Utah are shown in Figure 4.3, relative to the two-summer season average of PWAT over the southwestern Utah region. The PWAT averages of the 24-hourly forecasts available from the HRRR at lead times from 6, 12, and 18 h are compared to the averages of the 24-hourly analyses during those flash flood days. Generally, as might be expected for this parameter, the daily averages of forecasted PWAT values track closely the analyses. There are a couple days (e.g., 14 July and 16 August 2022) where the forecasts tended to have noticeably lower PWAT values than those analyzed over southwestern Utah.

Figures 4.4 and 4.5 repeat the previous two figures except for daily maximum CAPE. While all four panels exhibit the monsoonal seasonal distribution with higher CAPE values across northern Arizona and southern Utah, the CAPE forecasts are consistently lower than the CAPE analyses. As might be expected, differences in CAPE between the

analyses and forecasts tend to be larger during most events than was seen for PWAT. There are just a few cases where the CAPE was over forecasted, such as Aug 19, 2021, and September 13, 2022. The HRRR tends to have larger amount of forecasted CAPE at longer lead times likely due to the model spin up time.

Figure 4.6 compares over the two summers the daily-averaged accumulated precipitation from MRMS QPE analyses to those from the HRRR F06, F12, and F18 forecasts. The HRRR forecasts underestimate precipitation estimated from the MRMS in regions where there is adequate radar coverage (e.g., near the Promontory Point, Grand Junction, Cedar City, and Flagstaff radars) and might be more accurate in areas of poor radar coverage such as the Abajo Mountains in southeastern Utah. As the lead time decreases from 18 to 6 h, the forecasted precipitation amounts decrease as seen in Figure 4.7. Hence, it should not be surprising that the HRRR forecasts at all lead times tend to underestimate the average precipitation over southwestern Utah during flash flood days. A few exceptions exist later in the seasons (e.g., 1 September 2021 and 21 September 21 2022) where precipitation was over forecasted.

Diurnal statistics were also computed for the HRRR precipitation forecasts across southwestern Utah as seen in Figure 4.8. As expected, forecasted precipitation is much lower in magnitude than the MRMS analyses with lower amounts at shorter lead times. Figure 4.9 shows the spatial distribution of precipitation in southwestern Utah during the afternoon and early evening hours. The HRRR shows precipitation at higher elevations is stronger in the early afternoon and shifts to lower in the valleys in the evening. The HRRR under forecasted the intensity, but this shift is similar to what is estimated by the MRMS.

HRRR hourly forecasts can be combined into time-lagged ensembles to take advantage of some of the variability expected from one model run to the next. Table 4.2 illustrates two time-lagged ensembles developed to be potentially relevant for operational forecasts for the 4-h period during early afternoon when convection in this region is beginning to develop (18-21 UTC; 12-15 MDT). The "midnight" 3-h HRRR ensemble would be available to a forecaster by 6 UTC (midnight MDT) while the "early morning" ensemble would be available by 9 UTC (3 AM MDT). Hence, each ensemble set consists of 12 individual forecasts. This approach was adopted to help evaluate what might be available to a forecaster to assist in issuing flash flood watches.

Following from Figure 3.13, Figure 4.10 relates for each set of ensemble forecasts the variation in daily accumulated MRMS QPE to the ensemble CAPE and PWAT values. As before, days with very limited rainfall (domain averaged rainfall < 0.01 cm) are omitted. PWAT values in Figure 4.10a are the PWAT domain averages computed from the set of 12 ensemble members from HRRR forecasts initialized between 03-05 UTC and verifying during the 18-21 UTC (12-15 MDT) time period. Similarly, the CAPE domain averaged values in Figure 4.10a are the mean maximum CAPE computed from the same set of 12 ensemble members. As before, the size and color of each dot denotes the daily MRMS QPE. Also as before, the days when NCEI flash flood reports were made in southwestern Utah during the 2021 and 2022 seasons are shown as plus signs in Figure 4.10.

As seen in Figure 3.13, MRMS QPE amounts tend to be low either if forecasted PWAT averaged over southwestern Utah is less than 1.5 cm or maximum CAPE is less than ~350 J kg^{-1} for all days. This approximate lower CAPE threshold is consistent with the forecasted CAPE values during both seasons tending to be lower than those analyzed

as shown in earlier figures in this chapter. As PWAT and CAPE increase in the forecasts, then QPE tends to increase commensurately. There are no large differences between the time-lagged ensemble forecasts available from the midnight set (Figure 4.10a) vs those available from the early morning set (Figure 4.10b).

Table 4.3 follows the approach used in Table 3.1 and relies on the HRRR analysis thresholds of PWAT and CAPE (1.5 cm and 500 J kg^{-1}, respectively). Widespread rainfall and flash floods occur rarely when either set of time-lagged ensembles have low moisture and limited instability. When the forecasts are above those thresholds, Table 4.3 illustrates a tendency for lower CAPE forecasts when PWAT is above average from both time-lagged ensembles to result in missing more flash flood days with higher precipitation.

To relate the HRRR forecasts to the NWS forecasted FFPR (Table 4.1), PWAT and CAPE were categorized by their respective thresholds and the number of days with and without flash floods are seen in Table 4.4. If both PWAT and CAPE were under the thresholds then they were labeled as a FFPR of Not Expected, if only one was over the threshold, then these days were labeled as a FFPR of Possible. A FFPR of Probable was used for days where both thresholds were surpassed. The HRRR time lagged ensemble forecasts performed well distinguishing the probability of flash flood days occurring, comparable to the NWS FFPR for over the entire southwestern Utah domain. No designation was tried for a FFPR of Expected.

4.2 Forecasts For The Three Case Study Days

Rather than using the time-lagged ensembles as introduced in the previous section, averages of the HRRR forecasts of PWAT, CAPE, and precipitation at 6, 12, and 18 h lead

times for the duration of each case study as described in Chapter 3 are examined. These comparisons help to assess if the skill of HRRR model forecasts is related substantively to forecast lead time. Average values over the domain for each of these flash flood days are provided in the time series plots shown in Figures 4.3, 4.5, and 4.7 for PWAT, CAPE, and precipitation, respectively.

As shown in Figure 4.11, no such dependence on forecast lead time is evident for PWAT for the Springdale flood case (29 June 2021, Chapter 3.2) during the 5 h period from 18-22 UTC (12-16 MDT). One difference is that the forecasts do not catch elevated PWAT (> 2.5 cm) in western Garfield County, where a flash flood was reported across state route 12. While maximum CAPE values analyzed during the afternoon of this event were above 1000 J kg^{-1} across much of the domain (see also Figure 3.16), the forecasts only show limited areas above that value (Figure 4.12). The 18 and 6 h forecasts have higher CAPE values across much of the domain compared to the 12 h forecast

Figure 4.13 shows the hourly average precipitation from the 18, 12, and 6-h HRRR forecasts relative to that from the MRMS (previously shown in Figure 3.21). As discussed previously, the MRMS shows several areas of high average hourly precipitation running north and south over Zion National Park. All of the HRRR forecasts underestimate the precipitation across the domain during this afternoon. As shown in Figure 4.7, the areal averaged precipitation for the entire day forecasted at the three lead times were roughly half of those analyzed by the MRMS.

Returning to the Cedar City flood day (26 July 2021) discussed in Chapter 3.3, widespread monsoonal moisture was analyzed over the 7 h period from 12-15 MDT (Figure 4.14). Lower elevations in the domain are analyzed to have 2.5 - 3.0 cm PWAT values,

with much of the upper elevations still over 1.5 cm. All of the forecasts predict large amounts of PWAT for this afternoon as well. The analysis and forecast of CAPE for the event are shown in Figure 4.15. The analysis shows large areas of CAPE over 2000 J kg^{-1} with the highest values southwest of Cedar City. The HRRR under forecasted CAPE overall, but the afternoon CAPE values increased with shorter forecast lead times.

When averaged over the day and over the entire domain (Figure 4.7), the HRRR precipitation forecasts are roughly a third of the MRMS average precipitation. Averaged over the time period when precipitation was heaviest in the Cedar City area (Figure 4.16), the HRRR forecasts show much smaller amounts than analyzed by the MRMS.

Returning to the values of PWAT and CAPE averaged over the entire domain and day shown in Figures 4.3 and 4.5 respectively, analyzed and forecasted PWAT was elevated while the analyzed (forecasted) CAPE was above (below) the 500 J kg^{-1} threshold for the Capitol Reef flash flood. Further, precipitation forecasts (Figure 4.7) were near 0.1 cm for the day suggesting not much potential for storm initiation on this day.

During the afternoon period of the Capitol Reef event (11-18 MDT), the general tendency for higher PWAT and CAPE to be over the eastern third of the domain is generally captured by the forecast (Figures 4.17 and 4.18) although again the forecast CAPE values are much lower than those analyzed. With the larger distance from the KICX radar, the location of heavy precipitation near Capitol Reef analyzed by the MRMS may be underestimated. However, the HRRR precipitation forecasts clearly underestimate the precipitation across the entire domain including the eastern half of the domain (Figure 4.19). The precipitation from the event was very light (Figure 4.19).

Examining these three cases helps to reinforce that HRRR precipitation forecasts at lead times from 6-18 h are not useful for identifying subsequent afternoon periods of localized or regional heavy rainfall events. Compensating for the known low CAPE bias of HRRR model forecasts (Evans et al. 2018; MacDonald and Nowotarski 2023) is likely possible such that keying on periods of higher CAPE and PWAT may be useful for such purposes.

	Zion National Park		Bryce Canyon National Park		Capitol Reef National Park		Grand Staircase-Escalante NM	
Flash Flood Potential Rating (FFPR)	*NFF*	*FF*	*NFF*	*FF*	*NFF*	*FF*	*NFF*	*FF*
Expected	1	9	1	3	1	8	2	7
Probable	24	25	16	29	24	32	20	31
Possible	31	15	54	24	44	14	38	14
Not Expected	104	7	89	0	91	2	100	4

Table 4.1: Number of days when flash flood occurred (FF) or when no flash flood occurred (NFF) for each government entity in the southwestern Utah domain based upon the SLC NWS WFO FFPR during the 2021 and 2022 monsoon seasons.

	HRRR Initialization Time	FCST Hours			
Midnight	3	15	16	17	18
	4	14	15	16	17
	5	13	14	15	16
Early Morning	6	12	13	14	15
	7	11	12	13	14
	8	10	11	12	13
Valid Times (UTC)		**18**	**19**	**20**	**21**

Table 4.2: HRRR data that was utilized to make the time lagged ensembles as seen in Figure 4.9.

Midnight Forecast

Analysis \ Forecast	PWAT < 1.5 cm CAPE < 500 J kg^{-1}				PWAT ≥ 1.5 cm CAPE < 500 J kg^{-1}				PWAT < 1.5 cm CAPE ≥ 500 J kg^{-1}				PWAT ≥ 1.5 cm CAPE ≥ 500 J kg^{-1}			
	NFF		*FF*		*NFF*		*FF*		*NFF*		*FF*		*NFF*		*FF*	
	Days	*PPT*	*Days*	*PPT*	*Days*	*PPT*	*Days*	*PPT*	*Days*	*PPT*	*Days*	*PPT*	*Days*	*PPT*	*Days*	*PPT*
PWAT < 1.5 cm CAPE < 500 J kg^{-1}	85	0.0	1	0.01	2	0.06										
PWAT ≥ 1.5 cm CAPE < 500 J kg^{-1}	6	0.03	1	0.1	43	0.05	5	0.09					4	0.1	2	0.92
PWAT < 1.5 cm CAPE ≥ 500 J kg^{-1}									1	0.05						
PWAT ≥ 1.5 cm CAPE ≥ 500 J kg^{-1}					7	0.15	8	0.21					13	0.26	38	0.36

Early Morning Forecast

Analysis \ Forecast	PWAT < 1.5 cm CAPE < 500 J kg^{-1}				PWAT ≥ 1.5 cm CAPE < 500 J kg^{-1}				PWAT < 1.5 cm CAPE ≥ 500 J kg^{-1}				PWAT ≥ 1.5 cm CAPE ≥ 500 J kg^{-1}			
	NFF		*FF*		*NFF*		*FF*		*NFF*		*FF*		*NFF*		*FF*	
	Days	*PPT*	*Days*	*PPT*	*Days*	*PPT*	*Days*	*PPT*	*Days*	*PPT*	*Days*	*PPT*	*Days*	*PPT*	*Days*	*PPT*
PWAT < 1.5 cm CAPE < 500 J kg^{-1}	86	0.0	1	0.01	1	0.07										
PWAT ≥ 1.5 cm CAPE < 500 J kg^{-1}	9	0.02	1	0.1	41	0.05	5	0.09					3	0.15	2	0.92
PWAT < 1.5 cm CAPE ≥ 500 J kg^{-1}											1	0.05				
PWAT ≥ 1.5 cm CAPE ≥ 500 J kg^{-1}					11	0.2	10	0.2					9	0.24	36	0.37

Table 4.3: HRRR midnight and early morning time lagged ensembles compared to the analyses for the counts of days with no flash floods (NFF) and days with flash floods (FF) across southwestern Utah binned relative to CAPE and PWAT thresholds. Average daily precipitation (PPT, cm) across southwestern Utah during these sets of days also shown.

	HRRR Midnight Forecast		HRRR Early Morning Forecast	
Flash Flood Potential	NFF	FF	NFF	FF
Probable	17	40	12	38
Possible	52	14	53	16
Not Expected	91	2	95	2

Table 4.4: Counts of days with no flash floods (NFF) and days with flash floods (FF) in the southwestern Utah domain relative to the HRRR time lagged ensemble forecasts (Figure 4.10, Table 4.3). HRRR ensemble forecasts were categorized by the approximate two season averages to compare to the NWS FFPR discussed in the text.

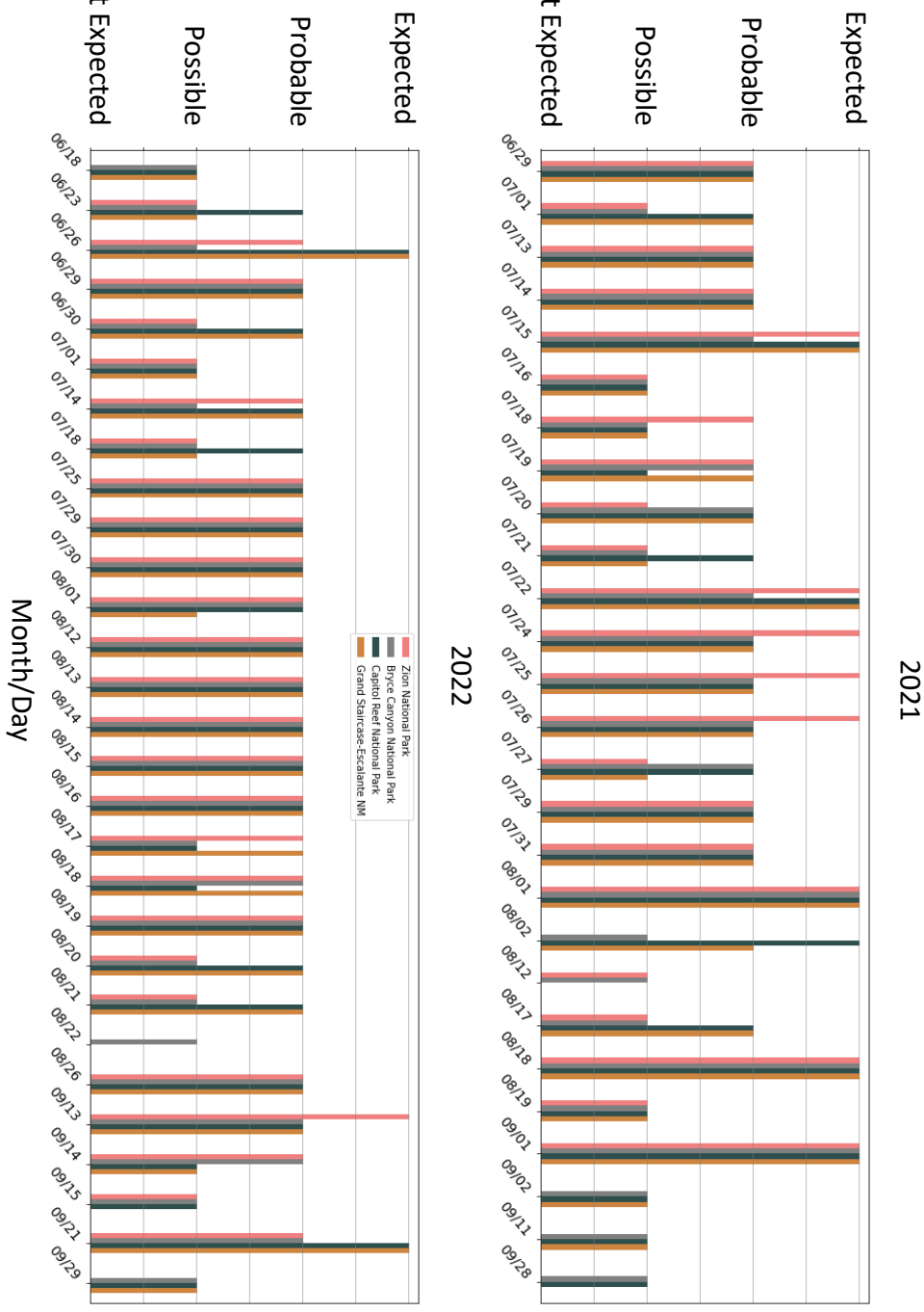

Figure 4.1: NWS issued FFPR for the 4 government entities in the southwestern Utah domain for days with a NCEI flash flood report.

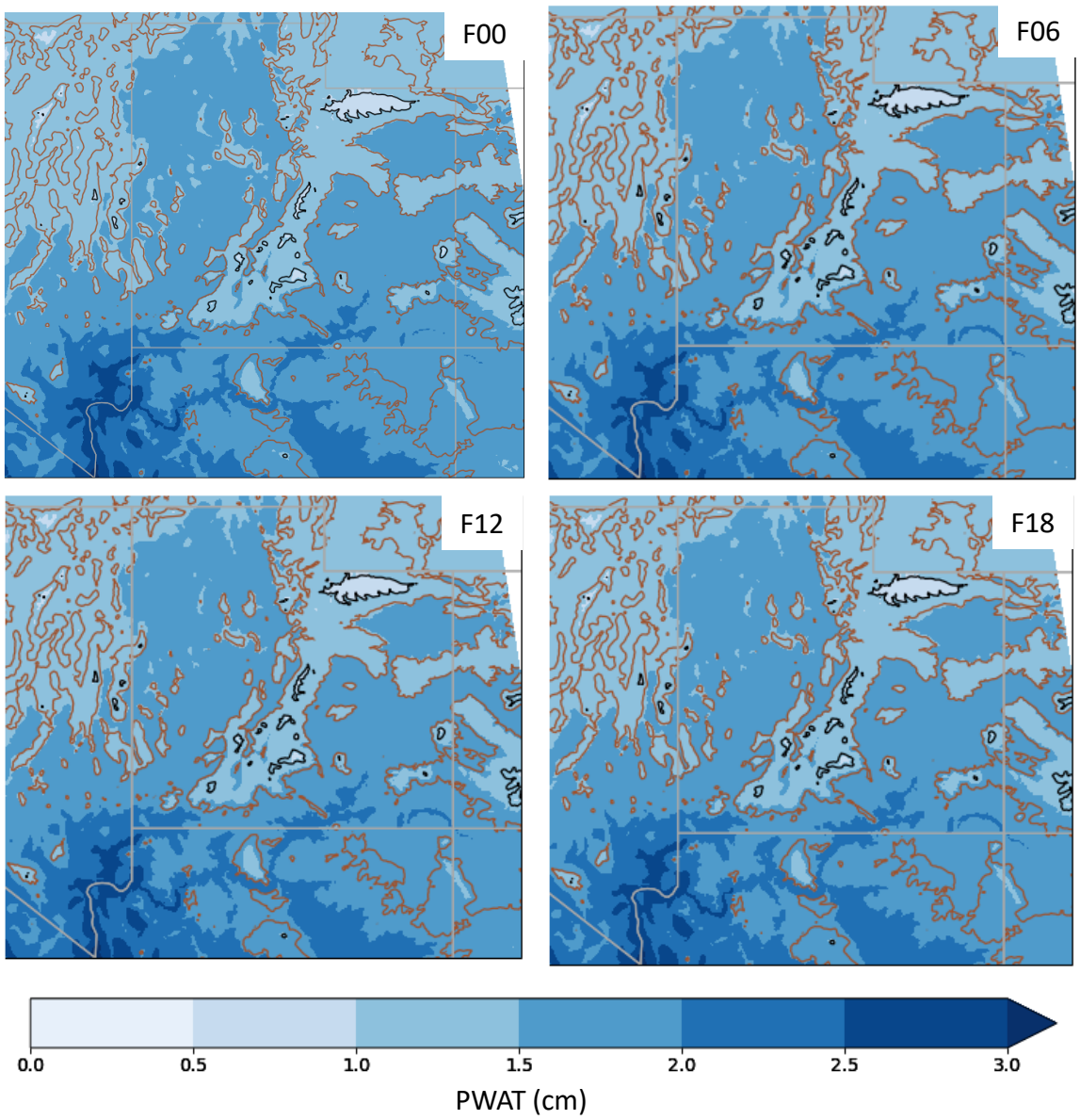

Figure 4.2: Mean HRRR PWAT (cm) during the 2021 – 2022 monsoon seasons from HRRR F00 analyses and F06, F12, and F18 forecasts. Heavy solid lines denote terrain elevation at 2000m (brown) and 3000m (black).

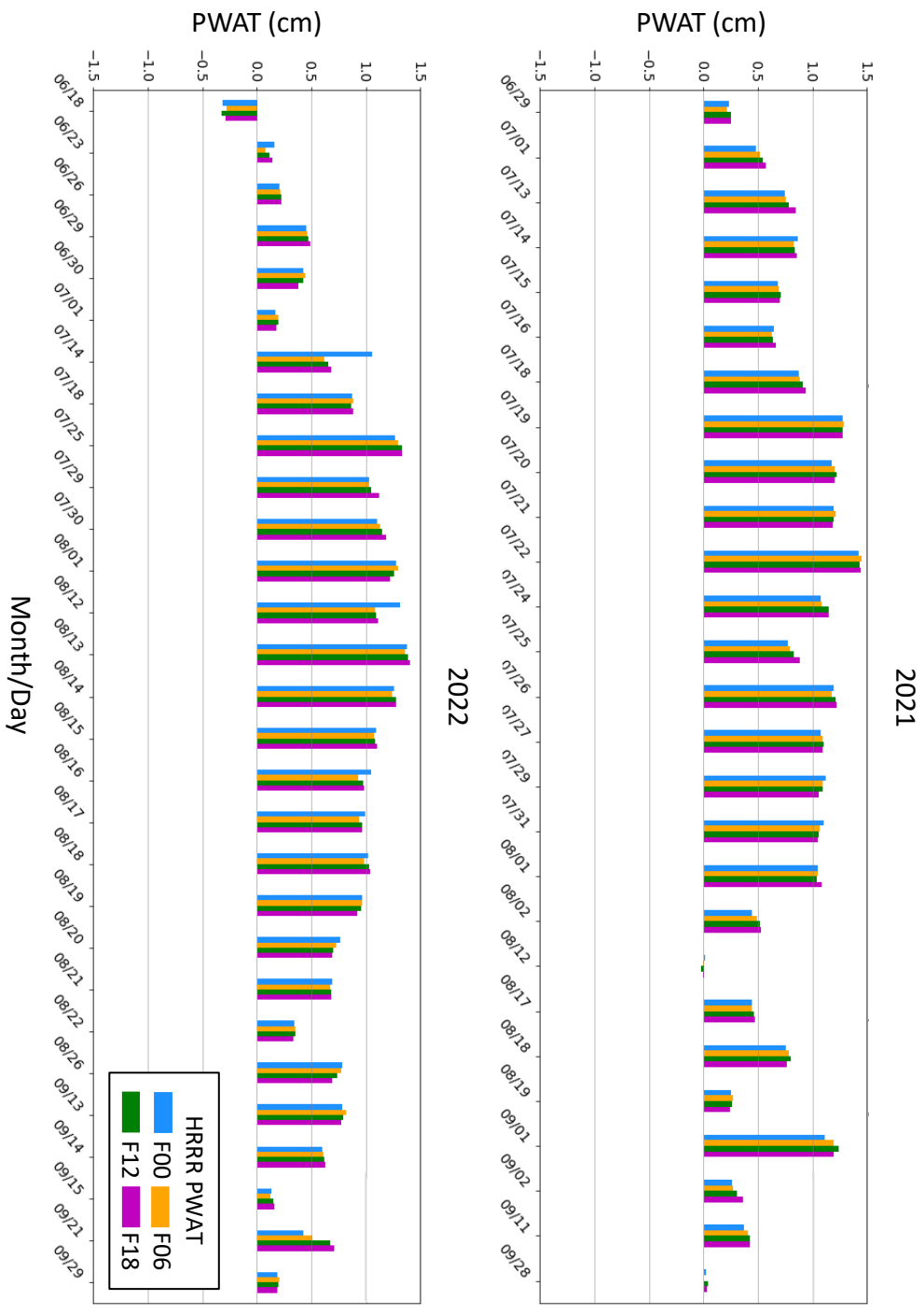

Figure 4.3: Departure from the approximate two season average of PWAT (cm) over southwestern Utah for days with a NCEI flash flood report from the HRRR F00 analyses and F06, F12, and F18 forecasts.

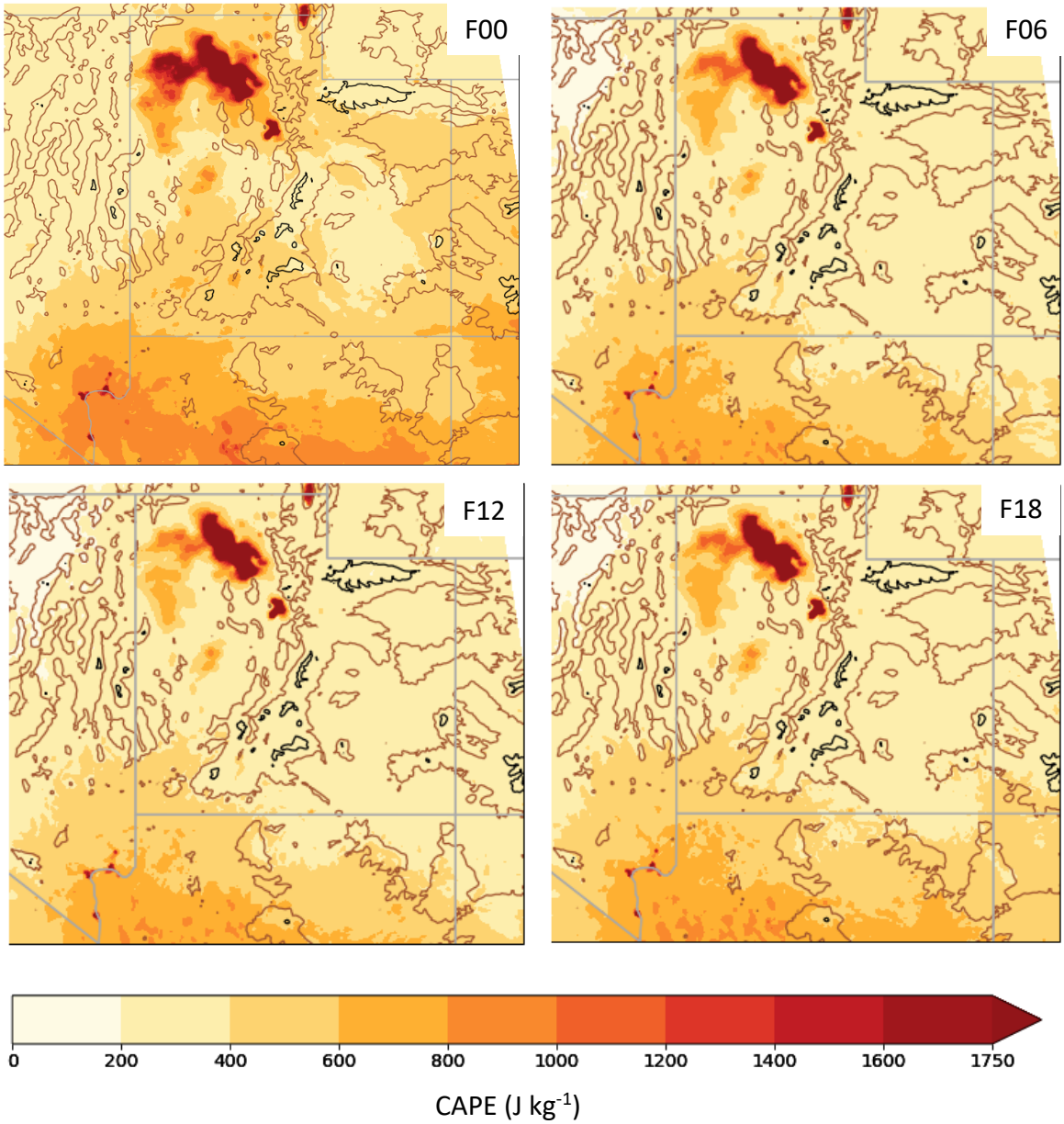

Figure 4.4: Mean HRRR daily maximum CAPE (J kg^{-1}) during the 2021 – 2022 monsoon seasons from HRRR F00 analyses and F06, F12, and F18 forecasts. Heavy solid lines denote terrain elevation at 2000m (brown) and 3000m (black).

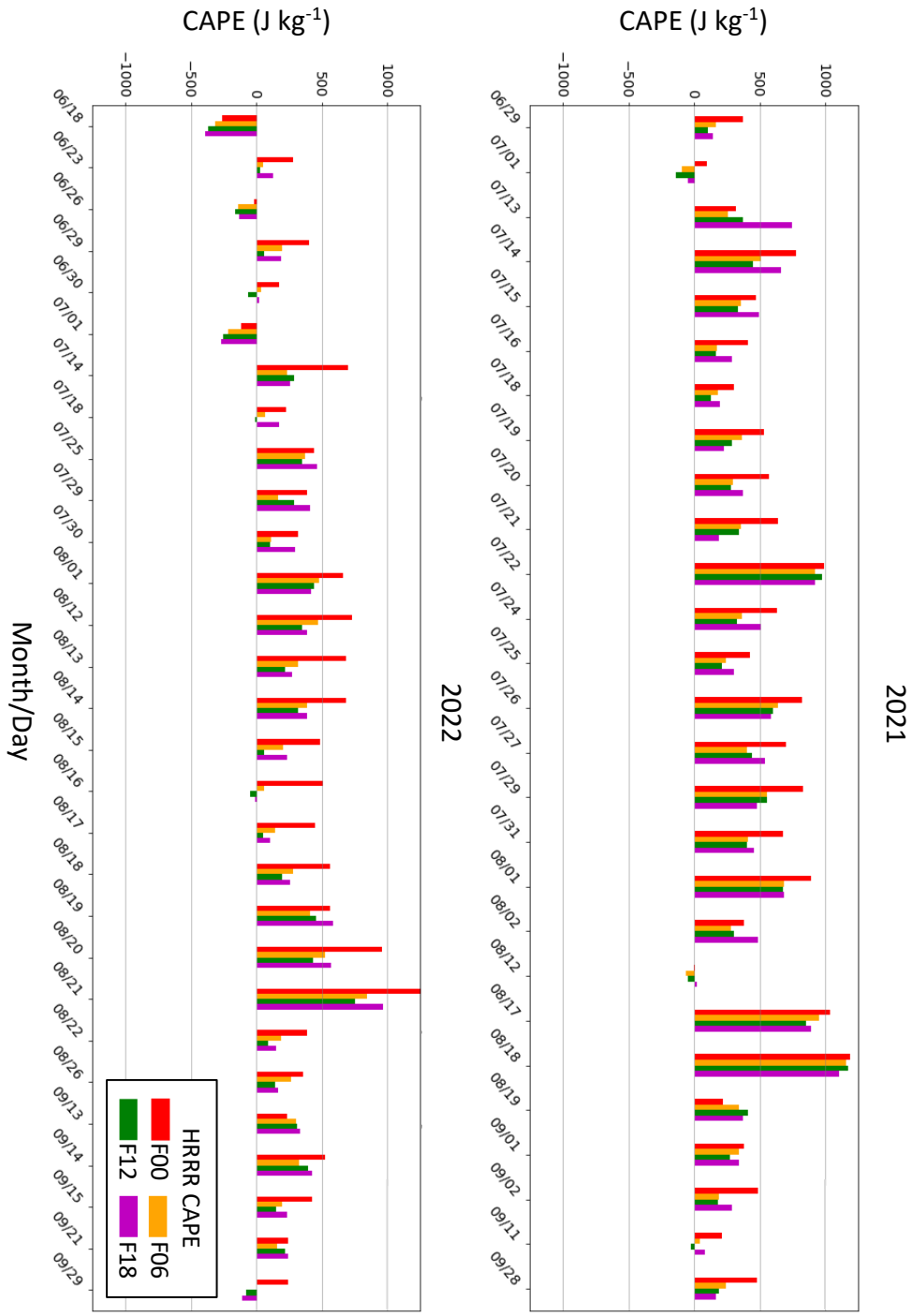

Figure 4.5: Departure from the approximate two season average of maximum CAPE (J kg^{-1}) over southwestern Utah for days with a NCEI flash flood report for HRRR F00 analyses and F06, F12, and F18 forecasts

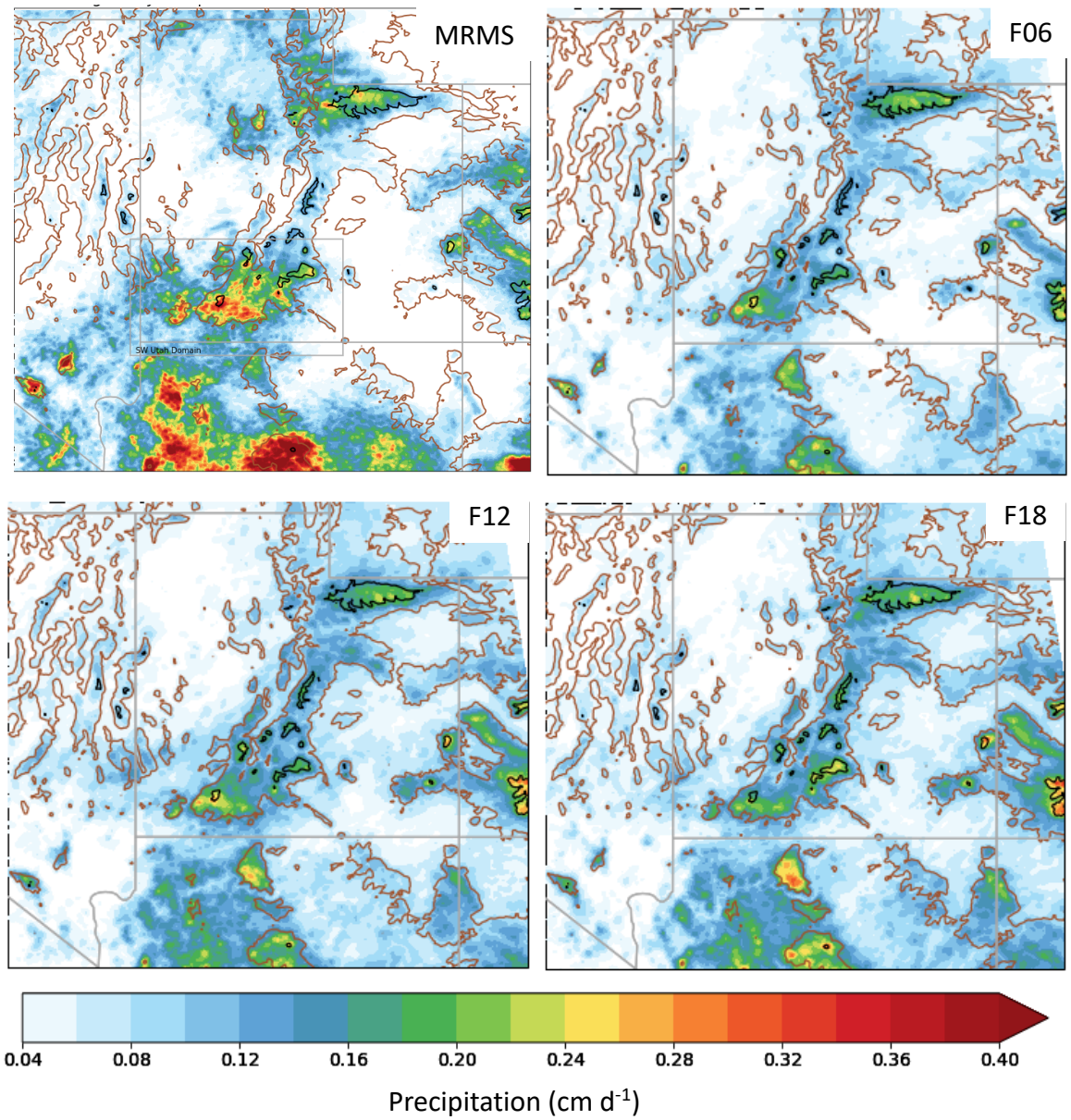

Figure 4.6: Average daily precipitation (cm d^{-1}) during the 2021 – 2022 monsoon seasons from the MRMS QPE and HRRR F06, F12, and F18 forecasts. Heavy solid lines denote terrain elevation at 2000m (brown) and 3000m (black).

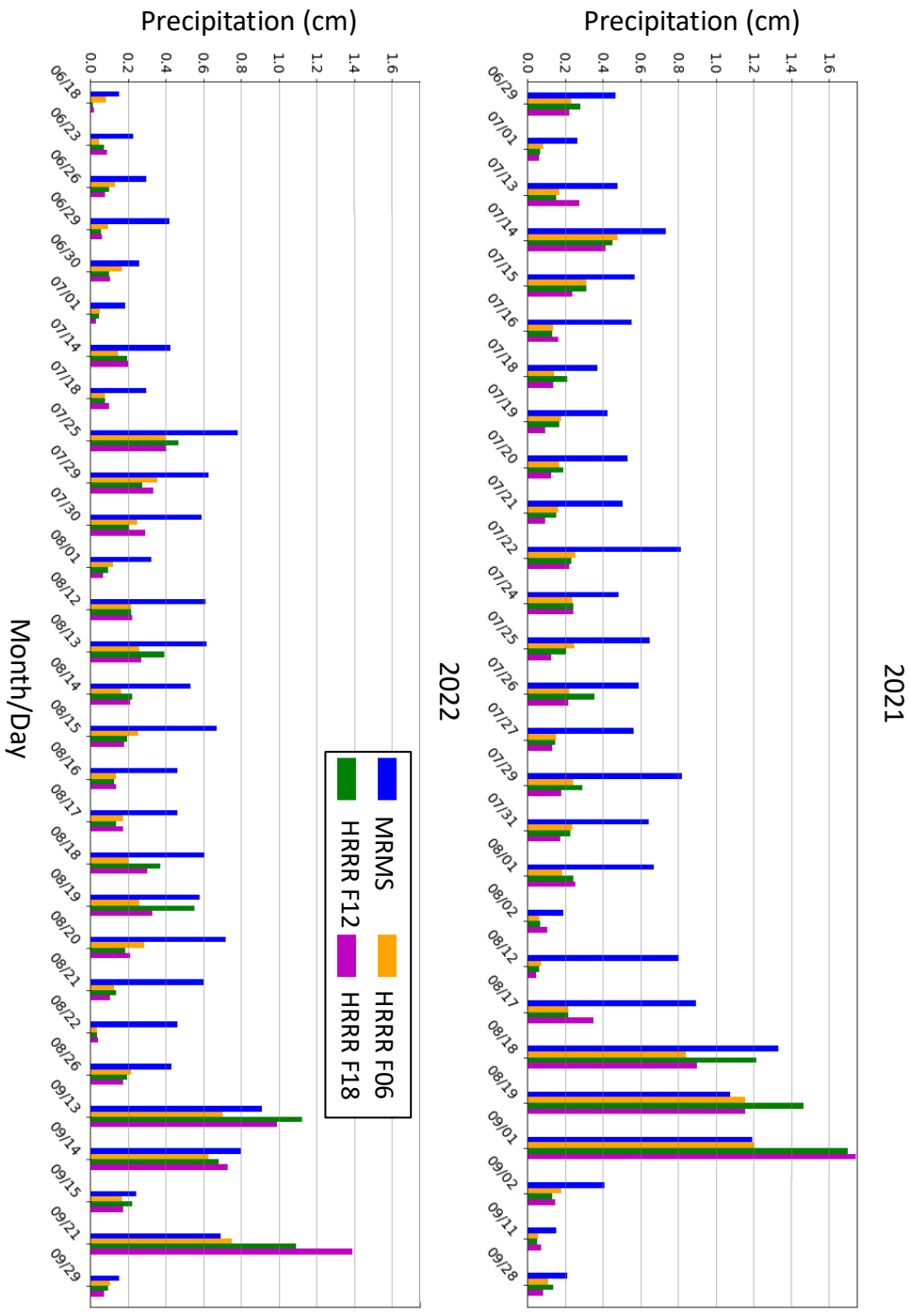

Figure 4.7: Average accumulated precipitation (cm) over southwestern Utah of MRMS and HRRR F06, F12, and F18 for days with a NCEI flash flood report.

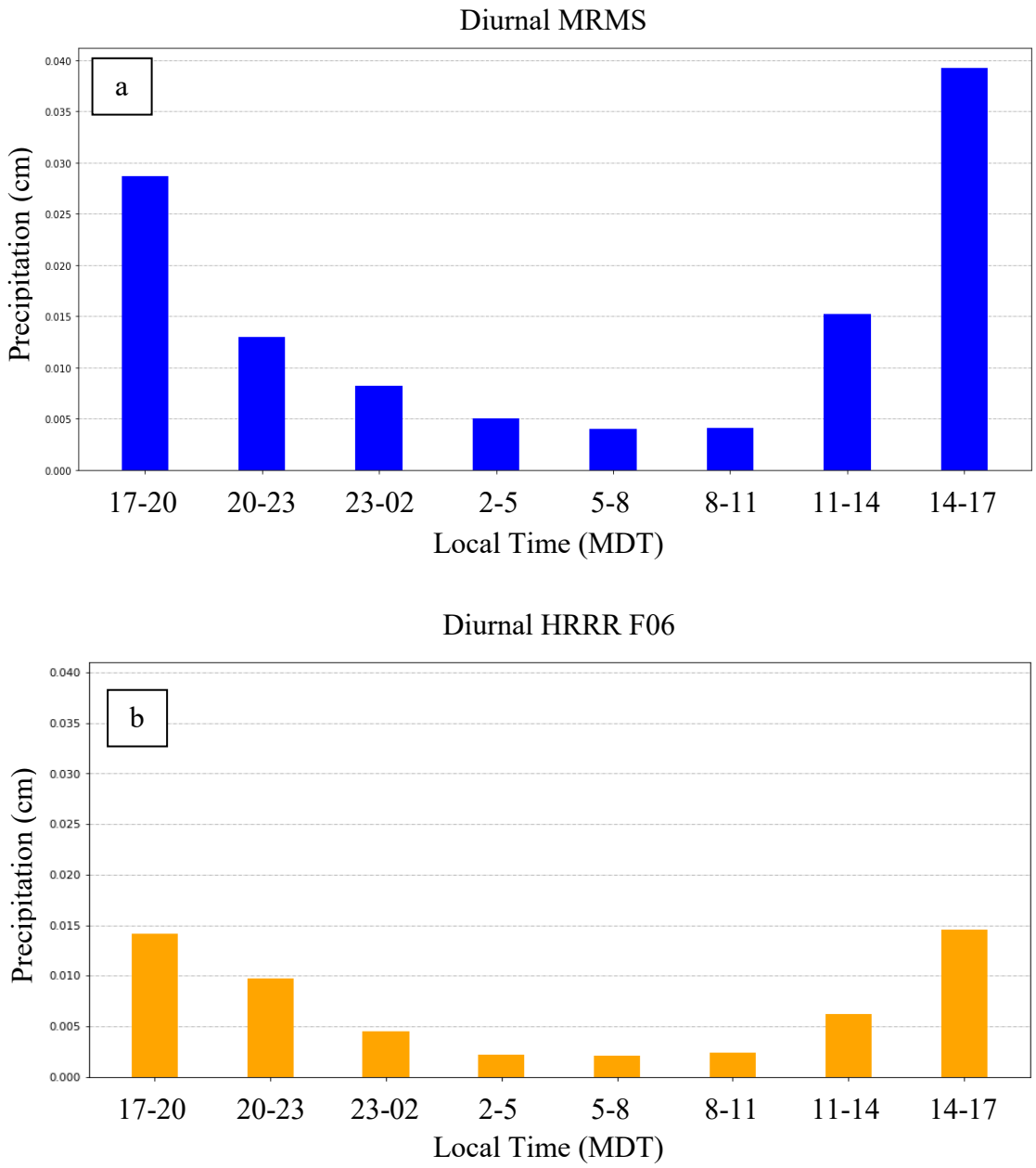

Figure 4.8: 3-h accumulated precipitation (cm) averaged during the 2021 – 2022 monsoon seasons and over the southwestern Utah domain for a) MRMS analyses; b) F06 HRRR forecasts; c) F12 HRRR forecasts; d) F18 HRRR forecasts.

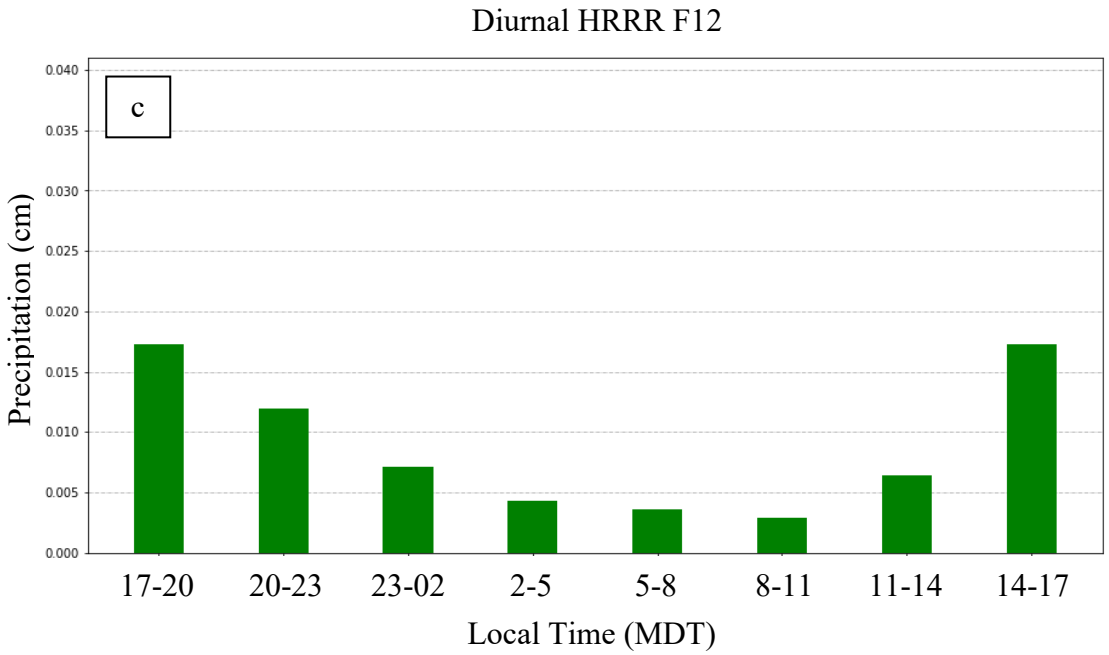

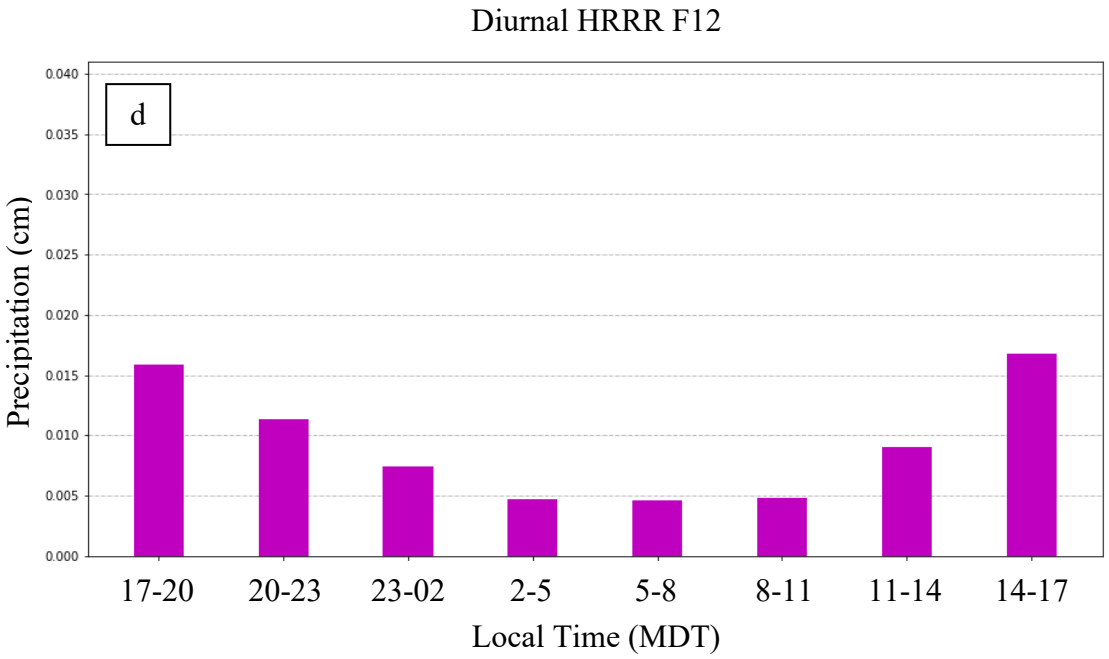

Figure 4.8 continued

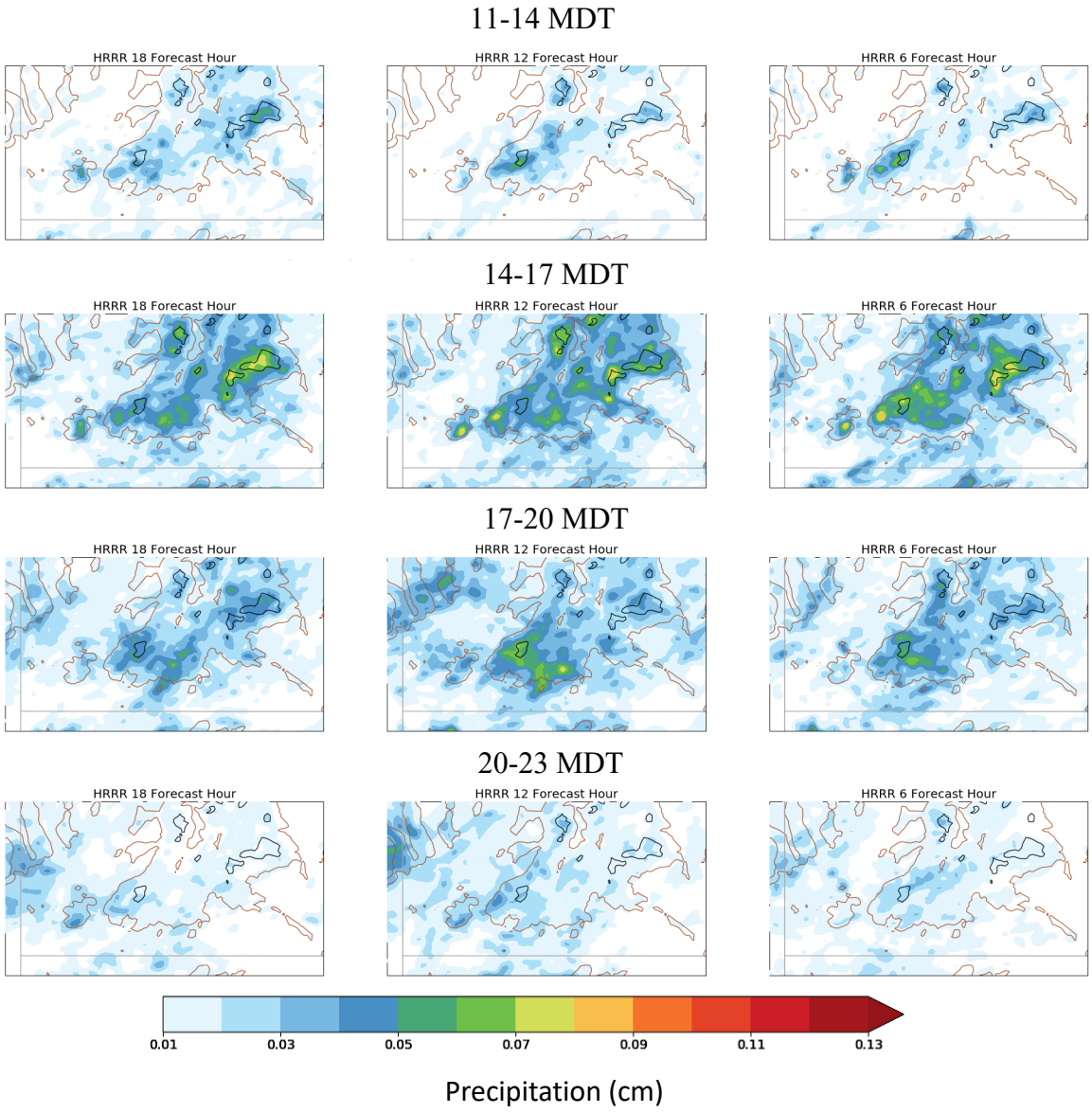

Figure 4.9: HRRR 3-h accumulated precipitation (cm) averaged during the 2021 – 2022 monsoon seasons of at F18, F12, and F06 lead times.

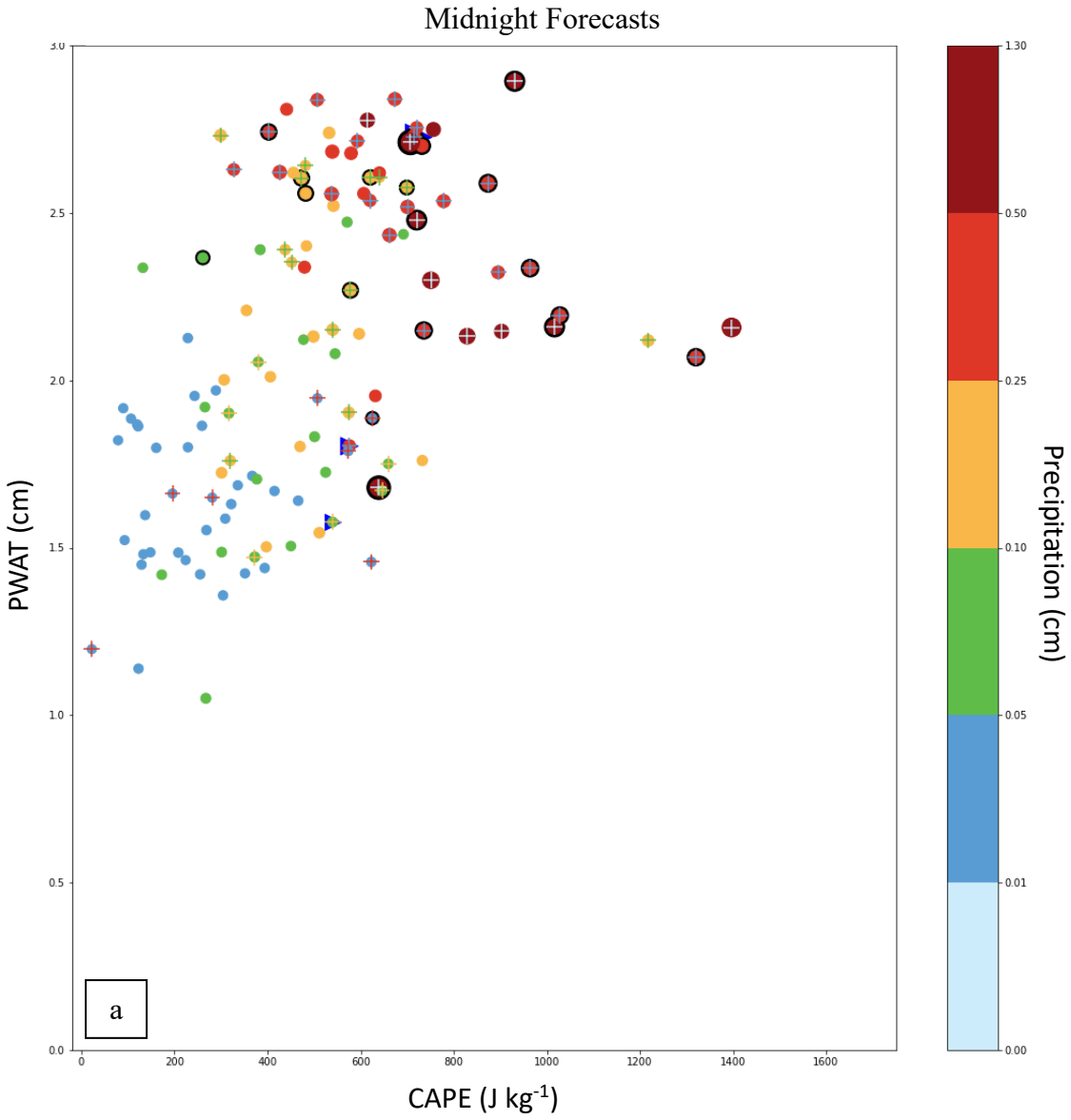

Figure 4.10: Daily maximum CAPE (J kg^{-1}) and PWAT (cm) from 18 – 21 UTC (12 – 15 MDT) for southwestern Utah domain with the color/size denoting daily MRMS precipitation (cm). (a) Midnight (3-5 UTC) time-lagged ensemble forecasts (b) Early Morning (6 – 8 UTC) time-lagged ensemble forecasts. Plus symbols denote days with at least one flash flood report. Blue sideways triangles are under the three case study days.

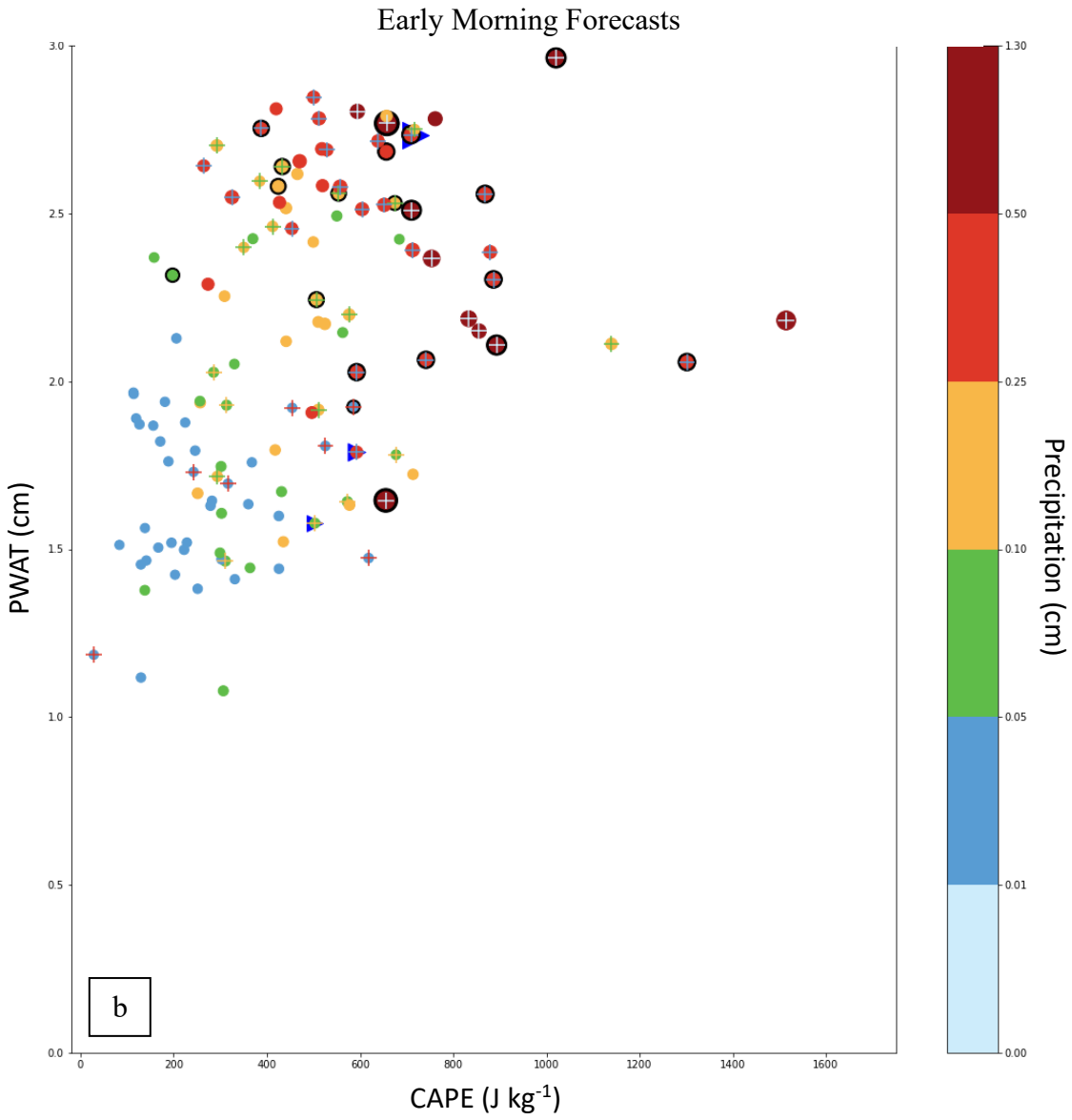

Figure 4.10 continued.

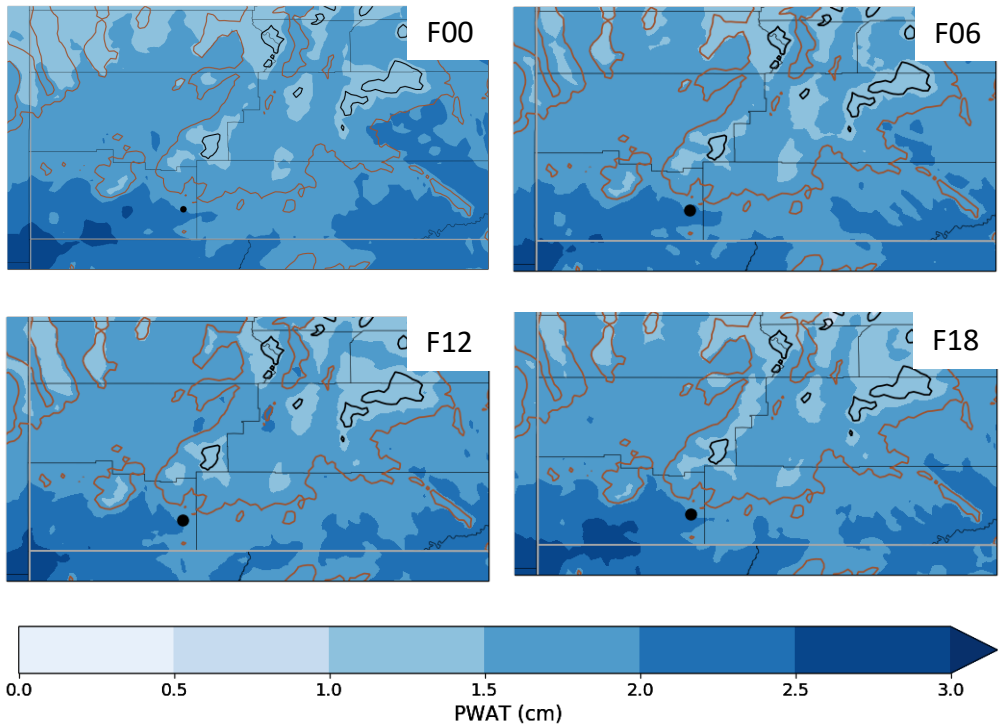

Figure 4.11: Mean HRRR PWAT (cm) from the F00 analysis, F06, F12, & F18 hour forecasts during the period 12 – 16 MDT 29 June 2021.

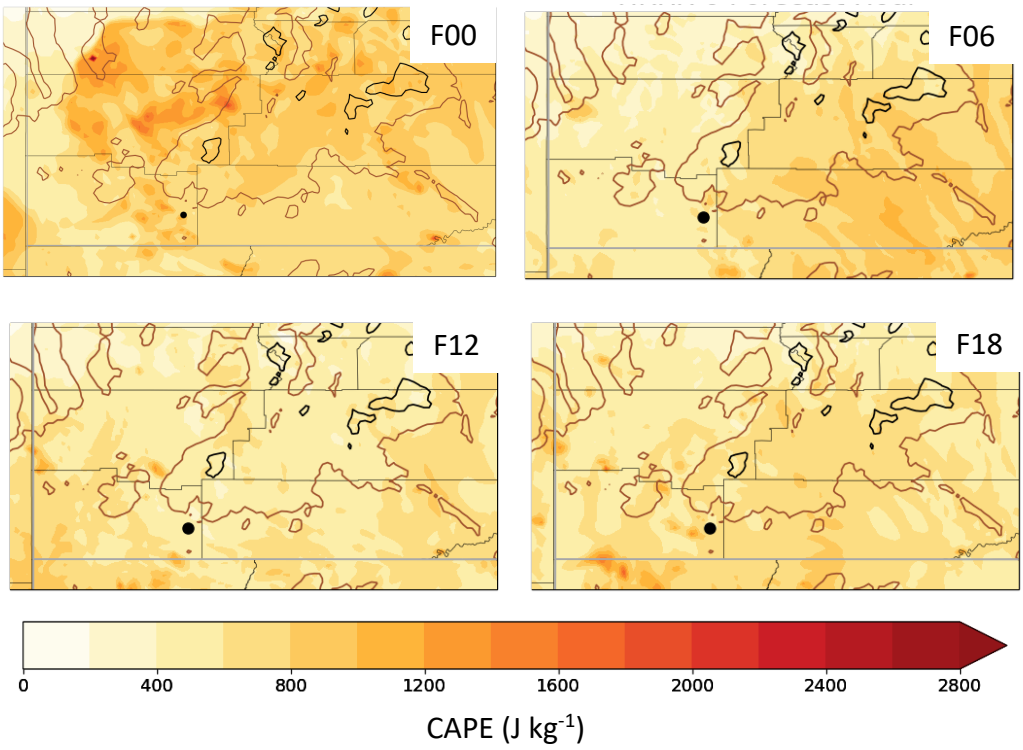

Figure 4.12: Maximum HRRR CAPE (J kg^{-1}) from the F00 analysis, F06, F12, & F18 hour forecasts during the period 12 – 16 MDT 29 June 2021.

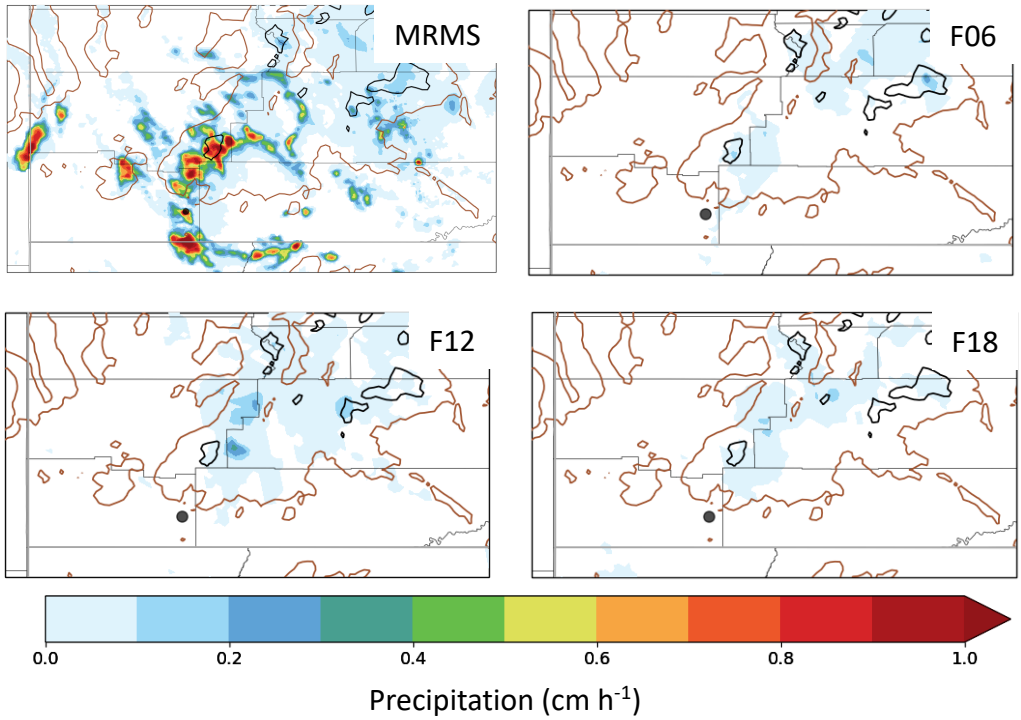

Figure 4.13: MRMS QPE and HRRR average hourly accumulated precipitation (cm h^{-1}) for HRRR F06, F12, & F18 forecasts during the period 12 – 16 MDT 29 June 2021.

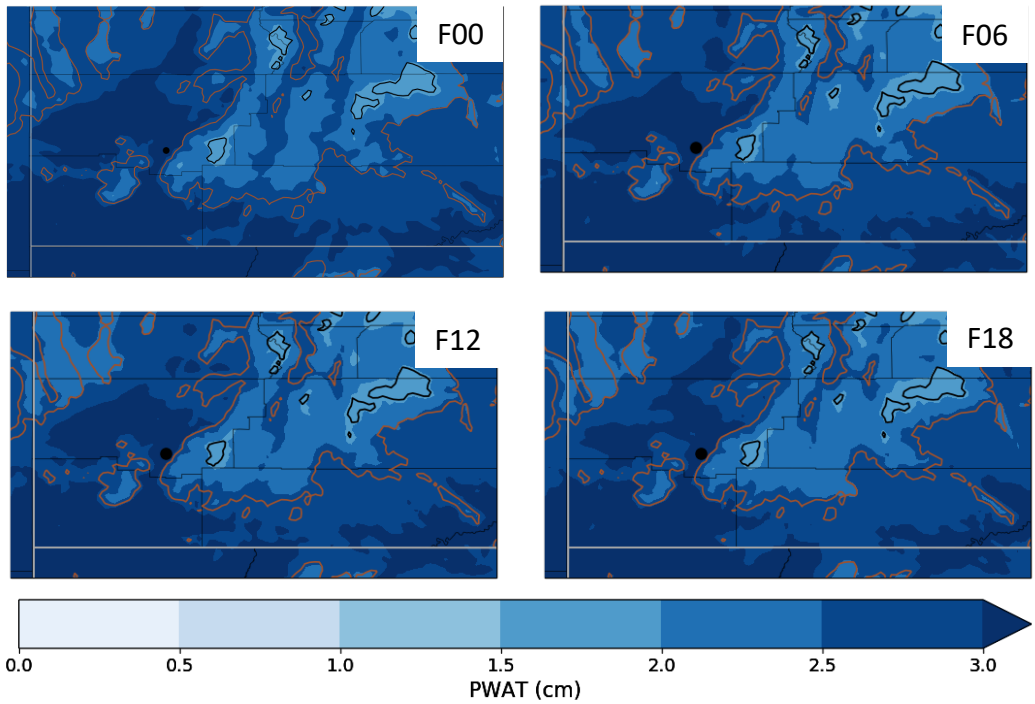

Figure 4.14: Mean HRRR PWAT (cm) from the F00 analysis, F06, F12, & F18 hour forecasts during the period 12 – 18 MDT 26 July 2021.

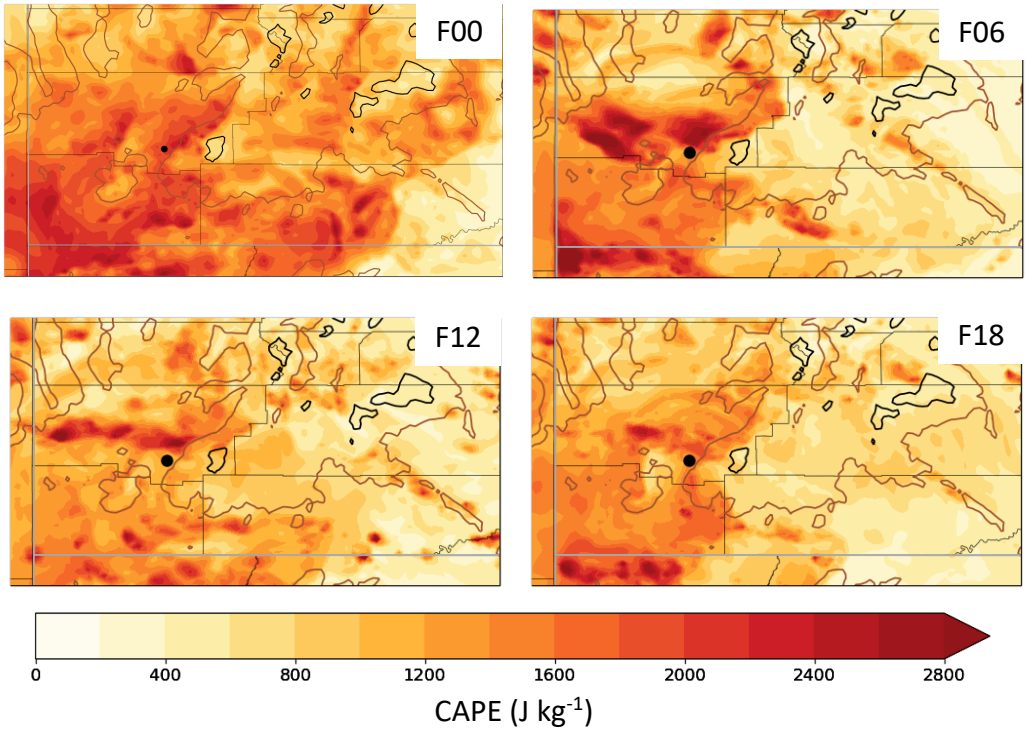

Figure 4.15: Maximum HRRR CAPE (J kg^{-1}) from the F00 analysis, F06, F12, & F18 hour forecasts during the period 12 – 18 MDT 26 July 2021.

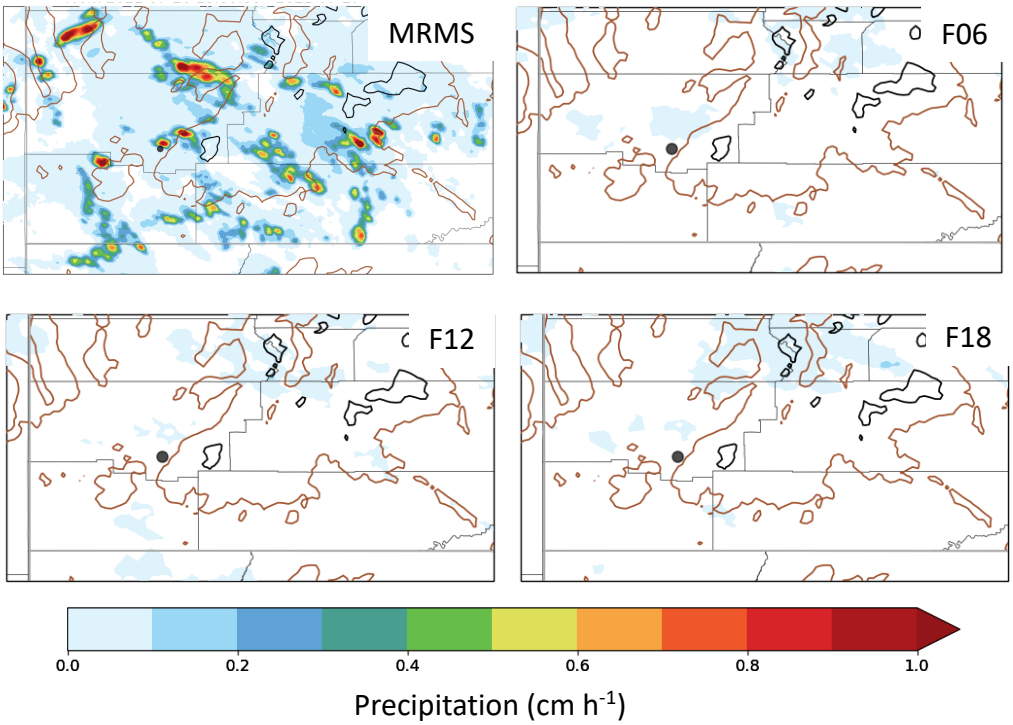

Figure 4.16: MRMS QPE and HRRR average hourly accumulated precipitation (cm h^{-1}) for HRRR F06, F12, & F18 forecasts during the period 12 – 18 MDT 26 July 2021.

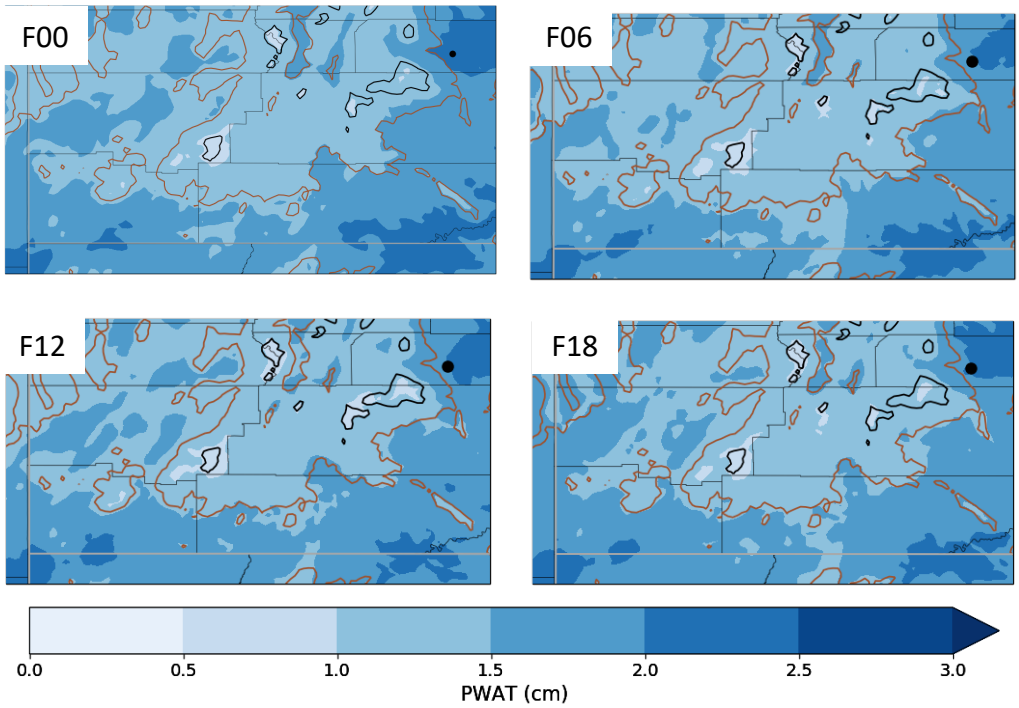

Figure 4.17: Mean HRRR PWAT (cm) from the F00 analysis, F06, F12, & F18 hour forecasts during the period 11 – 18 MDT 23 June 2022.

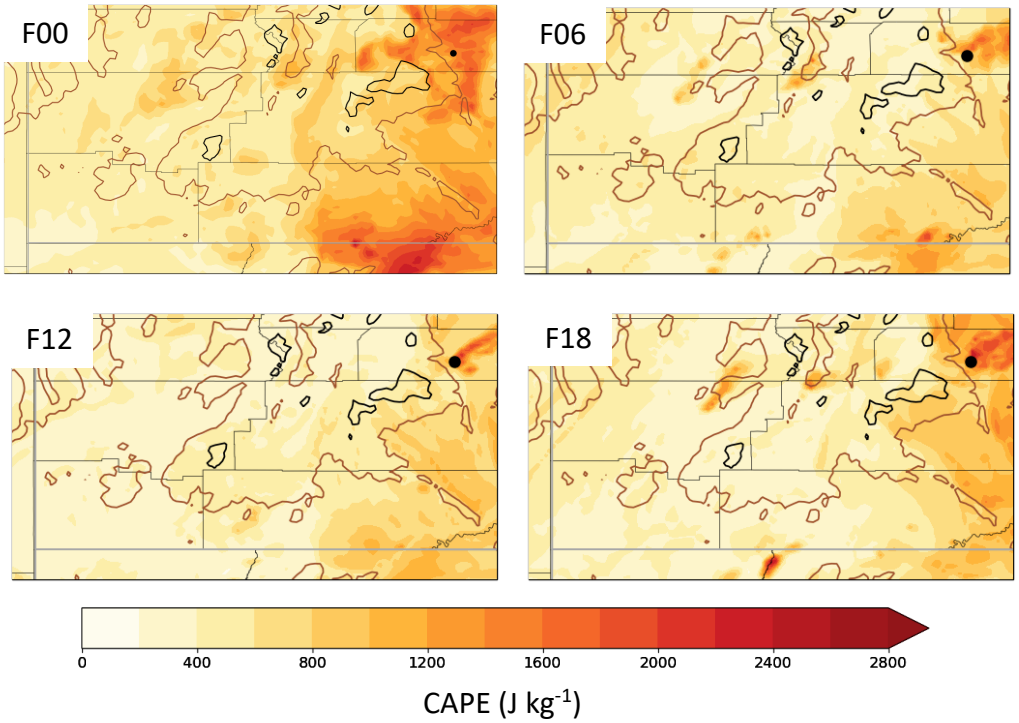

Figure 4.18: Maximum HRRR CAPE (J kg^{-1}) from the F00 analysis, F06, F12, & F18 hour forecasts during the period 11 – 18 MDT 23 June 2022.

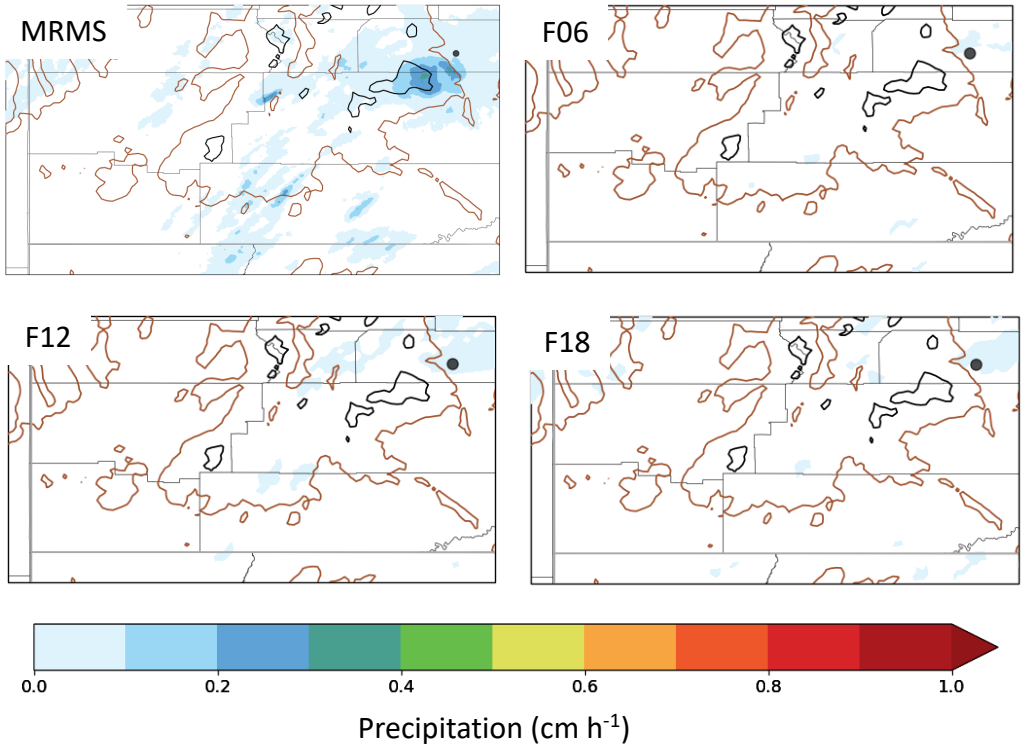

Figure 4.19: MRMS QPE and HRRR average hourly accumulated precipitation (cm h^{-1}) for HRRR F06, F12, & F18 forecasts during the period 11 – 18 MDT 23 June 2022.

CHAPTER 5

SUMMARY

The North American Monsoon brings extreme precipitation to Mexico, the southwestern United States, and at times southern Utah. Occasionally, fatalities and heavy damage can result from these extreme precipitation events often leading to flash floods. The monsoon seasons of 2021 & 2022 in southwestern Utah were two of the most active on record bringing many flash floods that would make 2021 the highest and 2022 the third-highest number of flash flood warnings during the past 36 years. As discussed in Chapter 1, much work has examined the NAM in Arizona and New Mexico, but the impact across its northern extent, including Utah, has not received as much attention. This study adapted similar techniques to those used to examine extreme summer precipitation events in Arizona by Mazon et al. (2016) and Yang et al. (2019) in order to examine the 2021 and 2022 monsoon season in southwestern Utah.

The analysis of the two seasons, as well as the three case studies, was focused on identifying the conditions conducive to heavy precipitation in southwestern Utah that may be conducive to flash floods in the areas that experience them. Intense rainfall over the sparsely visited elevated plateaus or desert floors of the region will have less impact than those along the region's plateau edges where streamflow is constricted, previous wildfires have affected soil permeability, or where people congregate for recreational activities.

This research helped to evaluate the usefulness of the predominantly radar-based precipitation analyses available from the MRMS. While precipitation far from the KICX radar is likely underestimated, rainfall estimates from the MRMS across southwestern Utah are likely reasonable. Estimates of rainfall and convection from station rain gauges, NLDN lightning, and MRMS QPE over the two seasons show the expected dependence on the underlying terrain with convection initiated at higher elevations during the afternoon. Also, as expected, widespread heavy summer rainfall events in southwestern Utah generally occur when the PWAT and CAPE are higher than typically observed in the region. The short time lag between maximum CAPE during the early afternoon followed by maximum lightning and precipitation is also to be expected in this region.

The spatial and temporal variations of rainfall, lightning, precipitation, moisture availability, and instability were examined during the 2021 and 2022 monsoon seasons. A closer study of three flash flood days helped illustrate the diversity and challenge to understand the details on convection in complex terrain beyond simply moisture availability and instability. For example, the Springdale and Capitol Reef flash flood days exhibited low-moderate PWAT and CAPE with considerable veering winds with height in the former and southwest unidirectional flow in the latter case. On the Cedar City flash flood day, PWAT and CAPE were unusually high relative to other days during the two summers with unidirectional flow from the southeast. Although the three flash flood days had differing environmental conditions and wind profiles, every case study resulted in storms with greater than composite reflectivity above 60 dBz and heavy precipitation. This would put all three cases near the 90th percentile of flash flood producing storms in the region estimated by Smith et al. (2019).

During the two monsoon seasons, the HRRR generally under forecasted CAPE and greatly under forecasted precipitation, similar to other findings of HRRR forecasted CAPE and precipitation for convective events (Evans et al. 2018; Yue and Gebremichael 2020). Counterintuitively, HRRR CAPE forecasts at lead times of 12-18 h tended to be higher and closer to those observed than at shorter range (F06). Although HRRR forecasts captured the general precipitation diurnal cycle, the model greatly under forecasts daytime precipitation.

Further research is needed to understand the accuracy of the HRRR analysis and why the HRRR is under forecasting CAPE in this region. The HRRR likely would improve for forecasting situational awareness parameters (FFPR) if other convective parameters, such as wind shear, were also used to help constrain the extreme precipitation. The HRRR is planned to be phased out of operation and replaced with an ensemble forecast system, run similar to the HRRR, called the Rapid Refresh Forecast System (RRFS; Dowell et al. 2022). It will need to be studied if this bias continues with the ensemble-based model. Other studies have suggested that the local bias of CAPE within the HRRR might be best handled by making adjustments on the regional scale (Evans et al. 2018, Macdonald et al. 2023).

Meyer and Jin (2016, 2017) and Zhang (2023) among many other studies have examined current and future trends in the NAM on the basis of downscaled global climate simulations. Since global and regional climate models have difficulty simulating precipitation and energy budget terms over limited domains such as southwestern Utah (a fraction typically of a general circulation model grid cell), downscaling proxy indicators

of monsoonal strength (e.g., CAPE and PWAT as used in this study) may provide an approach to evaluate future changes in the NAM's northern extent.

REFERENCES

Adams, D. K., and A. C. Comrie, 1997: The North American monsoon. *Bull. Amer. Meteor. Soc.*, **78**, 2197–2213, https://doi.org/10.1175/1520-0477(1997)078<2197:TNAM>2.0.CO;2.

Adams, D. K., and E. P. Souza, 2009: CAPE and Convective Events in the Southwest during the North American Monsoon. *Mon Weather Rev*, **137**, 83–98, https://doi.org/10.1175/2008MWR2502.1.

Blaylock, B. K., and J. D. Horel, 2020: Comparison of Lightning Forecasts from the High-Resolution Rapid Refresh Model to Geostationary Lightning Mapper Observations. *Weather Forecast*, **35**, 401–416, https://doi.org/10.1175/WAF-D-19-0141.1.

Boos, W. R., and S. Pascale, 2021: Mechanical forcing of the North American monsoon by orography. *Nature 2021 599:7886*, **599**, 611–615, https://doi.org/10.1038/s41586-021-03978-2.

CBS News, 2021: Hiker still missing after she was stranded by torrential rainfall in Utah - CBS News. https://www.cbsnews.com/news/zion-hiker-lost-jetal-agnihotri-dallas-cars-submerged-as-floods-hit-us/ (Accessed May 11, 2023).

Doswell, C. A., H. E. Brooks, and R. A. Maddox, 1996: Flash Flood Forecasting: An Ingredients-Based Methodology in: Weather and Forecasting Volume 11 Issue 4 (1996). *Weather Forecast*, 560–581. https://journals.ametsoc.org/view/journals/wefo/11/4/1520-0434_1996_011_0560_fffaib_2_0_co_2.xml (Accessed May 10, 2023).

Dougherty, K. J., J. D. Horel, and J. E. Nachamkin, 2021: Forecast Skill for California Heavy Precipitation Periods from the High-Resolution Rapid Refresh Model and the Coupled Ocean–Atmosphere Mesoscale Prediction System. *Weather Forecast*, **36**, 2275–2288, https://doi.org/10.1175/WAF-D-20-0182.1.

Douglas, M. W., R. A. Maddox, K. Howard, and S. Reyes, 1993: The Mexican Monsoon. *J Clim*, **6**, 1665–1677, https://doi.org/10.1175/1520-0442(1993)006<1665:TMM>2.0.CO;2.

Dowell, D. C., and Coauthors, 2022: The High-Resolution Rapid Refresh (HRRR): An Hourly Updating Convection-Allowing Forecast Model. Part I: Motivation and System Description. *Weather Forecast*, **37**, 1371–1395, https://doi.org/10.1175/WAF-D-21-0151.1.

Dunn, L. B., and J. D. Horel, 1994a: Prediction of Central Arizona Convection. Part I: Evaluation of the NGM and Eta Model Precipitation Forecasts. *Weather Forecast*, **9**, 495–507, https://doi.org/10.1175/1520-0434(1994)009<0495:POCACP>2.0.CO;2.

——, and ——, 1994b: Prediction of Central Arizona Convection. Part II: Further Examination of the Eta Model Forecasts. *Weather Forecast*, **9**, 508–521, https://doi.org/10.1175/1520-0434(1994)009<0508:POCACP>2.0.CO;2.

ElSaadani, M., W. F. Krajewski, and D. L. Zimmerman, 2018: River network based characterization of errors in remotely sensed rainfall products in hydrological applications. *Remote Sensing Letters*, **9**, 743–752, https://doi.org/10.1080/2150704X.2018.1475768.

Evans, C., S. J. Weiss, I. L. Jirak, A. R. Dean, and D. S. Nevius, 2018: An Evaluation of Paired Regional/Convection-Allowing Forecast Vertical Thermodynamic Profiles in Warm-Season, Thunderstorm-Supporting Environments. *Weather Forecast*, **33**, 1547–1566, https://doi.org/10.1175/WAF-D-18-0124.1.

Gowan, T. A., J. D. Horel, A. A. Jacques, and A. Kovac, 2022: Using Cloud Computing to Analyze Model Output Archived in Zarr Format. *J Atmos Ocean Technol*, **39**, 449–462, https://doi.org/10.1175/JTECH-D-21-0106.1.

Gutzler, D. S., and Coauthors, 2009: Simulations of the 2004 North American Monsoon: NAMAP2. *J Clim*, **22**, 6716–6740, https://doi.org/10.1175/2009JCLI3138.1.

Horel, J., and Coauthors, 2002: MESOWEST: COOPERATIVE MESONETS IN THE WESTERN UNITED STATES. *Bulletin of the American Meteorological Society2002*, 211–226. https://journals.ametsoc.org/view/journals/bams/83/2/1520-0477_2002_083_0211_mcmitw_2_3_co_2.xml?tab_body=abstract-display (Accessed February 22, 2023).

Hu, M., S. G. Benjamin, T. T. Ladwig, D. C. Dowell, S. S. Weygandt, C. R. Alexander, and J. S. Whitaker, 2017: GSI Three-Dimensional Ensemble–Variational Hybrid Data Assimilation Using a Global Ensemble for the Regional Rapid Refresh Model. *Mon Weather Rev*, **145**, 4205–4225, https://doi.org/10.1175/MWR-D-16-0418.1.

Iowa State University, 2023: Iowa Environmental Mesonet. https://mesonet.agron.iastate.edu/plotting/auto/ (Accessed April 16, 2023).

Iowa State University Automated Data Plotter, ISU NWS Watches/Warnings. Figure 3a: IEM generated line plot for all flash flood warnings issued for the entire state of Utah from 1986-2022. cite this proper: https://mesonet.agron.iastate.edu/plotting/auto/?_wait=no&q=44&plot=line&opt=state&station=SLC&state=UT&limit=no&c=single&phenomena=FF&significance=W&syear=1986&eyear=2022&s=jan1&_r=t&dpi=500&_fmt=png&_cb=1 (Accessed February 27, 2023).

James, E. P., and S. G. Benjamin, 2017: Observation System Experiments with the Hourly Updating Rapid Refresh Model Using GSI Hybrid Ensemble–Variational Data Assimilation. *Mon Weather Rev*, **145**, 2897–2918, https://doi.org/10.1175/MWR-D-16-0398.1.

MacDonald, L. M., and C. J. Nowotarski, 2023: Verification of Rapid Refresh and High-Resolution Rapid Refresh Model Variables in Tornadic Tropical Cyclones. *Weather Forecast*, **1**, https://doi.org/10.1175/WAF-D-22-0117.1.

Maddox, R. A., D. M. McCollum, and K. W. Howard, 1995: Large-Scale Patterns Associated with Severe Summertime Thunderstorms over Central Arizona. *Weather Forecast*, **10**, 763–778, https://doi.org/10.1175/1520-0434(1995)010<0763:LSPAWS>2.0.CO;2.

Martinaitis, S. M., S. B. Cocks, M. J. Simpson, A. P. Osborne, S. S. Harkema, H. M. Grams, J. Zhang, and K. W. Howard, 2021: Advancements and Characteristics of Gauge Ingest and Quality Control within the Multi-Radar Multi-Sensor System. *J Hydrometeorol*, **22**, 2455–2474, https://doi.org/10.1175/JHM-D-20-0234.1.

Mazon, J. J., C. L. Castro, D. K. Adams, H.-I. Chang, C. M. Carrillo, and J. J. Brost, 2016: Objective Climatological Analysis of Extreme Weather Events in Arizona during the North American Monsoon. *J Appl Meteorol Climatol*, **55**, 2431–2450, https://doi.org/10.1175/JAMC-D-16-0075.1.

Meyer, J. D. D., and J. Jin, 2016: Bias correction of the CCSM4 for improved regional climate modeling of the North American monsoon. *Clim Dyn*, **46**, 2961–2976, https://doi.org/10.1007/S00382-015-2744-5/METRICS.

——, and ——, 2017: The response of future projections of the North American monsoon when combining dynamical downscaling and bias correction of CCSM4 output. *Clim Dyn*, **49**, 433–447, https://doi.org/10.1007/S00382-016-3352-8/METRICS.

MRMS Decision Tree, 2022: Multi-Sensor QPE - Warning Decision Training Division (WDTD) - Virtual Lab. https://vlab.noaa.gov/web/wdtd/-/multi-sensor-qpe-3?selectedFolder=668043 (Accessed May 14, 2023).

Murphy, M. J., J. A. Cramer, and R. K. Said, 2021: Recent History of Upgrades to the U.S. National Lightning Detection Network. *J Atmos Ocean Technol*, **38**, 573–585, https://doi.org/10.1175/JTECH-D-19-0215.1.

NCEI, 2022: Storm Events Database. NOAA, accessed 10 February 2023, https://www.ncdc.noaa.gov/stormevents/.

NWS website, Flash Flood Definition. https://www.weather.gov/phi/FlashFloodingDefinition (Accessed February 21, 2022).

Risanto, C. B., C. L. Castro, A. F. Arellano, J. M. Moker, and D. K. Adams, 2021: The Impact of Assimilating GPS Precipitable Water Vapor in Convective-Permitting WRF-ARW on North American Monsoon Precipitation Forecasts over Northwest Mexico. *Mon Weather Rev*, **149**, 3013–3035, https://doi.org/10.1175/MWR-D-20-0394.1.

Serra, Y. L., and Coauthors, 2016: The North American Monsoon GPS Transect Experiment 2013. *Bull Am Meteorol Soc*, **97**, 2103–2115, https://doi.org/10.1175/BAMS-D-14-00250.1.

Sharif, R. B., E. H. Habib, and M. ElSaadani, 2020: Evaluation of Radar-Rainfall Products over Coastal Louisiana. *Remote Sens (Basel)*, **12**, https://doi.org/10.3390/rs12091477.

Smith, J. A., M. L. Baeck, L. Yang, J. Signell, E. Morin, and D. C. Goodrich, 2019: The Paroxysmal Precipitation of the Desert: Flash Floods in the Southwestern United States. *Water Resour Res*, **55**, 10218–10247, https://doi.org/https://doi.org/10.1029/2019WR025480.

Smith, T. L., S. G. Benjamin, J. M. Brown, S. Weygandt, T. Smirnova, and B. Schwartz, 2008: 1.1 CONVECTION FORECASTS FROM THE HOURLY UPDATED, 3-KM HIGH RESOLUTION RAPID REFRESH (HRRR) MODEL. *American Meteorological Society 24th Conference on Severe Local Storms*,.

Sun, J., and Coauthors, 2014: Use of NWP for Nowcasting Convective Precipitation: Recent Progress and Challenges. *Bull Am Meteorol Soc*, **95**, 409–426, https://doi.org/10.1175/BAMS-D-11-00263.1.

Yang, L., J. Smith, M. L. Baeck, and E. Morin, 2019: Flash Flooding in Arid/Semiarid Regions: Climatological Analyses of Flood-Producing Storms in Central Arizona during the North American Monsoon. *J Hydrometeorol*, **20**, 1449–1471, https://doi.org/10.1175/JHM-D-19-0016.1.

Zhang, J., and Coauthors, 2016: Multi-Radar Multi-Sensor (MRMS) Quantitative Precipitation Estimation: Initial Operating Capabilities. *Bull Am Meteorol Soc*, **97**, 621–638, https://doi.org/10.1175/BAMS-D-14-00174.1.

Zhang, W., 2023: The dry and hot American Southwest under the present and future climates. *Atmospheric and Oceanic Science Letters*, 100340, https://doi.org/10.1016/J.AOSL.2023.100340.